Dissertation

Development of a Surrogate Diesel Fuel

ausgeführt zum Zwecke der Erlangung des akademischen Grades eines Doktors
der technischen Wissenschaften / der Naturwissenschaften under der Leitung von

Ao.Univ.Prof. Dipl.-Ing. Dr.techn. Ernst Pucher
E 315
Institut für Verbrennungskraftmaschinen und Kraftfahrzeugbau
Technische Universität Wien

Prof. Dr. Kalyanasundaram Seshadri
Department of Mechanical and Aerospace Engineering
University of California at San Diego, USA

eingereicht an der Technischen Universität Wien
Fakultät für Maschinenwesen und Betriebswirtschaften

von

Dipl.-Ing. Stefan Helmuth Humer
Matrikel Nr. 9121399
10922 Ivy Hill Dr. #1
San Diego, CA 92131 USA

Wien, Jänner 2007
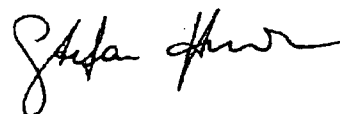
Diese Dissertation haben begutachtet:
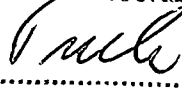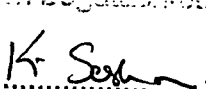
Development of a Surrogate Diesel Fuel

PhD. Thesis

Stefan H. Humer

Institute for Internal Combustion Engines and
Automotive Engineering

Vienna University of Technology, Austria

Advisor:

Ao.Univ.Prof. Dipl.-Ing. Dr.techn. Ernst Pucher
Institute for Internal Combustion Engines and Automotive Engineering
Vienna University of Technology, Austria

Prof. Dr. Kalyanasundaram Seshadri
Department of Mechanical and Aerospace Engineering
University of California at San Diego, USA

San Diego, January 2007

Abstract

Diesel and jet fuels are composed of several hundred different compounds with many of them are in low concentration. The large number of different species in these fuels makes it difficult to use them in numerical calculation of combustion, in addition for only a few compounds detailed chemical-kinetic mechanism are currently available. An approach to solve this problem is by developing a surrogate that consists of only a few compounds for which detailed chemical kinetic mechanism exist or will exist in the near future. This surrogate should have similar characteristics as the "real" fuel. Surrogate fuels are mixtures of few hydrocarbon compounds. The relative concentrations of these compounds are so adjusted that the physical and chemical properties of the mixture approximate those of jet fuels. Chemical-kinetic mechanism for large compounds are based on mechanism for smaller molecules. The high molecular weight compounds, used as reference fuels here, undergo a sequential reduction to lower molecular weight hydrocarbons during combustion. Therefore chemical-kinetic mechanisms for these fuels include those for lower molecular weight compounds. Large molecules break down to species of 3 or smaller carbon numbers. Species with a carbon number of 3 and less are the most important compounds in the chemical kinetic mechanism. Therefor it is important to verify mechanisms which describe these reactions perfectly. To verify these mechanism experimental studies are carried out to obtain critical condition on autoignition and extinction for ethane (C_2H_4), ethylene (C_2H_6), propane (C_3H_6), and propylene, (C_3H_8) in a counterflow setup. Nonpremixed and premixed conditions are investigated over a wide range of fuel mass fraction and equivalence ratios, respectively. The experimental results are compared with numerical calculations.

To obtain data for liquid fuels (fuels with a large carbon number), experiments are conducted on a liquid pool counterflow burner. Several single component fuels are investigated to find out which one is feasible to be used as a reference fuel for a surrogate of diesel and jet fuel. Experimental and analytical studies are performed to elucidate the mechanisms of extinction and autoignition of various liquid hydrocarbon fuels under nonpremixed conditions. Experiments are conducted in a counterflow configuration. In this configuration an oxidizer stream made up of air and nitrogen flows toward a pool of liquid fuel. A boundary layer is established over the surface of the liquid fuel. A formulation is given for describing autoignition in nonpremixed systems. Steady laminar flow of an oxidizer stream toward a stagnation plane is considered. The chemical reaction that takes place between fuel and oxygen is described by a one-step overall process. The activation energy of the reaction is presumed to be large in comparison to the thermal energy. The asymptotic theory developed here makes available explicit formulas for predicting autoignition. From these results a simple but reasonably accurate method is developed for deducing the activation energy, E, and frequency factor, B, of the rate

of the one-step reaction between the fuel and oxygen.

Experimental and numerical studies are carried out to construct reliable surrogates that can reproduce aspects of combustion of JP-8 and Jet-A. Surrogate fuels are defined as mixtures of few hydrocarbon compounds with combustion characteristics similar to those of commercial fuels. The combustion characteristics considered here are extinction and autoignition in laminar nonpremixed flows. Several single component fuels are considered as components for a surrogate for jet fuel. The fuels tested are the components of the surrogates, the surrogates, and the jet fuels. A fuel stream made up of a mixture of fuel vapors and nitrogen is injected into a mixing layer from one duct of a counterflow burner. Air is injected from the other duct into the same mixing layer. The strain rate at extinction is measured as a function of the mass fraction of fuel in the fuel stream. The temperature of the air at autoignition is measured as a function of the strain rate at a fixed value of the mass fraction of fuel in the fuel stream or as a function of the fuel mass fraction in the fuel stram at a fixed value of strain rate. The measured values of the critical conditions of extinction and autoignition for the surrogates show that they are slightly more reactive than the jet fuels. Numerical calculations are carried out using a semi-detailed chemical-kinetic mechanism. The calculated values of the critical conditions of extinction and autoignition for the reference fuels and for the surrogates are found to agree well with experimental data. Sensitivity analysis is used to highlight key elementary reactions that influence the critical conditions of autoignition of an alkane fuel and an aromatic fuel. A surrogate made up of 60% n-dodecane, 20% methylcyclohexane, and 20% o-xylene is suggested as a surrogate for JP-8 and Jet A fuel.

Acknowledgments

I am glad to have here the opportunity to thank all people who supported me and helped to finish this work.

At first i want to thank my advisor Prof. Dr. Ernst Pucher at the Vienna University of Technology without whom i would have never gotten the idea to go to California. He is always on the lookout to find opportunities to support (his) students with scholarships and good advice. I am also very thankful to Prof. Dr. Kalyansasundaram Seshadri, who advised me here at the University of California, San Diego. I am always amazed about the ability to remember tons of equations. Both advisors have a very fruitful and ongoing cooperation between both institutes.

Furthermore I want to thank Dr. Reinhard Seiser with whom i worked together on many problems and who has always an idea how to solve a problem - even if they are not always working afterwards, but i had to make the same experience.

I want to acknowledge the following institutions for granting me financial support in conducting research at the University of California, San Diego: STEP Program, Vienna University of Technology, U.S. Army Research Office Grant # W911NF-04-1-0139.

Special thanks go of course to my wife, Miyuki, who had heard the sentence "I'm nearly finished", or "I'll finish soon", quite often. For that and that she kept her patient all my love goes to her. I guess I drove her crazy saying that one more experiment should go into my thesis - I promise this one is really the last one!

Also special thanks go to my parent who supported me in the idea to go abroad. I guess they didn't think at the first point that I will stay in the US. I also want to thank my sister Ingrid whom i could tell news usually my parents would hear much later and her two very fun kids Katharina and Florian.

John Pulsifer for our daily CAR-talk during our lunch and coffee break. And that he helped me keeping my Volvo cruising - Yeah, Volvo rules (OK - Alfa Romeo too).

All my friends back in Austria - especially Dr. "Roberto" who usually had to do some paperwork for me in Austria and Dorli. I could always stay at their place when I was in Vienna. I would also like to mention Bernd, Pressomat, Julia, ... who keep me updated what's going on in Austria.

Last but not least i want to thank all students which i was advising and working with: Woiferl (aka. el lobo), Joshua, Martin, Jappe (also a very good car mechanic), Ulrich, and Ibrahim. They gave me always a very good supply on "Mozart Kugeln".

And finally to the guy who invented voice over IP, who decreased my telephone bill.

Contents

List of Figures

List of Tables

Chapter 1

Introduction

Mobility is a fundamental need for human beings and the basis for economic development. Countries that are entering the phase of intensified industrialization are likely to follow the path of today's industrialized nations that based their transportation on fossil fuels, mainly crude oil [5]. We globally experience an increase demand of transport and mobility of commodities and individuals. Today's fuel supply is mainly covered by fossil fuels, causing urging challenges for the global climate and emission situation. The internal combustion engine serves as a universal propulsion system for trucks, railways, navigation, and passenger cars. Emission of ground transportation (mainly internal combustion engines) and aviation gets more and more restricted because of nonrenewable sources of crude oil and global warming.

Combustion is a complex process that is still in its beginning of understanding. The earliest studies of flames were mostly experimental – an observer could easily identify flames visually and physically. By means of senses humans could notice that the temperature was much higher near or in the flame than further away from the flame. Observation became eventually more detailed and scientific. By 1000 A.D. furnaces had been developed, by 1300 A.D. first guns were used. With the invention of the steam engine, the industrial revolution started in the 18th century. With all the advantages the industrial revolution brought, the first environmental problems occurred, such as the London fog that was caused mainly by domestic fuel in coal stoves. The Bunsen burner was developed around 1866 [6] and the first internal combustion engine was presented in 1867 by Nikolaus August Otto [7].

Around the early 1900s analytical studies about combustion began to develop (the work of Mikhel'son, Chapman, and Jouget). Since then, Burke and Schumann, Zel'dovich, Frank-Kamenetskii, Liñán, and many others have greatly expanded the useful realm of analytical work [6].

A flame can be describe analytically in terms of interaction of convection and molecular diffusion with many chemical reactions in small length scales [8]. These interactions can be expressed by developing balance equations for continuity, mo-

mentum, energy, and mass fraction of the chemical species involved. Chemical kinetics involved however many species and reactions. To solve such a system analytically was a difficult task. Detailed knowledge could be gathered and used in judicious selection of simplification in order to obtain an analytical solution. The fast development of computational power since the 50's made it possible to solve the sets of equation numerically without the need to simplifying equations. Computer simulation has become an important tool in modeling combustion processes. It provides a detailed prediction of the process occurring in a combustion chamber. Computer simulation helps to optimize the combustion process in a combustion engine so that such is more efficient and produces less emissions.

1.1 History

The improvement of the internal combustion engine went hand in hand with the improvement of the used fuels. The development of the internal combustion engine began in the late 18th century. Slow but steady progress was made over the next hundred years. By 1892, Rudolf Diesel received a patent for a compression ignition reciprocating engine. But his original design, which used coal dust as fuel, didn't work.
Thirty-three years earlier, in 1859, crude oil had been discovered in Pennsylvania. The first product refined from crude oil was lamp oil (kerosene). Since only a fraction of the crude made good lamp oil, refiners had to figure out what to do with the rest of the barrel. Rudolf Diesel, recognized that the liquid petroleum by-products might be better engine fuels than coal dust, began to experiment with one of them. The fuel change, coupled with some mechanical changes, resulted in a successful prototype in 1895. Today, both the engine and the fuel still bear his name.
The first commercial diesels were large engines operating at low speeds. They were used to power trucks and buses. An effort in the late 30s to extend the engine's use to passenger cars was interrupted by World War II. After the war, the automotive diesel became very popular in Europe due to it's better gas mileage, efficiency and fuel price. [9]
The early aircraft engines were similar to those used in automobiles and burned the same fuels. The need for increased power led to the development of specialized engines and aviation gasolines (avgas) tailored to their requirements. In the 1940's the turbine engine emerged as the answer to the ques in still more power. In a replay of avgas development, kerosene - the fuel used in the first aircraft turbine engine - was eventually replaced by specialized aviation turbine fuels (jet fuels).
Liquid fuels have higher energy contents per unit volume than gases, and are easier to handle and distribute than solids. Among liquids, liquid hydrocarbons offer the best combination of energy content, availability, and price. [10]

The development of military jet fuel went from JP-1, JP-2, to JP-3 in the early stage of the turbine engine. The development was driven by an attempt to balance the conflict requirements of volatility, freezing point, and availability/cost. In the late 1940s and early 1950s two fuels emerged from this situation: JP-4 (wide-cut naphta/kerosene mixture) and Jet A-1 (kerosene fuel with a -50°C freeze point). The military aircraft used JP-4 until converting to JP-8 in the 1980s.

Speciality fuels were developed for various applications throughout the second-half of the 20th century. JP-5 was developed in the early 1950s to enhance safety onboard of U.S. Navy ships. The development of higher Mach aircrafts made it necessary to develop speciality fuels. The fuels used in high Mach aircrafts are exposed to larger amounts of heat in the tank and in the engine because of aerodynamic heat. The cutoff point between the use of conventional Jet A-1/JP-8 fuels and special produced fuels is between Mach 2.2 and 3. Thus, the Concorde used Jet A-1, whereas the Mach 2-3 XB-70 and SR-71 required JP-7. The U-2 high altitude reconnaissance aircraft required both improved thermal stability and lower freezing point in its fuel (JP-TS) because of its high altitude, long duration cruises. These speciality fuels gave higher performance than conventional aviation kerosene, at the expense of higher fuel and logistic costs (JP-7 and JP-TS are roughly three times the cost of JP-8 and Jet A-1). [11]

To cut costs and logistic problems the Department of Defense issued Directive 4140.43 on fuel standardization, specifying JP-8 as the primary fuel support for all air and land forces in March 1988 [12]. The result of this logistical simplification was that the U.S. Army's compression ignition (CI) engines designed to operate on DF-2 diesel, now had to operate on the military aviation fuel JP-8. An extensive field study was conducted between 1989 to 1992 at Fort Bliss, TX involving over 2800 U.S. Army vehicles and other equipment to see the influence in operation of JP-8 instead of DF-2 [12]. A similar process is occurring in the U.S. Navy, where a large variety of liquid fuels have compressed down to just two fuels – JP-5 for aircrafts and F-76 diesel for all other liquid fuel requirements.

In the following chapter the properties of Jet-8 and Diesel are presented. Although Diesel and JP-8 are different in their physical and chemical properties they are quite similar. JP-8 is used for this study to simplify the process.

Chapter 2

Fundamentals

Most aviation fuels and diesel fuels are mixtures of a large number of hydrocarbons that meet general physical property specifications. The research is concentrated on Diesel fuel and JP-8, since these two fuels represent a majority of the used fuels in the military. JP-8 is a "kerosene" fuel used by the USAF for jet aircraft. Jet-A fuel is used in the commercial aviation. The difference between Jet-A and JP-8 are in the additives. JP-8 is very similar to Jet-A except three additives: a lubricity improver/corrosion inhibitor, an antistatic additive, and a fuel system icing inhibitor. Kerosene fuels and diesel have similar physical and chemical properties. Both fuels consists mainly of straight chain paraffins, branched paraffins, cycloparaffins, aromatics, and alkenes. Diesel fuel and also JP-8 are formulated to meet general property limits, such as a maximum aromatic content, rather than a specified chemical composition. These specification are fairly wide and can be met by a wide variety of hydrocarbons mixtures [13].

2.1 Fuel Refining

Diesel and jet fuel are made from petroleum. Crude oil is the liquid part of the naturally occurring organic material composed mostly of hydrocarbons that is trapped geologically in underground reservoirs. It is by no means uniform and varies in density, chemical composition, boiling range, etc. from oil field to oil field and also with time for any given oil field. Petroleum crude oil consists primarily out of the paraffinic, naphthenic, and aromatic classes. Each class contains a very broad range of molecular weights. As it comes out of the ground it can be thin and light colored or thick and dark. Thin crudes have relatively low density and thus high API gravities. High-gravity crudes contain more lighter products and generally have a lower sulfur and nitrogen content, which makes them easier to refine. Refining means to turn low-gravity fuels into high-value products.
The refining process can be divided into three basic categories:

Separation process Two or more components are separated on some physical property, like boiling point. Figure 2.1 shows the boiling curve for Diesel and Jet-fuel. The most common separation process is *distillation*.

Upgrading process Catalytic reactions remove certain components that give undesired quality (eg. lowering the sulfur content). The most common one is *hydrotreating*.

Conversion process This process changes the molecular structure of the crude oil by "cracking" large molecules into small ones. Hydrocarbons with a higher boiling point can be broken apart (cracked) into lower boiling hydrocarbons by using high temperature or by a catalyst.

Crude oil is separated in groups depending on its boiling point and density in a fractionating column. The main products after the distillation of crude oil is shown in Figure 2.2. These groups are further processed and are treated with additives.

A schematic layout of a modern, fully integrated refinery is shown in figure 2.3. Jet fuel and diesel may be a blend of straight-run, hydroprocessed, and/or hydroprocessed product. The refinery blends the available stream to meet all performance, regulations, and inventory requirements. The refinery has only limited control over detailed composition of the final fuel. It depends primarily on the composition of the crude oil. [9, 10]

2.2 Types of Fuels

Illuminating kerosene, produced for wick lamps, was used to fuel the first turbine engines. Since the engines were thought to be relative insensitive to fuel properties, kerosene was chosen mainly because of availability. The war at the time required every drop of gasoline.

After World War II, the U.S. Air Force started using "wide-cut" fuel, which basically is a hydrocarbon mixture spanning the gasoline and kerosene boiling ranges. Again, the choice was driven by availability: it was assumed that a wide-cut fuel would be available in larger volumes than either gasoline or kerosene alone.

However, compared to a kerosene-type fuel, wide cut jet fuel was found to have operational disadvantages due to higher volatility:

- greater losses due to evaporation at high altitudes

- greater risk of fire during handling on the ground

- crashed planes fueled with wide-cut fuels were less survivable
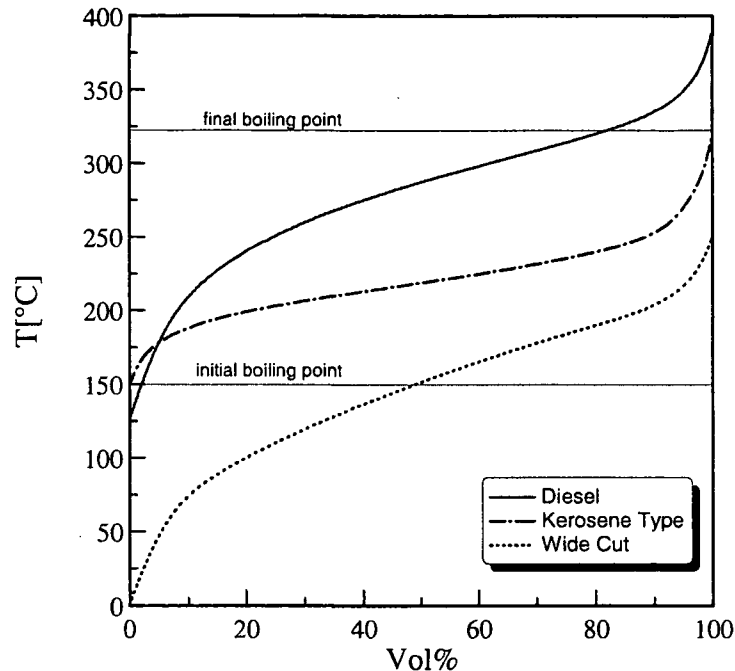
Figure 2.1: Boiling curve of Diesel and Jet Fuel [9].

So the Air Force started to change back to kerosene-type fuel in the 1970s and has essentially completed the process of converting from wide-cut (JP-4) to kerosene-type (JP-5) on aircraft carriers because of safety considerations since the early 1950s. When the commercial jet industry was developed in the 1950s, kerosene-type fuel was chosen as having the best combinations of properties. See table 2.1 for a list of U.S. Military jet fuels. Wide-cut fuel (Jet-B) still is used in some parts of Canada and Alaska because it is suited to cold climates. But kerosene-type fuels - Jet-A and Jet A-1 - predominate in the rest of the world. [1] Jet A is used in the United States while most of the rest of the world uses Jet A-1. the important difference between the two fuels is that Jet A-1 has a lower maximum freezing point than Jet A (Jet A: -40°C, Jet A-1: -47°C). The lower freezing point makes Jet A-1 more suitable for long international flights, especially on polar routes during winter. However, the lower freezing point comes at a price. Other variables being constant, a refinery can produce a few more percent more Jet A than Jet A-1 because of the higher freezing point allows the incorporation of more higher boiling components, which in turn, permits the user of a broader distillation cut. The choice of Jet A for use in the Untied States is driven by concerns about fuel price and availability. Many years of experience have shown that Jet A is suitable

---

[1]The difference between JP-8 and Jet A jet fuel is in the additives.

C₁ to C₄ gases
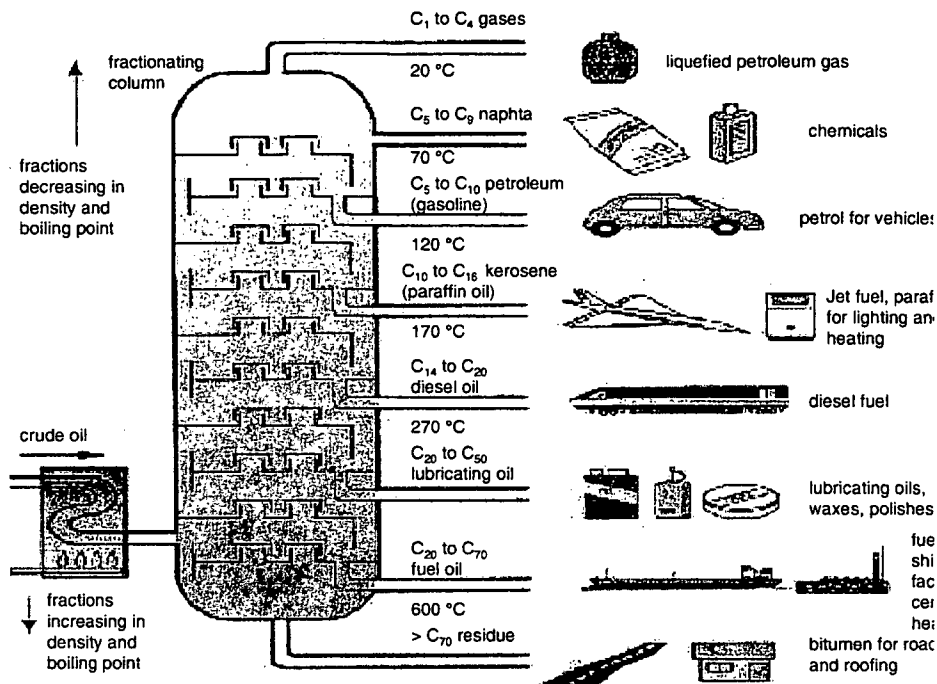
Figure 2.2: Products made out of crude oil after distillation in a refinery.

for use in the Unites States, especially for domestic flights.

Automotive and aviation industry must produce vehicles and jet turbines which operate satisfactorily in all countries under all climatic and geographic conditions. This can only be achieved by extensive testing and developing with the appropriate fuels. Fuels can vary considerably around the world and manufactures need to 'mimic' different fuels to support their test and development programmes. Therefor special fuels are designed for manufacturing, experimentation, test and calibration applications to satisfy the automotive CEC standards. In Europe RF-03-A-84 and DIN EN 590 is used for diesel.

2.2.1 Fuel Properties

As mentioned before aviation fuel and diesel fuel consists of a large variety of hydrocarbons. The content varies from refineries to refineries and country to country respectively. Therefore only a average of the chemical composition can be given. The physical properties are fixed by the specification. Table 2.2 gives an overview of the physical properties. The chemical properties are listed in table 2.3. Refineries are required to deliver fuel with certain physical properties. The chemical
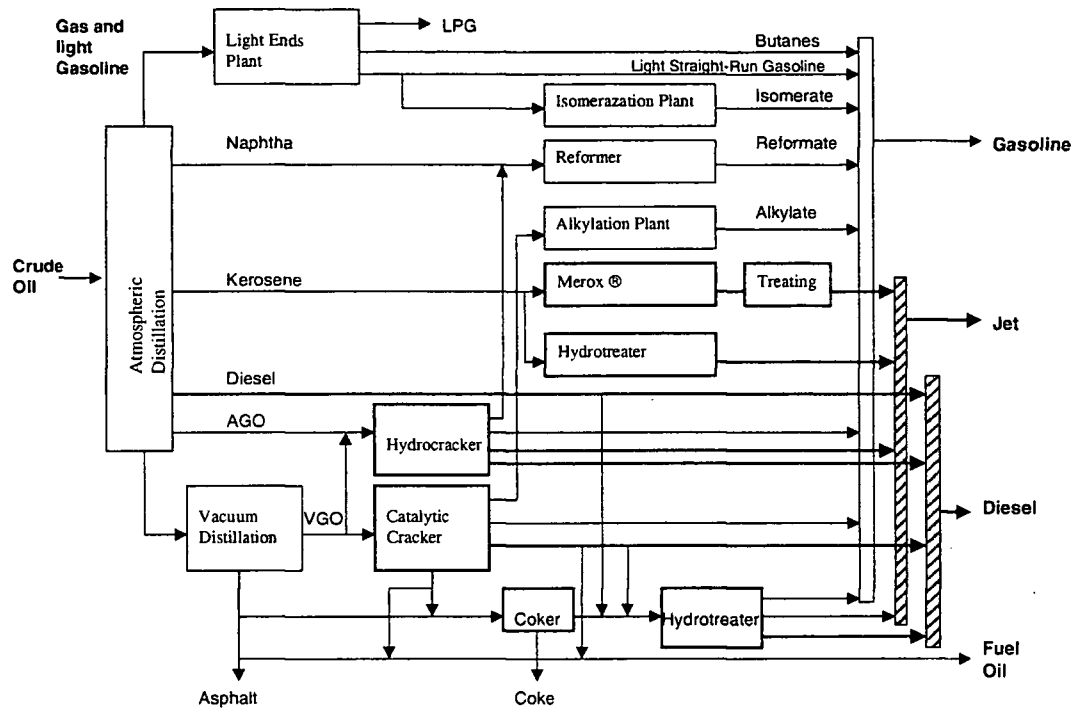
Figure 2.3: A schematic layout of a modern, fully integrated refinery. [9] .

composition is not regulated by the government except the content of aromatics. The content is limited to less than 11% in Europe and 10% in California for diesel. Figure 2.4 illustrates the carbon content of Diesel and Jet A fuel. The carbon number distribution in Fig. 2.4 is interpreted as, for example, Jet A consists of about 20% (by mass) molecules that contain 11 carbon atoms. The typical average and prevalent carbon number for Jet A and auto diesel fuel is C_{11} and C_{16}, respectively. Diesel fuel contains heavier components compared to aviation fuel and has a wider cut. Diesel consists of hydrocarbons with carbon numbers mostly between the C_9–C_{23} range, while Jet A has a range of mostly C_7–C_{17}. This fact can be also seen from the distillation curve. The range of diesel distillation is about 50 to 90 K higher compared to aviation fuel (see therefor 2.1). Aviation fuel require a lower freezing point what's understandable when considering the environment these turbines are operating.

Table 2.1: U.S. Military Jet Fuels [10]

Fuel	Year introduced	Type	RVP, psi	Freeze Point, °C max	Flash Point, °C min	Comments
JP-1	1944	kerosene		-60	43	obsolete
JP-2	1945	wide-cut	≤ 2	-60		obsolete
JP-3	1947	wide-cut	5-7	-60		obsolete
JP-4	1951	wide-cut	2-3	-72		U.S.Air Force fuel
JP-5	1952	kerosene		-46	60	U.S. Navy fuel
JP-6	1956	kerosene		-54		XB-70 program, obsolete
JPTS	1956	kerosene		-53	43	Higher thermal stability
JP-7	1960	kerosene		-43	60	Lower volatility, higher thermal stability
JP-8	1979	kerosene		-47	38	U.S. Air Force fuel
JP-8+100	1998	kerosene		-47	38	U.S. Air Force fuel containing an additive that provides improved thermal stability

2.2.2 Civil Jet Fuels

Aviation turbine fuels are used for powering jet and turbo-prop engined aircraft and are not to be confused with Avgas. Outside former communist areas, there are currently two main grades of turbine fuel in use in civil commercial aviation : Jet A-1 and Jet A, both are kerosine type fuels. There is another grade of jet fuel, Jet B which is a wide cut kerosine (a blend of gasoline and kerosine) but it is rarely used except in very cold climates.

Jet-A1 is a kerosine grade of fuel suitable for most turbine engined aircraft. It is produced to a stringent internationally agreed standard, has a flash point above 38°C (100°F) and a freeze point maximum of -47°C. It is widely available outside the U.S.A. Jet-A-1 meets the requirements of British specification DEF STAN 91-91 (Jet A-1), (formerly DERD 2494 (AVTUR)), ASTM specification D1655 (Jet A-1) and IATA Guidance Material (Kerosine Type), NATO Code F-35. Jet A is a similar kerosine type of fuel, produced to an ASTM specification and normally only available in the U.S.A. It has the same flash point as Jet A-1 but
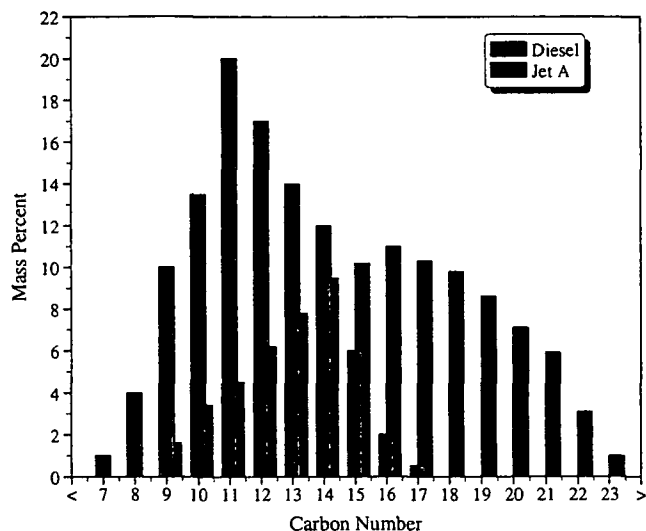
Figure 2.4: Carbon number distribution for Diesel [9] and Jet A [11].

a higher freeze point maximum (-40°C). It is supplied against the ASTM D1655 (Jet A) specification. JP-8 is the military equivalent of Jet A-1 with the addition of corrosion inhibitor and anti-icing additives; it meets the requirements of the U.S. Military Specification MIL-T-83188D. JP-8 also meets the requirements of the British Specification DEF STAN 91-87 AVTUR/FSII (formerly DERD 2453). NATO Code F-34. An excerpt of these specifications is given in the appendix in Chapter B.

Jet B is a distillate covering the naphtha and kerosine fractions. It can be used as an alternative to Jet A-1 but because it is more difficult to handle (higher flammability), there is only significant demand in very cold climates where its better cold weather performance is important. In Canada it is supplied against the Canadian Specification CAN/CGSB 3.23

2.2.3 Military Jet Fuels

JP-4 is the military equivalent of Jet B with the addition of corrosion inhibitor and anti-icing additives; it meets the requirements of the U.S. Military Specification MIL-PRF-5624S Grade JP-4. JP-4 also meets the requirements of the British Specification DEF STAN 91-88 AVTAG/FSII (formerly DERD 2454),where FSII stands for Fuel Systems Icing Inhibitor. NATO Code F-40.

JP-5 is a high flash point kerosine meeting the requirements of the U.S. Military Specification MIL-PRF-5624S Grade JP-5. JP-5 also meets the requirements of the British Specification DEF STAN 91-86 AVCAT/FSII (formerly DERD 2452). NATO Code F-44.

JP-8 is the military equivalent of Jet A-1 with the addition of corrosion inhibitor and anti-icing additives; it meets the requirements of the U.S. Military Specification MIL-T-83188D. JP-8 also meets the requirements of the British Specification DEF STAN 91-87 AVTUR/FSII (formerly DERD 2453). NATO Code F-34. An excerpt of these specifications is given in the appendix in Chapter B.

Both JP-8 and Jet-A (or more commonly used Jet-A1 in Europe) fuel are distillate fuels consisting of distilled process streams refined from crude petroleum. There is no standard formula for jet fuels. Their exact composition depends on the crude oil from which they were refined. Variability in fuel composition occurs of differences in the original crude oil and individual additives. As a result of this varaiability, little information exists on the exact chemical and physical properties of jet fuel. However, the differences are minimal. The primary ingredient of jet fuel is kerosene, and the composition of JP-8 and Jet-A fuel is basically the same as kerosene, with the exemption that they are made under more stringent conditions and contain various additives not found in kerosene. Typical additives include antioxidations (including phenolic antioxidationts), static inhibitors, corrosive inhibitors, fuel system icing inhibitors, lubricate improvers, biocides, and thermal stability improvers. These additives are used only in specific amounts , as governed by military specifications. Straight-run kerosene, the basic component of kerosene used in jet fuels, consists of hydrocarbons with carbon numbers mostly between the $C_6 - C_{16}$ range. Like all the jet fuels, straight-run kerosene consists of a complex mixture of aliphatic and aromatic hydrocarbons.

2.2.4 Diesel

The specification of diesel fuel for the European Community are given in norm EN 590, the specification for the US are given in ASTM D 975. There don't exist different grades as there are aviation jet fuels, although lately oil companies try to introduce diesel fuels as Diesel-Ultimate (Exxon/Mobile) or V-Power (Shell) with a better and cleaner combustion. This is achieved with different kind of additives, what makes the fuel more expensive. The chemical composition of Diesel is given by OMV with 20-25 % mono-aromats, 1-5% di-aromats, and less then 3% poly-aromats. The rest consists of paraffins. As is can be seen from EN 590 and ASTM D 975, only physical properties are required. Norm EN 590 can be seen in the appendix, Table B.1, Diesel fuel specification in the US, Table B.3, and a comparison of US, European, and Japanese Specification for comparable Grade of Diesel fuel, Table B.4.

Table 2.2: Physical fuel properties [14, 15, 16, 17, 18]

Property	Diesel	Jet-A/JP-8
approx. formula	$C_{14.17}H_{26.8}$	$C_{12}H_{23.3}$
H/C ratio	1.96	1.91
boiling range, °C	172-384	165-265
freezing point, °C	NA	-51 (JP-8)
		-50 (Jet-A)
flash point, °C	60	48.9
net heat of combustion,MJ/kg	42.35	42.8
specific gravity @ 15 °C	0.82-0.95	0.81
critical T, °C	NA	410
critical P, bar	NA	65.77

Table 2.3: Average composition of fuels [13, 16, 19]

avg. composition	Diesel [19]	Jet-A/JP-8 [13]
aromatics, vol%	~ 29	18
cycloparaffins	~ 30	20
paraffins	~ 41	60
alkenes	NA	2
sulfur, ppm	510*	490
cetane no.	40.2	45

Since 2005 only 350ppm are allowed by the European Community (EU) - Austria and few other countries of the EU even lowered this level voluntarily to less than 10ppm, called sulfur-free diesel fuel.

2.2.5 Ignition quality, cetane number, cetane index

Because the diesel engine dispense with an externally supplied ignition spark, the fuel must ignite spontaneously (auto-ignition) and with minimal delay (ignition lag) when injected into the combustion chamber. Ignition quality is an expression of the fuel's suitability for spontaneous auto-ignition in a diesel engine. The higher the cetane number, the greater the fuel's tendency to ignite. The cetane number 100 is assigned to n-hexadecane (cetane), which ignites very easily, while slow-burning methyl-naphthalene is allocated the cetane number 0. The cetane number is determined using a test engine. A cetane number in excess of 50 is desirable for optimal operation in modern engines (smooth operation, emissions). High-quality diesel fuels contain a high proportion of paraffins and with elevated CN ratings. Conversely, the aromatic compounds found in cracked components

have a detrimental effect on ignitability.

Yet another indication for ignitability is provided by the the cetane index, which can be calculated on the basis of the density and various points on the boiling curve. In contrast to the cetane number, this index does not reflect the positive influence of "ignition enhancers" on the fuel's ignitability. [20]

Methyl-naphthalene as been replaced by the isoparaffin 2,2,4,4,6,8,8- heptamethyl-nonane (iso-cetane) with a cetane number of 15, mainly due the cost, instability and very bad ignition behavior of the methyl-naphthalene in the CFR-test engine. The cetane number is a measure of the ignition quality of a diesel fuel. It is often mistaken as a measure of the fuel quality. The cetane number is actually a measure of the fuel's ignition delay. This is the time period between the start of injection and start of combustion (ignition) of the fuel. Fuels with higher cetane number have shorter ignition delay periods than lower cetane fuels in a particular diesel engine (which means at the same initial temperature and density).

The measure of the cetane number is standardized in the procedure of ASTM D-613 (America Society for Testing and Material) and is based on the experimental CFR engine test. This method requires the use of an industry standard test engine equipped with accepted instrumentation and operated under specific conditions. In this test, the engine compression ratio is varied for the test sample and reference fuels of known cetane number to obtain a fixed ignition delay. The compression ratio of the sample is bracketed by those of two reference fuels. The cetane number of the sample fuel is determined by estimating between the two reference fuel points. The measured cetane number is itself subject to measurement errors. ASTM D-613 reproducibility of 5% of cetane rating is ~ 3.

Because the ASTM D-613 test is time consuming and expensive, calculated cetane index (ASTM D-976 or D-4737) is often substituted for cetane number. The calculated cetane index is derived from the fuel's density and boiling range. While useful for estimating the cetane number of distillate fuels, this technique can not be applied to fuels containing additives that raise cetane number. These additives do not change the fuel density or distillation profile, so they do not alter the calculated cetane index.

The following equation 2.1 is applied to calculate the cetane number of a mixture of i components, with the volumetric constraint represented by equation 2.2. Equation 2.1 is based on the assumption of linear blending.

$$CN_{mixture} = \sum_i V_i \cdot CN_i \qquad (2.1)$$

$$\sum_i V_i = 1 \qquad (2.2)$$

Cetane index is widely used for routine monitoring of diesel fuel ignition quality.

It is a calculated value, derived from physical properties of the fuel, as density and volatility. The calculations gives a good approximation to the cetane number to avoid expensive and time consuming tests with the CFR cetane engine. Several equations have been developed for this purpose. These equations are mostly empirical derived and specially for fossil fuels.

N. Ladommatos compared in his paper [21] several equations in comparison calculated cetane index to measured cetane number. All equations take physical properties to predict the cetane number. According to [21] equation 2.3 - which is in fact the Canadian General Standard Board cetane index (CGSB) [22] - predicts the cetane number the best of the 22 investigated equations. It can be seen that equation 2.3 can predict the CN over a wide range of values, from $\sim$25 to $\sim$65.

$$CI = 77.7628 + (0.1765AP) + (0.003867AP^2) -$$
$$- (11.615KC) + (0.5844KC^2) - (0.635\nu) \tag{2.3}$$

$$KC = \frac{T_{10} + T_{50} + T_{90} + 820}{200\rho^2}$$

N.Lammotos published a ranking in [21]. In this ranking, the CGSB index was more accurate then all other tested ones as the ASTM cetane index equation, which was taken from [23].The formula has been revised from time to time, as fuels have evolved, to maintain its predictive validity. The equation of the ASTM cetane index from 1993 given in [21] differs to the newer equation for calculating the cetane index, ASTM D 4737, given by [24]. The equation of ASTM D 4737 2.4 is given below:

$$CI = 45.2 + 0.0892(T_{10} - 215) + 0.131(T_{50} - 260) +$$
$$+ 0.0523(T_{90} - 310) + 0.901B(T_{50} - 260) -$$
$$- 0.420B(T_{90} - 310) + 0.0049(T_{10} - 215)^2 -$$
$$- 0.0049(T_{90} - 310)^2 + 107.0B + 60.0B^2 \tag{2.4}$$

$$B = e^{[-3.5(\rho - 0.85)]} - 1$$

Unfortunately the predictive capability of these equations is poor for untypical diesel fuels, such as containing vegetable oils, alcohols and single hydrocarbon compounds.

The ignition quality does not only depend on the physical properties, it also depends on the chemical structure of the hydrocarbons. The physical characteristics affect the time the fuel takes to vaporize and to mix with the hot compressed air.

Several relations between the hydrocarbon structure and/or the class can be made. Generally the CN increases in following order: n-alkanes, olefins, cycloalaknes, and aromatics. A high proportion of normal (unbranched) paraffins (C_nH_{2n+2}) in the fuel, especially those with longer molecular chains (high carbon numbers), generally improves the cetane number. Large n-alkanes have a greater CN than smaller or branched iso-alkanes. On the other hand, cycloparffins and aromatics with their stable ring structure are more difficult to break down and ignite [21]. The CN of naphthenes ranges from 40 to 70, whereas aromatics from 0 to 60. A single ring-structure with a long alkyl side chain has a higher CN than molecules with two or three aromatic rings fused together. [25]

The specification in EN 590 and ASTM D 975 states a required minimum cetane number and cetane index of 47 and 46, respectively. Although JP-8 was successfully tested in reciprocal engines of the U.S. Army, the specifications MIL-DTL-83133E and DefStand 91-87 list no cetane number or index.

2.3 Surrogates in Literature

A considerable amount of research has been conducted on the chemistry of small hydrocarbons. Since the complexity increases with the number of components, only a few studies have been focused on combustion aspects of complex mixture of hydrocarbons. Fuels like gasoline, diesel and aviation fuels are made up of thousands of components. This gives a high complexity to simulate and calculate these fuels. Gaseous fuels have seen a much higher interest of research compared to liquid fuels. This is mainly because liquid fuels are harder to handle and operate in experiments to receive data for comparison.

In 1973, Barnard and Harwood [26, 27] studied the low and intermediate temperature oxidation of both iso-octane and n-heptane using a sub-atmospheric conditions in a static reactor. They noticed a two stage ignition for n-heptane while iso-octane showed a very weak and slow combustion process. Later in 1980s, Lignola and others [28, 29] reexamined the oxidation of these two important reference fuels. In this expertise a jet stirred flow reactor was used where operation conditions up to 12 atmospheres could be accomplished. Iso-octane showed the classic two-stage ignition behavior.

A study at Drexel University [30] deals with low and intermediate temperature hydrocarbon chemistry of iso-octane, n-heptane and their blends. This study investigated several mixtures of the two gasoline reference fuels comparing autoignition behavior of these surrogates comparing it with real fuel. The study showed that a blend of two components is not enough accurate to reproduce the behavior of complex real fuels, even if they match the real fuel MON/RON values. The two component surrogate ignites earlier compared to the real fuel. The real fuel ignition behavior was finally achieved by using a surrogate with 4 hydrocarbon

components (n-heptane, iso-octane, 1-pentene (an olefin), and toluene (an aromatic)).

In a study of autoignition chemistry of gasoline primary fuels and of mixtures of paraffins and olefins, Leppard [31] and Kowalski [32] identified a synergistic behavior for the binary mixtures of paraffins and olefins. Lepard related this inhibiting behavior to the alkenes acting as radical scavengers in the lot temperature chemistry of the alkanes, and the alkanes slowing the faster alkenes high temperature chemistry.

In 1989, Wilk et al. [33] researched in this work the autoignition tendency of several compounds representative of the main hydrocarbon classes and their binary mixtures with n-heptane. The alkenes inhibited the alkane chemistry of n-heptane in the low temperature region but promoted the oxidation in the intermediate temperature region. The aromatic and branched alkane showed inhibiting behavior. Furthermore the study related the amount of CO produced by the combustion of the mixtures to their octane number, providing a simple correlation to predict the non-linear behavior of binary hydrocarbon mixtures. A comparable cetane correlation was developed based on the experimental data for n-heptane, n-octane, and n-decane, but could not be confirmed.

Kinetic studies of real fuels like diesel and aviation fuels are considered impossible due their high order of complexity. Maurice and Lindstedt [34] reduced the complexity of the kerosene type aviation fuels using a surrogate model of 89 mol% n-decane and 11 mol% various aromatics including benzene, toluene, ethylbenzene, and ethylbenzene/naphtalene as an input to a detailed kinetic model. Wood et al. [35] performed experimental combustion studies with JP-4 and JP-5 surrogates. The surrogates are listed in Table 2.4 and 2.5 and were developed with the goal to establish a set of surrogate fuels for modeling and a study of fuel properties and chemical composition effects. Wood reported that these surrogates had good agreement with the physical and chemical properties of the real fuel except for the smoke point. Edwards and Maurice [13] used these surrogates in their swirl-stabilized combustor. The fuel hydrogen content of the fuel may be a good predictor for the soot level.

Starting from the pioneering work of Schulz [1], who proposed a 12-component surrogate mixture for JP-8, several investigators have proposed surrogates for jet fuels. Some examples are shown in Table 2.6 [1, 2, 3, 4]. The surrogate developed by Schulz et al. [1] was designed to reproduced the general oxidation behavior of the JP-8, but could not reproduce the deposition levels in thermal stability testing. This fact has been related by Edwards and Maurice [13] to the key role that trace species, such as metals and hetero-atoms, play in the deposition process. The surrogate mixture of Ref. [2] is called the Drexel surrogate, and that of Ref. [4] the Utah surrogate. Quasi global chemical-kinetic models have been developed previously to reproduce experimental data. Lindstedt and Maurice [36] modeled the

Table 2.4: JP-4 Surrogate - Wood et al. [35]

COMPOUND CLASS	JP-4 Vol.%	SURROGATE COMPONENT	Vol.%
PARAFFINS	61.2	n-hexane	5.5
		n-heptane	8.0
		n-octane	8.0
		n-nonane	10.0
		n-decane	10.0
		n-dodecane	10.0
		n-tetradecane	10.0
METHYLCYCLO-PARAFFINS	24.2	cyclohexane	8.0
		methylcyclohexane	8.0
		cycooctane	8.0
DICYCLOPARAFFINS	4.9	decalin	5.0
ALKYLBENZENE	8.2	toluene	8.0
INDANS & TETRALINS	1.1	tetralin	1.0
NAPHTHALENES	0.5	a-methylnaphthalene	0.5

Table 2.5: JP-5 Surrogate - Wood et al. [35]

COMPOUND	Blend #1 Vol.%	Blend #2 Vol.%
n-decane	2.5	2.5
decalin	11.5	11.5
n-undecane	0.0	5.0
n-pentylcyclohexane	11.0	0.0
1,3-diisopropylbenzene	3.0	3.0
tetralin	9.5	9.5
n-dodecane	25.0	31.0
1-phenylhexane	5.0	5.0
n-tridecane	10.0	15.0
n-heptylcyclohexane	11.0	0.0
a-methylnaphthalene	1.5	1.5
n-tetradecane	5.0	5.0
n-pentadecane	5.0	5.0

Table 2.6: Surrogate mixtures for Jet fuels [1, 2, 3, 4]

	Surrogate Compounds	Schulz[1]	Drexel[2]	Montgomery[3]	Utah[4]
normal Alkanes	n-decane	15		32.6	
	n-dodecane	20	26	34.7	30
	n-tetradecane	15			20
	n-hexadecane	10			
branched Alkanes	iso-octane	5			10
	iso-cetane		36		
cyclo Alkanes	methyl-cyclo-hexane	5	14	16.7	20
	cyclooctane	5			
	decaline		6		
Aromatics	toluene				
	o-xylene	5			15
	butyl-benzene	5		16	
	tetra-methyl-benzene	5			
	α-methyl-naphthalene	5	18		
	tetralin	5			5

structure of kerosene flames using a surrogate blend comprising 89-mol% n-decane and 11-mol% aromatic fuel. Montgomery et al. [3] proposed a surrogate mixture made up of four components shown in Table 2.6. They developed a reduced chemical-kinetic mechanism for the surrogate using CARM (Computer Assisted Reduction Method) [3, 37]. The Utah surrogate for JP-8 is made up of six components shown in Table 2.6. It was used to model a kerosene flame using a semi-detailed chemical-kinetic scheme [4]. Recently, Montgomery et al. [38] developed a reduced chemical-kinetic mechanism starting from the semi-detailed chemical-kinetic scheme of the Utah surrogate for the simulation of a two-dimensional supersonic jet flame. They successfully demonstrated the feasibility of employing chemistry of commercial fuels into computational fluid dynamic (CFD) codes.

Two surrogate fuels for JP-8 have been developed by Sarofim and coworkers [39] in their work for fire simulation. Six pure hydrocarbons were blended in such a way as to create a surrogate that reproduce the distillation curve of the parent fuel, as well as its sooting propensity. It was determined that a six-component surrogate provides sufficient flexibility to simulate the major properties of interest to pool

Table 2.7: JP-8 Surrogate - Sarofim et al. [39]

Surrogate #1		Surrogate #2	
COMPOUND	Vol.-%	COMPOUND	Vol.-%
iso-octane	10.0	iso-octane	5.0
methylcyclohexane	20.0	methylcyclohexane	5.0
m-xylene	15.0	toluene	20.0
n-dodecane	30.0	n-decane	25.0
tetralin	5.0	n-dodecane	25.0
n-tetradecane	20.0	n-tetradecane	20.0

fires of real jet fuels. These two fuels are listed in Table 2.7.

Based on carbon distribution (Fig.2.4), hydrogen–carbon ratio (Tab.2.2), average composition (Tab.2.3), and other fuel properties, single component fuels can be selected to mimic the characteristics of the real fuel. It is fairly easy to find a mixture or even only one single component fuel if only one characteristic of the real fuel is desired to replicate. The challenge is to find a fuel mixture/surrogate that imitates several characteristics of the real fuel and is not too complicated to handle. The more properties that should be emulated by the surrogate fuel the more species are necessary. Also availability of the fuel itself, its costs, and the availability of chemical kinetic mechanism for these species have to be considered. Usually a surrogate is designed to mimic certain characteristics of the real fuel. The less components the surrogate contains, the less characteristics the surrogate will mimic. It is possible to design a surrogate by using a few components if the aim of this surrogate is to imitate a few characteristics of the real fuel.

2.4 Adiabatic Flame Temperature

The adiabatic flame temperature is a theoretical temperature of the flame that results from a complete combustion process that occurs without any work, heat transfer or changes in kinetic or potential energy at either constant volume or pressure. This is the maximum temperature that can be achieved for given reactants because any heat transfer from the reacting substances and/or any incomplete combustion would tend to lower the temperature of the products. The reactants reach a chemical equilibrium at a given initial temperature and pressure. The adiabatic flame temperature depends on the pressure, the initial temperature and its initial compositions of reactans. The reactants (index r) and the products

(index p) have the same specific enthalpy, h.

$$h^{(r)} = \sum_{j=1}^{S} w_j^{(r)} w_j^{(r)} = \sum_{j=1}^{S} w_j^{(p)} w_j^{(p)} = h^{(p)} \qquad (2.5)$$

And for constant pressure:

$$h_j^{(p)} = h_j^{(r)} + \int_{T_0}^{T_{ad}} c_{p,j} dT \qquad (2.6)$$

with T_{ad} the adiabatic flame temperature, T_0 the initial temperature, and $c_{p,j}$ the specific heat capacity of species j. Using both equations, the adiabatic flame temperature, T_{ad} can be determined.

A diffusion flame in a counterflow configuration has always the position of stoichiometric conditions, where the highest energy output happens. In an ideal combustion process hydrocarbon fuel gets completely burned to carbon dioxide and water. The one-step reaction is given in Equ. 2.7.

$$C_m H_{n(l)} + \nu_{O_2} O_2 + \nu_{N_2} N_2 \Leftrightarrow \nu_{CO_2} CO_2 + \nu_{H_2O} H_2O_{(g)} + \nu_{N_2} N_2$$

$$\qquad (2.7)$$
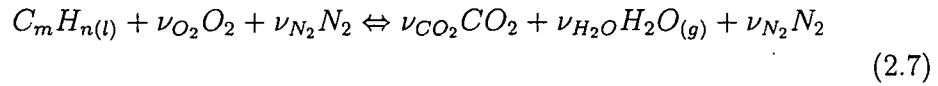
$$\nu_{CO_2} = m, \quad \nu_{H_2O} = \frac{n}{2}, \quad \nu_{O_2} = m + \frac{n}{4}, \quad \nu_{N_2} = \nu_{O2} \frac{M_{O_2}}{M_{N_2}} \cdot \frac{1 - y_{O_2,\infty}}{y_{O_2,\infty}}$$

Assuming that the reaction is processed in one step and produces only CO_2, and H_2O as a product results in the highest adiabatic temperature.

2.5 Experiments

Practical combustion engines such as internal combustion engine (gasoline), turbines need turbulence to mix the reactants (fuel) with the oxidizer (air) to achieve a (nearly) complete combustion. In a diesel engine, fuel droplets are injected at high velocity into hot air. The flame burns in a highly turbulence environment. That means that flow velocities of gases have an influence on the flame and therefor its combustion. Although a candle is an example for a laminar diffusion flame, it is a simple example to see the influence of flows when the flame gets blown out. Blowing air against the burning candle means to deliver more oxygen into the flame, and more oxygen means that the flame burns better. Everybody knows this by trying to ignite the coal for their barbecue. By blowing air onto the glowing coal, the reaction increases and with it the temperature. But if there is a critical value of velocity reached, the flame of the candle will extinguish. In an internal combustion engine this phenomena is called quenching. The flame in the combustion chamber can be blown out by turbulence in the combustion chamber,

the upwards movement of the piston against the cylinder head, where the flame is "quenched". Similar things happen in a turbine engine. If the velocity in the combustor is too high, the flame extinguishes. Aircraft turbine manufacturer are required to test their engines under which conditions the flame in the combustor extinguishes. It is important to understand this phenomena to simulate exactly combustion processes in an internal combustion engine.

Except the gasoline engines and HCCI engines, all of the above mentioned engines are nonpremixed systems. The reactants and the oxidizer are not mixed before entering the combustion chamber. The mixing of fuel and oxidizer occurs simultaneously with the combustion process.

Previous investigations on fuels were conducted in constant volume bombs, flow reactors, and shock tubes to get experimental data. These experimental studies were conducted on premixed systems in the absence of fluid flow. The counterflow setup takes the influence of a flow field into account. As a characterizing value the strain rate, a, is used here which is a function of the opposing velocities. The strain rate is given in Equ. 3.1.

The flame is characterized if it is a premixed or non-premixed flame. The combustion is influenced by its chemical time, t_c, and its time of transport and mixing of reactants, t_m. The chemical time, t_c, depends on the fuel and characterizes its reactivity. The time of transport and mixing of reactants, t_m, depends on the flow field. Gustave Damköhler introduced the Damköhler Number:

$$Da = \frac{t_m}{t_c} \tag{2.8}$$

It defines the ratio of characteristic residence time or fluid motion time scale to characteristic reaction time. Large Damköhler number Da $\gg$ 1 corresponds to very rapid chemical reaction in comparison to all other processes. Small Damköhler number Da $\ll$ 1 corresponds to very slow chemical reaction in comparison to all other processes. Following Eqn. 2.8, the Damköhler number becomes very small for premixed combustion, since the reactants are already mixed and with that $t_m \ll 1$. For a diffusion flame the Damköhler number is large, since $t_m \gg 1$.

Although the combustion in an internal combustion engine takes place in a turbulent environment, on a micro-scale the combustion is locally laminar. For simplicity the experimental setup assumes laminar premixed and nonpremixed flames. Simple examples for nonpremixed laminar flames include candles, oil lamps, and camp fires. The flame in the laminar nonpremixed condition exists at the interface between the fuel and oxidizer. The rate of combustion is generally controlled by the rate of diffusion of reactants to the interface.

Two commonly used configurations for research are the laminar counter-flow and the co-flow nonpremixed configuration as shown in Fig. 2.5 and Fig. 2.6, respectively. Because of the two-stream nature of a nonpremixed flame the whole range of equivalence ratio ϕ from 0 (air) to ∞ (pure fuel) is covered. The flame front is
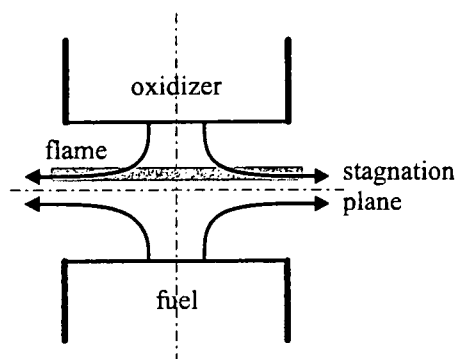
Figure 2.5: Schematically illustration of a nonpremixed laminar counterflow configuration.
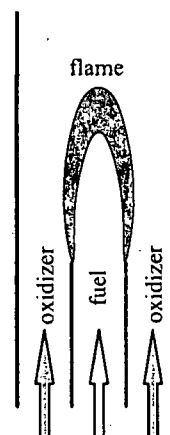
Figure 2.6: Schematically illustration of a nonpremixed laminar coflow configuration.

fixed to regions near the location of the stoichiometric composition and is usually characterized by the intensity of its luminescence. The more intense the luminescence the higher the temperature. Also the highest temperature occurs close to stoichiometric.

Calculating the maximum temperature in the reactive flow-field a well-known result can be obtained for steady strained counterflow – the characteristic S-shaped curve [40], shown in Fig. 2.7. Three solutions can be obtained at a certain value of strain rate. The upper branch represents the temperature of a burning flame, the lower branch gives the temperature of the reactants before ignition. The branch in the middle is physically unstable. Two opposing stream with a certain composition and temperature can mix as frozen flow at high strain rate. Here, the reaction rate is negligible and the maximum temperature in the flow-field will be the higher one of the reactant stream (lower branch). By decreasing the strain rate the residence time for the reactants in the mixing layer is increased. Exothermic reactions can take place and the steady-state temperature in the reaction zone will be higher than that of the frozen flow. At a certain strain rate below a critical value the heat release and formation of radicals will become so large that no steady-state solution in the non-burning regime can be maintained. The mixture will ignite and the maximum temperature of the resulting flame is given by the upper branch of the S-shaped curve. Increasing the strain rate in the upper regime results in decreasing the residence time of the reactants in the mixing layer and decreasing temperature. A flame can not be maintained anymore – the extinction limit is reached. The maximum temperature "falls" down the the lower branch. This hysteresis between ignition and extinction is due to the activation energy found in
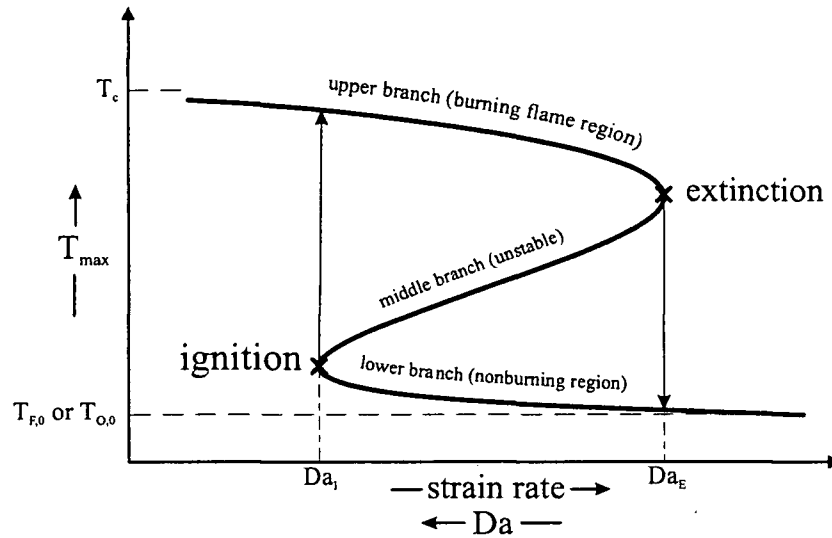
Figure 2.7: The maximum temperature T_{max} as a function of the strain rate and Damköhler number – the well-known S-curve, where $T_{F,0}$ is the temperature at the fuel duct boundary, $T_{O,0}$ the temperature at the oxidizer duct boundary, and T_c the adiabatic flame temperature.

combustion reactions. Similar S-shaped curves can be obtained for the maximum concentration of certain radicals like OH, H, or O. The numerical calculation of extinction can be performed by establishing a burning-flame solution and increasing the strain rate until the maximum temperature decreases and no burning solution can be obtained anymore. [41]

Chapter 3

Setup

Fundamental studies on extinction and autoignition of strained premixed flames provide knowledge for modelling turbulent combustion. Previous studies on liquid hydrocarbon fuels were focused on measuring ignition delay times in shock tubes [42, 43] and rapid compression machines [44]. These experimental studies were conducted on premixed systems in the absence of fluid flow. In diesel and jet engines (turbines) fuel gets injected into hot, compressed air in the combustion chamber. The temperature of the compressed air ignites the fuel - so called self-ignition or autoignition. Because of the principle of the working process in diesel engines and jet engines it is of interest to know the ignition and extinction behavior of the used fuels. To achieve a good (homogeneous) mixture between air and fuel, turbulence is desired in the combustion chamber. That means that high flow velocities occur inside the combustion chamber which can be equaled to the strain rate. The combustion process in the chamber is a function of the strain rate. With the counterflow setup the strain rate can be implemented into the experimental setup.

The opposed-flow configuration makes an attractive experimental configuration, because the flames are flat, allowing for detailed study of the flame chemistry and structure. The two or three-dimensional flow is reduced mathematically to one dimension by assuming that the y- or radial velocity varies linearly in the y- or radial direction, which leads to a simplification in which the fluid properties are functions of the axial distance only. The one dimensional model then predicts the species, temperature, and velocity profiles in the core flow between the nozzles. Both premixed and non-premixed can be simulated. [45]

3.1   Counterflow Burner

The counterflow (or also often called opposed-jet flow) setup is a well known configuration. [46] In practical devices, fuel and air are brought together by convection

where they mix as a result of diffusion. In general, this is a three-dimensional problem. With a counterflow setup this problem can be reduced to one spatial dimension. Using the boundary layer approximation of Prandtl (i.e. neglect of diffusion in the direction orthogonal to the stream line, here y-direction), the problem reduces to one spatial coordinate, namely the coordinate orthogonal to the stagnation plane. Using the assumption that

- the temperature and mass fraction of all species are functions only of the coordinate x normal to the flame plane,

- the normal velocity v_x is a function of x only (shown in Figure 3.2),

- the tangential velocity v_y is proportional to the coordinate tangential to the flame y, $v_y = Gy$,

- the system is considered to be steady-state ($\partial/\partial t = 0$).

The counterflow configuration is made up of two axis symmetric ducts opposing each other. The lower duct is called reactant duct and indicated by the index 1. The upper duct is either called oxidizer duct for non-premixed experiments or inert gas duct for premixed experiments and indicated by index 2. To shield the reaction zone from the surrounding environment, both ducts are surrounded by another centered duct, called curtain duct. In this duct pure nitrogen is flowing, so that the surrounding has no influence on the reaction zone. Additionally the exhaust gases get mildly sucked into the exhaust, which surrounds the curtain duct, and cooled down by a water spray inside the exhaust duct. With this it is made sure that the hot reactants/products do not ignite in the exhaust duct. Figure 3.1 shows on the left side a schematic illustration of the counterflow, on the right side a velocity profile calculation for a strain rate of a $= 300$ s^{-1} at room temperature for this dimensions. The stagnation plane gets pulled down on the corner since the exhaust gases are mildly sucked into an exhaust exit. The velocity profile between the fuel-duct and oxidizer-duct exit along the x-axis is shown for a strain rate of a $= 300$ s^{-1} in Figure 3.2. The stagnation plane is kept in the middle of both ducts by mass balancing both flows. Steady, axisymmetric, laminar flow of two counterflowing streams toward a stagnation plane is considered. The distance between the exits of the ducts is L. Studies on nonpremixed systems are carried out by injecting a fuel stream made up of fuel and nitrogen (N_2) from one duct and an oxidizer stream made up of air and N_2 from the other duct. The mass fraction of fuel, the temperature, and the component of the flow velocity normal to the stagnation plane at the exit of the fuel duct are $Y_{F,1}$, T_1, and V_1, respectively. The mass fraction of oxygen, the temperature, and the flow velocity at the exit of the oxidizer duct are $Y_{O_2,2}$, T_2, and V_2, respectively. Studies on premixed systems are carried out by injecting a premixed reactant stream made up of fuel, oxygen,
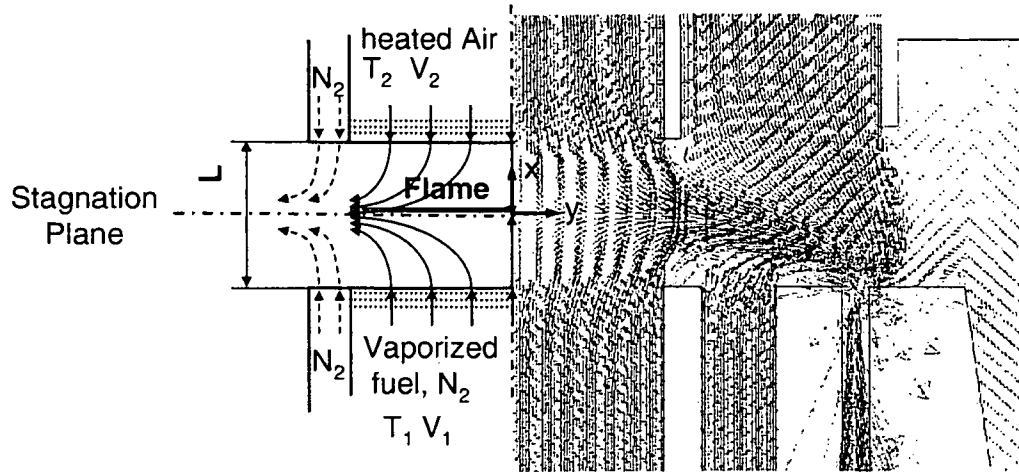
Figure 3.1: Schematic illustration of the counterflow setup. The velocity on the right side is calculated for a strain rate of a $= 300$ s^{-1}.
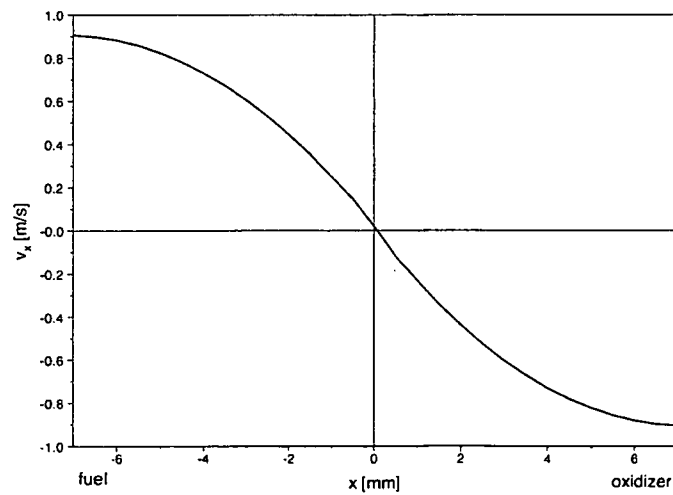
Figure 3.2: Velocity profile along x-axis between fuel-duct and oxidizer-duct exit at a strain rate a $= 300$ s^{-1}.

and nitrogen from one duct and an inert-gas stream of N_2 from the other duct. The mass fraction of fuel, the mass fraction of oxygen, the temperature, and the flow velocity in the premixed reactant stream at the exit of the duct are $Y_{F,1}$, $Y_{O_2,1}$, T_1, and V_1, respectively. The temperature and the flow velocity in the inert-gas stream at the exit of the duct are T_2 and V_2, respectively. Experimental studies are conducted with the momenta of the counterflowing streams $\rho_i V_i^2$, $i = 1, 2$ kept equal to each other. Here, ρ is the density. The tangential components of the flow velocities at the exits of the ducts are presumed to be equal to zero (plug-flow boundary conditions). The value of the strain rate, a, defined as the normal gradient of the normal component of the flow velocity, changes from one duct exit to the other [47]. The value of a on the oxidizer side of the stagnation plane, a_2, for non-premixed systems and on the inert gas side of the stagnation plane for premixed systems is presumed to be given by [47]

$$a_2 = \frac{2|V_2|}{L}\left(1 + \frac{|V_1|\sqrt{\rho_1}}{|V_2|\sqrt{\rho_2}}\right) \tag{3.1}$$

A detailed description of the burner is given elsewhere [48].

3.2   Numerical Calculation

The numerical computations are carried out using a computer program called FlameMaster, that was developed at RWTH-Aachen [49]. The program can also calculate liquid phases as it was needed for the liquid pool in Chapter 5 (Chemkin is not capable to do so.) At the boundaries of the computational domain the mass flux of the reactants and the velocities are specified corresponding to those used in the experiments. Plug-flow boundary conditions are employed in the calculations. The conservation equation of mass, momentum and energy and the species balance equations used in the formulation of the numerical problem are summarized elsewhere [50, 49, 8]. The species balance equations include thermal diffusion and the energy conservation equation includes radiative heat losses from carbon dioxide and water vapor [49]. Buoyancy is neglected.

3.3   Temperature Measurement

The temperature measurements of the gas flows as well as the temperature of liquid fuels are carried out by employing a thermocouple. Two different thermocouple are used. For the measurement of the oxidizer gas flow temperature at autoignition experiments, a Pt-Pt 13% Rh type R is used. It consists of two different wire materials that are welded together. One wire is made of platinum (Pt), the other of platinum with 13% rhodium (Rh). The diameter of both wires is 0.076 mm,
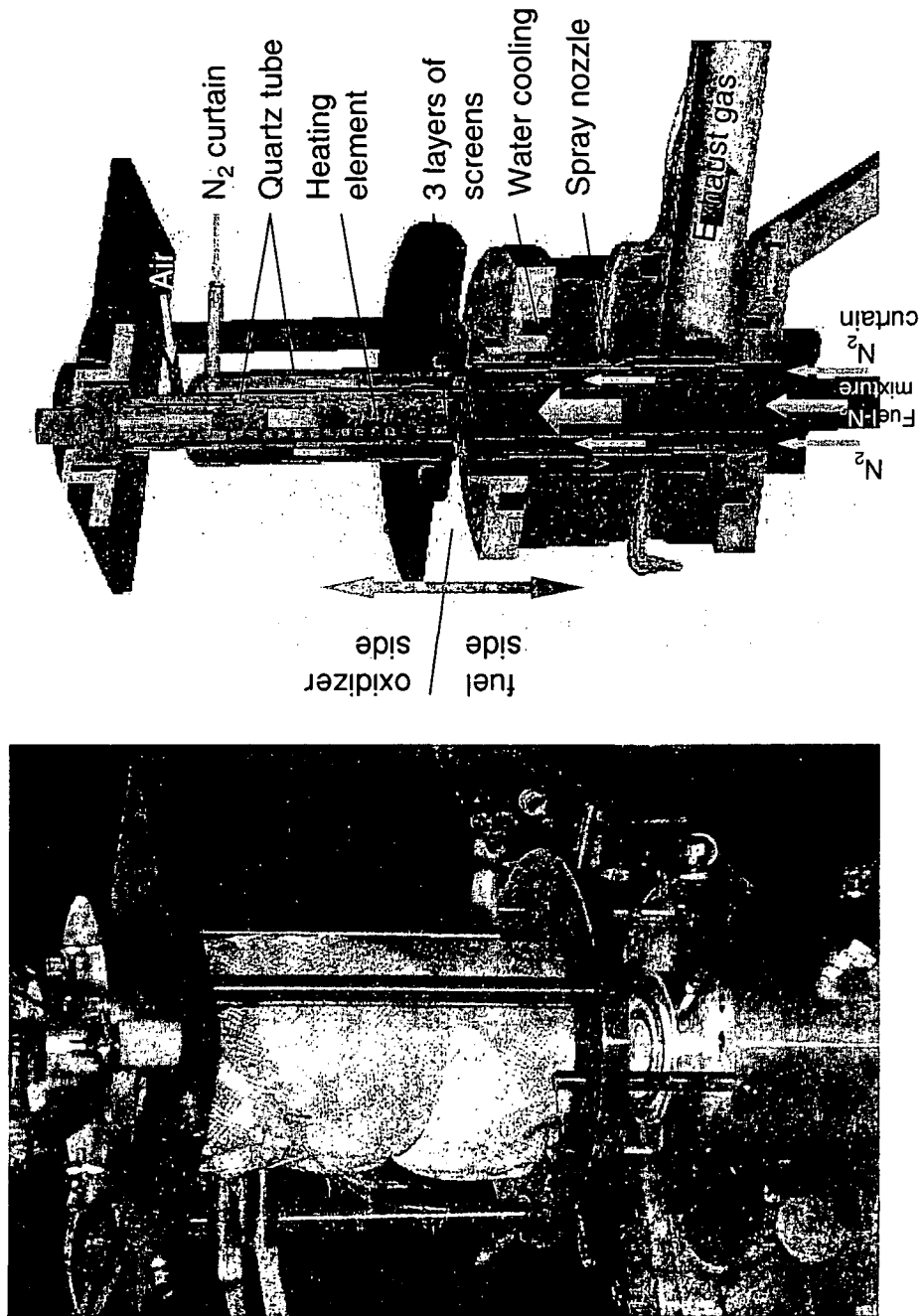
Figure 3.3: Section view of a 3-D Model of the counterflow setup and picture of the "red" glowing heating top.

the beat of the welding is 0.21 mm in diameter. A ceramic tube, that contains
two holes for each wire to prevent it from electrical short-circuiting, supports
the thin wires. On the side with the bead, the wires stuck about 1.0 cm out of
the tube. The other ends of the wires are hooked up to a connector mounted
on a 2-dimensional stage, to move the thermocouple in the correct location. To
obtain accurate measurements of the gaseous flow temperature, the wire of the
thermocouple has to be inserted into the flow horizontal to prevent heat conduction
along the wire and be radially centered and positioned close to the exit of the upper
duct to get the reading of the highest temperature. It was demonstrated that the
axial temperature does not change significantly close to the duct exit. Also the
thermocouple wire gets slightly bent down at higher flow rates, the measured
temperature is still accurate [51]. The temperature profile along the radial axis is
flat over nearly the whole diameter of the upper duct (see Fig.6.2 in chapter 6).

The temperature is displayed by a digital unit made by Omega Engineering,
Inc. The indicated temperature at the readout is corrected for radiative heat loss
of the bead (assuming a spherical shape) according to the following equation

$$T_g = T_{tc} + \frac{\varepsilon \sigma d T_{tc}{}^4}{2\lambda} A \qquad (3.2)$$

where T_g is the corrected gas temperature and T_{tc} the indicated temperature, σ is
the Boltzmann constant $(5.67x10^{-8} W/m^2 K^4)$, λ the thermal conductivity, d the
diameter of the bead, ε the emissivity, and A the view factor, which is chosen to be
0.5 since only the lower part of the thermocouple can emit radiation. The thermal
conductivity is calculated according the the equation derived from [52]

$$\lambda = 4.6942x10^{-3} + 8.1225x10^{-5} T_{tc} - 1.4547x10^{-8} T_{tc}{}^2. \qquad (3.3)$$

The value of emissivity $\varepsilon = 0.128$ according to previous study [53]. The estimated
accuracy of the corrected temperature is about $\pm$ 25 K.
The temperature of the vaporizer stream or liquid pool is measured by a Cromel/
Constantan type E thermocouple. This thermocouple is used for a lower temperature range and nearly constant temperature. This allowed a bigger sized
thermocouple with a wire diameter of 0.125 mm with a bigger time delay.

Chapter 4

Chemical Kinetic Mechanisms Implementation

The high molecular weight compounds of diesel and jet fuels undergo a sequential reduction to lower molecular weight hydrocarbons during combustion process. Therefor chemical-kinetic mechanisms for these fuels include those for lower molecular weight compounds. Species with a carbon number of 3 and less are the most important compounds in the chemical kinetic mechanism. Large molecules break down to species of 3 or smaller carbon numbers. Therefor it is important to verify mechanisms which describe these reactions perfectly. In the following the "base-skeleton" for all mechanisms is tested on ethane (C_2H_4), ethylene (C_2H_6), propane (C_3H_6), and propylene, (C_3H_8). Mechanisms for methane (CH_4) have been compared with experimental results elsewhere [54].

4.1 Non-Premixed and Premixed Extinction and Autoignition of C_2H_4, C_2H_6, C_3H_6, C_3H_8

Combustion is a complex chemical and physical process that in practice takes place in a nonuniform, turbulent flow-field. To compute the dynamics of combustion process in engines it is necessary to have knowledge of chemical-kinetic mechanisms of autoignition and combustion of practical fuels such as gasoline, diesel and jet fuels. These fuels are made up of numerous different hydrocarbon compounds with high molecular weight [55]. A number of experimental and numerical studies have addressed combustion of high molecular weight compounds such as n-heptane [56, 50, 57, 58, 59, 60], n-decane [61, 62], and n-hexadecane [63] because knowledge of chemical-kinetic mechanisms os combustion of these fuels are presumed to be useful in modeling combustion of diesel and jet fuels. These studies show that the chemical-kinetic mechanisms of oxidation of low molecular weight fuels such as hydrogen, carbon monoxide, methane, ethene (C_2H_4), ethane (C_2H_6), propene

(C_3H_6), and ethane (C_3H_8) can be presumed to be subset of chemical-kinetic mechanisms of oxidation of n-heptane, n-decane, and n-hexadecane. Therefore accurate description of mechanisms of oxidation of these low molecular weight fuels are necessary first steps in the development of chemical-kinetic mechanisms of oxidation of practical fuels [64]. Chemical-kinetic mechanisms are developed for certain experimental data and compared with other experimental results. Therefor it is important to provide accurate experimental data over a wide range of different conditions and configurations to test the chemical-kinetic mechanisms of their performance.

Several studies including laminar nonpremixed flames, laminar premixed flames, and shock induced ignition in homogeneous systems have been performed by previous investigators [64, 65, 66, 67, 68, 69, 70, 71, 72, 73, 74]. Autoignition in counterflow premixed systems have been investigated for C_2H_4 [65] and C_2H_6 [65]. The structure and concentration of various species have been measured in counterflow nonpremixed flames for C_2H_6 [66] and C_3H_8 [67]. Burning velocities of laminar premixed flames have been measured for C_2H_4 [68], C_2H_6 [68, 70], C_3H_6 [71], and C_3H_8 [68, 70]. Ignition delay times of homogeneous premixed reactive mixtures in shock tubes have been measured for C_2H_4 [72, 73] and C_3H_8 [64, 74]. These experimental data have been used to test the accuracies of predictions of various chemical-kinetic mechanisms. The principal elementary reactions that describe fuel breakdown and oxidation in nonpremixed systems need not necessarily be the same as those in premixed systems. In nonpremixed systems the reactants are not mixed at a molecular level prior to combustion. As a consequence mixing, and diffusion of reactants and intermediate species control the combustion process. In premixed systems the reactants are mixed on a molecular level prior to combustion. Rates of chemical reaction control the combustion process rather than mixing. the reaction kinetics are characterized by relative amounts of each reactant given by fuel-lean, stoichiometric, of fuel-rich conditions. A chemical-kinetic mechanism describing the oxidation of any fuel must be capable of describing combustion processes in premixed and nonpremixed systems. Here are experimental data presented for extinction and autoignition under premixed and nonpremixed conditions in the counterflow configuration. It particular these date highlights the influence of nonuniform flow-field on autoignition in premixed systems that were not available from previous studies that used shock tubes [64, 72, 73, 74]. The experimental data obtained here are compared with numerical calculations using the San Diego mechanism [75].

4.2 Description of Experiential and Numerical Studies

4.2.1 Experimental Apparatus and Procedures

The experimental apparatus is described in Chapter 3.1. The flow rates of gases are measured by computer-regulated mass flow controllers. The calibrated accuracy of these mass flow controllers is $\pm 1\%$. The velocities of the reactants at the exit of the ducts are presumed to be equal to the ratio of their volumetric flow rates to the cross-section areas of the ducts. The duct from which the oxidizer stream is injected in the non-premixed system and from which the inert-gas stream is injected in the premixed system is equipped with a heating device that allows the streams to be preheated up to 1350 K. The temperature of the heated stream at the exit of the duct is measured using a Pt-Pt 13% Rh thermocouple with wire diameter of 0.07 mm and a junction diameter of 0.21 mm. The measured temperatures are corrected for radiative heat losses assuming spherical shape of the junction, a constant Nusselt number of 2.0, and a constant emissivity of 0.2 [76]. The accuracy of the corrected temperature is expected to be better than ± 25 K. The experiments are carried out at a pressure p = 1.013 bar. The experimental procedures are described in the following sections.

4.2.2 Non-Premixed Flames

Extinction experiments, under nonpremixed conditions, are carried out allowing only small changes in the flame position in the reactive flow field [59]. Is is convenient to express the flame position in terms of a conserved scalar quantity ξ = 1.0 in the fuel stream and ξ = 0 in the oxidizer stream [77]. The location of the flame sheet, ξ_{st}, where the flux of the fuel and the flux of the oxygen are in stoichiometric proportion, is given by $\xi_{st} = [1 + \nu_{O_2} Y_{F,1} W_{O_2}/(Y_{O_2,2} W_F)]^{-1}$, where W_F and W_{O_2} represent the molecular weights of fuel and oxygen, respectively, and ν_{O_2} is the stoichiometric oxygen/fuel mole ratio. Extinction experiments are performed keeping ξ_{st} constant at 0.1. The temperature of the fuel stream, T_1, and the temperature of the oxidizer stream T_2 are 298 K. The distance between the exits of the ducts is L = 10 mm. Extinction experiments are conducted by establishing a flame at strain rate a_2 smaller then the strain rate at extinction, $a_{2,E}$, and increasing the strain rate until extinction is observed. Autoignition experiments are conducted with the mole fraction of fuel, $X_{F,1}$, maintained at 0.15. The temperature of the fuel stream, T_1, is 298 K. The oxidizer stream is air with a mass fraction of oxygen $Y_{O_2,2}$ = 0.233. The distance between the fuel and oxidizer duct is L = 12 mm. At a given strain rate, a_2, and oxidizer temperature $T_2 < T_{2,I}$ the flow field is established, where $T_{2,I}$ is the value of T_2 at autoignition. The temper-

ature of the oxidizer stream is gradually increased until autoignition takes place. The experimental data can be accurately compared to numerical calculations if autoignition takes place close to the axis of symmetry, where the concentration profile of species and the temperature profiles are nearly one-dimensional and are functions of the axial coordinate. A high-speed CCD video camera is used to observe the onset of ignition at a frame rate of 500 s^{-1}. Only those experimental data where autoignition is observed to take place close to the axis of symmetry are recorded.

4.2.3 Premixed Flames

The premixed reactant mixture, made up of fuel, air and nitrogen, is characterized by the equivalence ratio, $\phi_1 = \nu_{O_2} Y_{F,1} W_{O_2} / (Y_{O_2} W_F)$. The quantity, $Y_{O_2,ox} = Y_{O_2,1}/(Y_{O_2,1} + Y_{N_2,1})$, is a measure of dilution of air with nitrogen. In a reactive mixture of fuel and air the value of $Y_{O_2,ox}$ is 0.233. A premixed flame can be stabilized in the mixing layer between the counter-flowing streams of reactive mixture and nitrogen for values of strain rate less then $a_{2,E}$, where $a_{2,E}$ is the strain rate at extinction. In addition the velocity of the premixed reactant stream at the exit of the duct, V_1, must be greater than the laminar burning velocity, to prevent flash back. In the extinction experiments the distance between the ducts is L = 12 mm, the temperature of the premixed reactant stream, T_1, and the temperature of the inert-gas stream, T_2, are 298 K. Two sets of experiments are conducted. In one set, $\phi_1 = 1.0$ and $a_{2,E}$ is measured for various values of $Y_{O_2,ox}$. In the other set, $Y_{O_2,ox}$ is held constant and $a_{2,E}$ is measured as a function of ϕ_1.

In the autoignition experiments the temperature of the inert-gas stream at which autoignition takes place, $T_{2,I}$, is recorded. The separation distance is $L = 15$ mm and the temperature of the reactant stream is 298 K. Values of $T_{2,I}$ are obtained as a function of the strain rate for $\phi_1 = 1.0$ and mole fraction of fuel, $X_{F,1} = 0.054$, as a function of $Y_{O_2,ox}$ for $a_2 = 300$ s^{-1} and $\phi_1 = 1.0$, and as a function of ϕ_1 for $a_2 = 300$ s^{-1} and $Y_{O_2,ox} = 0.195$.

4.2.4 Numerical Procedure

A chemical-kinetic mechanism, called the San Diego Mechanism, developed at the University of California at San Diego is used [75]. This mechanism is made up of 184 reversible reactions among 38 species. This mechanism was previously employed to predict various aspects of premixed and nonpremixed combustion of ethyne (C_2H_2), ethene and ethane [66, 78, 79]. Chemical species containing three carbon atoms such as propene are included, but considered as intermediate products. Therefore, this mechanism can be used to predict extinction and autoignition of ethene and ethane flames.

4.3 Results and Discussion

4.3.1 Nonpremixed Flames

Figure 4.1 and 4.2 show critical conditions of extinction and autoignition. In these figures the symbols represent measurements and the lines are results of numerical calculations. In Figures 4.1 and 4.2 experimental data are shown for C_2H_4, C_2H_6, C_3H_6, and C_3H_8 and results of numerical calculations for C_2H_4 and C_2H_6.

Figure 4.1 shows the oxygen mass fraction, $Y_{O_2,ox}$, in the oxidizer stream as a
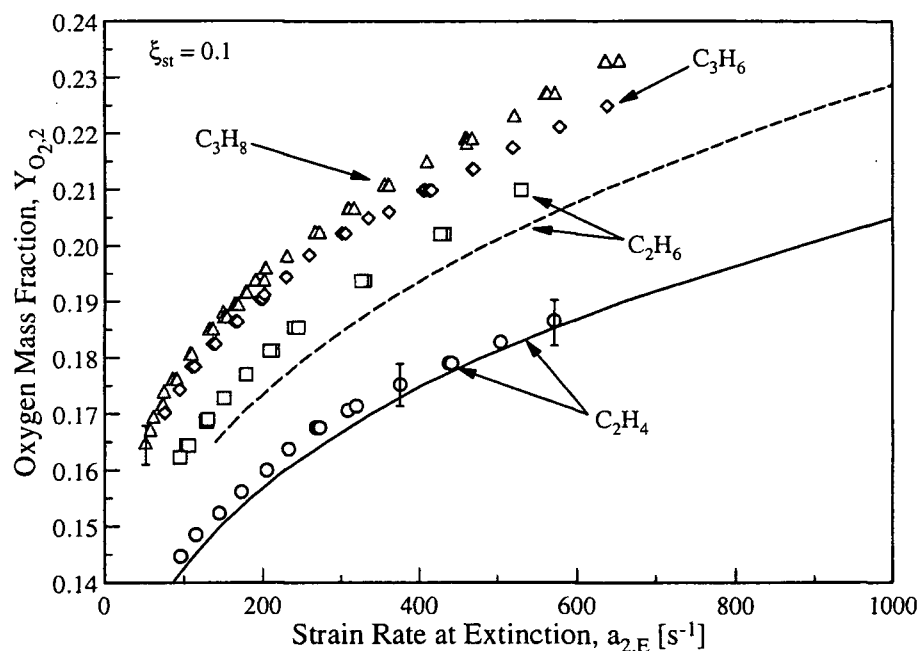
Figure 4.1: The oxygen mass fraction, $Y_{O_2,2}$, in the oxidizer stream as a function of the strain rate at extinction, $a_{2,E}$, for non-premixed flames. The symbols represent measurements, the lines are results from numerical calculations. The stoichiometric mixture fraction, ξ_{st}, is maintained at a constant value of 0.1.

function of the strain rate at extinction, $a_{2,E}$. The stoichiometric mixture fraction, ξ_{st}, for all fuels is maintained at a constant value of 0.1. For given values of $Y_{O_2,2}$, the region $a_2 < a_2, E$ represents flammable mixtures. The numerically calculated values of critical conditions of extinction of C_2H_4 and C_2H_6 agree well with the experimental data. For any value of the strain rate Fig. 4.1 shows that the amount of oxygen, necessary to maintain flammable conditions, increases for the tested fuels in the order of C_2H_4, C_2H_6, C_3H_6, and C_3H_8. This order is also

maintained if the fuel mass fraction of mole fraction is plotted as a function of $a_{2,E}$. Therefore this order is a measure of decreasing reactivity of the tested fuels.

Figure 4.2 shows the temperature of the oxidizer stream at autoignition as a
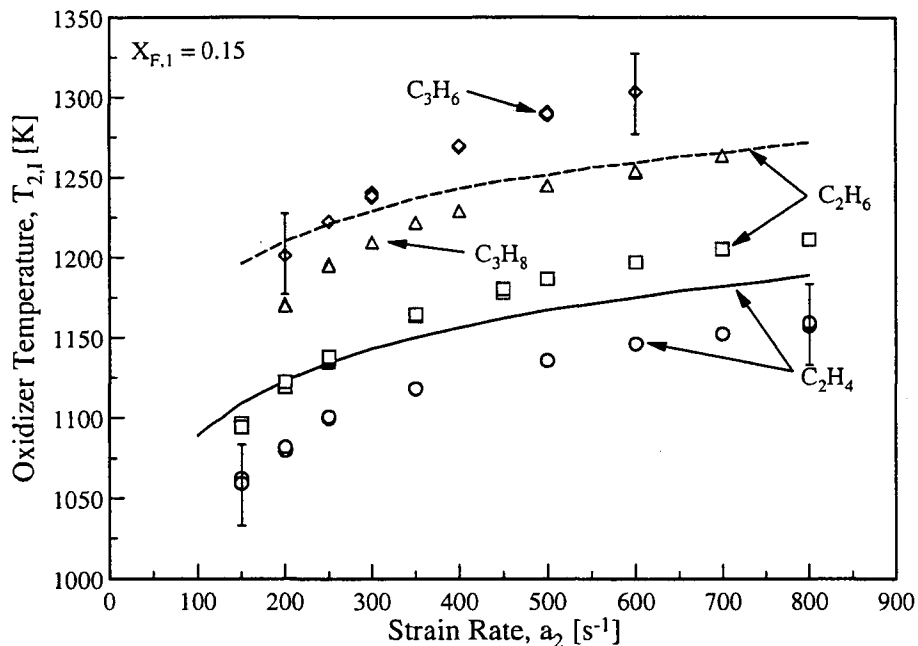
Figure 4.2: The oxidizer temperature at autoignition as a function of the strain rate for non-premixed systems. The symbols represent measurements, and the lines are results from numerical calculations. The mole fraction of fuel, $X_{F,1}$, and the temperature, T_1, of the fuel stream are 0.15 and 298 K, respectively. The oxidizer is air.

function of the strain rate, a_2. For all fuels the mole fraction of the fuel, $X_{F,1}$, and the temperature, T_1, of the fuel stream are 0.15 and 298 K, respectively. The oxidizer is air. For a given value of the strain rate, autoignition will take place in the nonpremixed system if the temperature of the oxidizer stream is greater than $T_{2,I}$. For all fuels, $T_{2,I}$ increases with increasing strain rate. Figure 4.2 shows that for a given value of strain rate the numerically predicted values of $T_{2,I}$ for ethene are not more than 50 K above the measured values, and for ethane numerical results are not more than 100 K above experimental data. The value of $T_{2,I}$ for C_2H_4 is the lowest followed by C_2H_6, C_3H_8, and C_3H_6. This order represents decreasing reactivity of the fuels. It is noteworthy that autoignition experiments show that propane is easier to ignite than propene, while extinction experiments show that propane is easier to extinguish than propene.

4.3.2 Premixed Flames

Figure 4.3 and 4.4 show critical conditions of extinction of the counterflow pre-mixed flames. Figures 4.5, 4.6, and 4.7 show critical conditions of autoignition. In these figures the symbols represent measurements for all the fuels tested and the lines are results of numerical calculations for C_2H_4, C_2H_6. For all cases the temperature of the premixed reactant stream is, T_1, is 298 K.

Figure 4.3 shows the values of $Y_{O_2,ox}$ as a function of the strain rate at extinc-
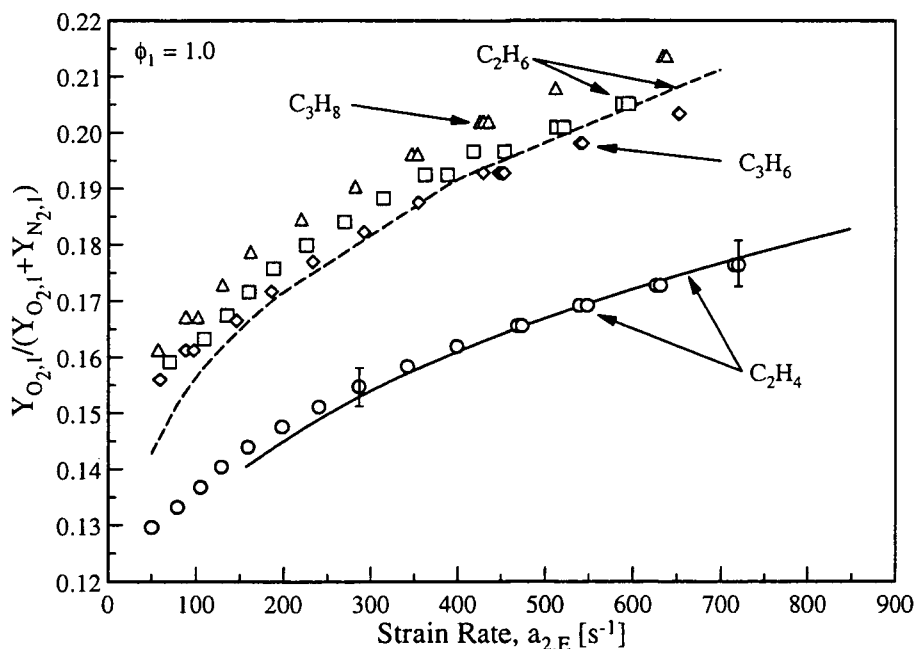
Figure 4.3: Values of $Y_{O_2,ox}=Y_{O_2,1}/(Y_{O_2,1}+Y_{N_2,1})$ in the premixed reactant stream as a function of the strain rate at extinction, $a_{2,E}$. The symbols represent measurements. The lines are results of numerical calculations for C_2H_4 and C_2H_6. For all fuels the equivalence ration of the premixed reactant stream is $\phi_1=1.0$. The temperature of the premixed reactant stream, T_1, and of the inert-gas stream, T_2, is 298 K.

tion, $a_{2,E}$. For all fuels, the equivalence ratio of the premixed reactant stream is $\phi_1 = 1.0$. For a given value of $Y_{O_2,ox}$ of premixed reactant mixture is flammable for values of strain rate less than $a_{2,E}$. Figure 4.3 shows that the critical conditions of the extinction obtained from numerical calculations for C_2H_4, C_2H_6 agree well with the experiments. Ethane is found to be less reactive than ethene, and propane is found to be less reactive than propene. The reactivity of ethane and

propane are nearly the same.

Figure 4.4 shows $a_{2,E}$ as a function of the equivalence ration, ϕ_1. For C_2H_4,
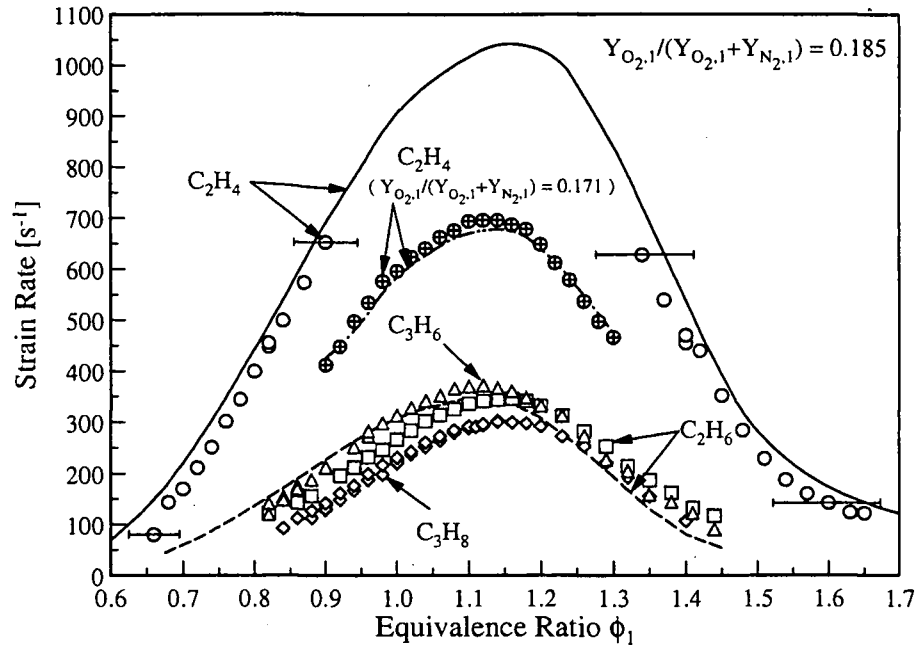
Figure 4.4: The strain rate at extinction, $a_{2,E}$, as a function of the equivalence ratio, ϕ_1, of the premixed reactant stream. The symbols represent measurements, the lines show results of numerical calculations for C_2H_4 and C_2H_6. For C_2H_4, C_2H_6, C_3H_6, and C_3H_8 results are shown for $Y_{O_2,ox} = Y_{O_2,1}/(Y_{O_2,1} + Y_{N_2,1}) = 0.185$. For C_2H_4 additional results are shown for $Y_{O_2,ox} = 0.171$. The temperature of the premixed reactant mixture, T_1, and of the inert-gas stream, T_2, is 298 K.

C_2H_6, C_3H_6, and C_3H_8 results are shown for $Y_{O_2,ox} = Y_{O_2,1}/(Y_{O_2,1} + Y_{N_2,1}) = 0.185$. For C_2H_4 additional results are shown for $Y_{O_2,ox} = 0.171$. Critical conditions of extinction obtained from numerical calculations agree well with experiments. For all fuels with increasing ϕ_1, the values of $a_{2,E}$ first increase up to a value slightly above stoichiometric and then decreases. The peak value of $a_{2,E}$ is found to be in the region $1.1 < \phi_1 < 1.15$. It is noteworthy that changes in the values of $a_{2,E}$ with equivalence ratio is similar to previous observations of changes in burning velocities of laminar flames with equivalence ratio [68]. For laminar premixed flames the highest burning velocity for ethane was found to be 0.43 m/s ($\phi = 1.1$), for propane to be 0.45 m/s ($\phi = 1.1$), and for ethene to be 0.72 m/s ($\phi = 1.2$) [68].

Figure 4.5 shows the temperature of the inert-gas stream at autoignition, $T_{2,I}$,
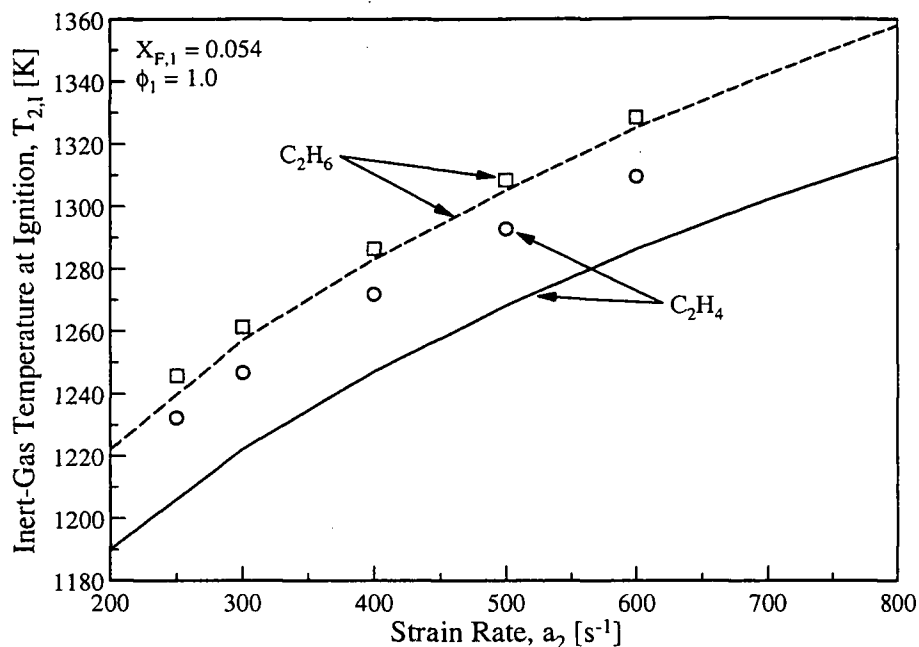
Figure 4.5: The temperature of the inert-gas stream at autoignition, $T_{2,I}$ as a function of the strain rate. The symbols represent measurements, the lines show results of numerical calculation of C_2H_4 and C_2H_6. The mole fraction of fuel, $X_{F,1}$, and the equivalence ratio, ϕ_1 of the premixed reactant mixture are 0.054 and 1.0, respectively. The temperature of the premixed reactant stream, T_1, is 298 K.

as a function of the strain rate. The mole fraction of fuel, $X_{F,1}$, and the equivalence ratio, ϕ_1, of the premixed reactant mixture are 0.054 and 1.0, respectively. Numerical calculations of critical conditions of autoignition agree well with the measurements. Experimental data and numerical calculations show the value of $T_{2,I}$ to increase with increasing strain rate. At a given value of strain rate, the value of $T_{2,I}$ for C_2H_6 is greater than for C_2H_4.

Figure 4.6 shows $T_{2,I}$ as a function of $Y_{O_2,ox} = Y_{O_2,1}/(Y_{O_2,1} + Y_{N_2,1})$. Here $\phi_1 = 1.0$, and $a_2 = 300s^{-1}$. The results of numerical calculations agree with experiments. Figures 4.5 and 4.6 show that ethene is easier to ignite compared to ethane. Experimental data for propene and propane are not shown because the values of $T_{2,I}$ are very high and cannot be accurately obtained i the present setup. For example at $\phi_1 = 1.0$, $Y_{O_2,ox} = 0.235$, and $a_2 = 400 \ s^{-1}$, autoignition for propane was found at $T_{2,I} = 1366K$. This temperature is close to the limit of heating the gas stream for the present experimental setup.
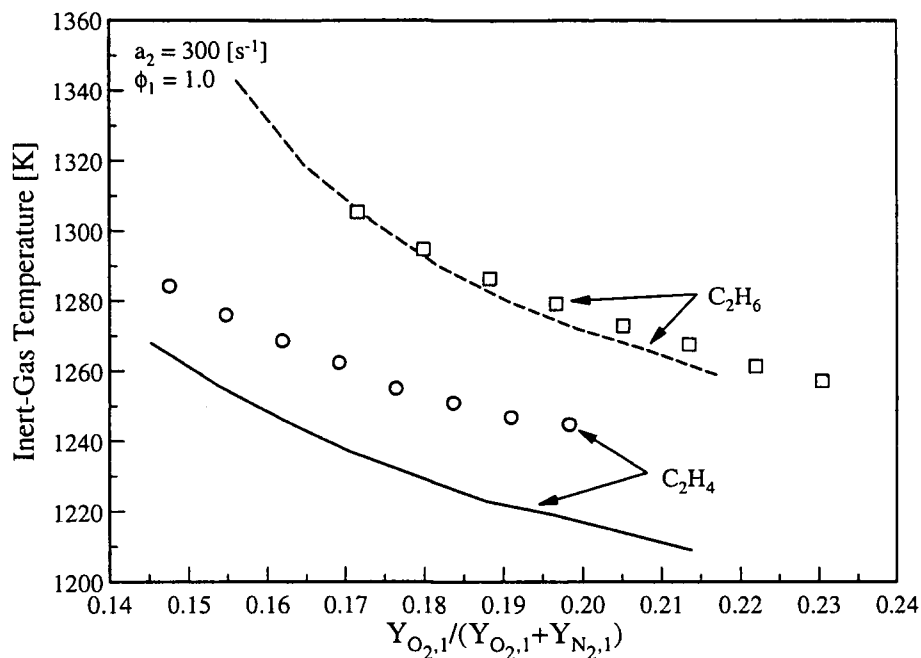
Figure 4.6: The temperature of the inert-gas stream at autoignition, $T_{2,I}$, as a function of $Y_{O_2,ox} = Y_{O_2,1}/(Y_{O_2,1} + Y_{N_2,1})$. The symbols represent measurements, the lines show results of numerical calculation of C_2H_4 and C_2H_6. The equivalence ratio, ϕ_1, of the premixed reactant mixture is 1.0. The strain rate, a_2, is 300 s^{-1}. The temperature of the premixed reactant stream, T_1, is 298 K.

Figure 4.7 shows $T_{2,I}$ as a function of the equivalence ratio, ϕ_1. . Results are shown for $Y_{O_2,ox} = Y_{O_2,1}/(Y_{O_2,1}+Y_{N_2,1}) = 0.195$ and for strain rate $a_2 = 300$ s^{-1}. The numerical calculation agrees well with the experiments. The experimental data and numerical calculations show that with increasing ϕ_1, the values of $T_{2,I}$ decreases and then increases. The experimental data show that for C_2H_4, the values of $T_{2,I}$ is the lowest around $\phi_1 = 0.85$, and for C_2H_6, the value of $T_{2,I}$ is the lowest at $\phi_1 = 1.0$. To check if the lowest value of $T_{2,I}$ for ethene depends on the strain rate, pressure, and $Y_{O_2,ox}$, the experimental data for $T_{2,I}$ were obtained as a function of ϕ_1 for $Y_{O_2,ox} = 0.195$ and $a_2 = 600$ s^{-1}. Numerical calculations were performed for $0.7 < p < 1.5$ bar, $100 < a_2 < 900$ s-1, and $0.195 < Y_{O_2,ox} < 0.233$. The experimental data and numerical calculations showed that for ethene the value of $T_{2,I}$ was the lowest in all cases around $\phi_1 = 0.85$. In the numerical calculations if the diffusivity of the ethene is presumed to be the same as that of ethane, then the value of $T_{2,I}$ was the lowest around $\phi_1 = 0.95$. If the diffusivity of ethane is presumed to be same as that of ethene, then the value of $T_{2,I}$ was the lowest around $\phi_1 = 0.9$. Thus, the lowest value of $T_{2,I}$ appears to be related to prefer-
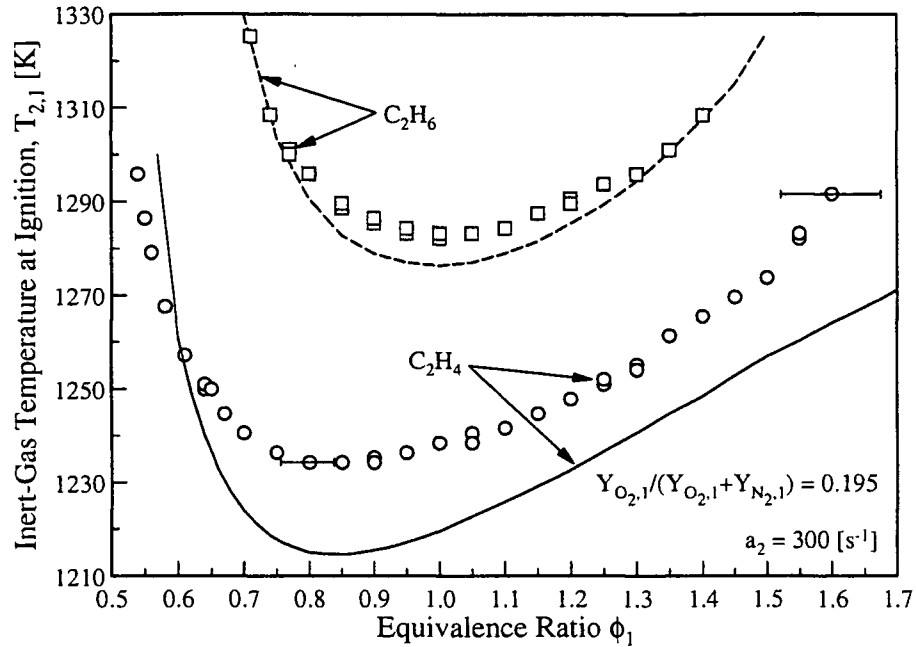
Figure 4.7: The temperature of the inert-gas stream at autoignition, $T_{2,I}$, as a function of the equivalence ratio, ϕ_1, of the premixed reactant stream. The symbols represent measurements, the lines show results of numerical calculation of C_2H_4 and C_2H_6. The results are shown for $Y_{O_2,ox} = Y_{O_2,1}/(Y_{O_2,1} + Y_{N_2,1}) = 0.195$ and for a strain rate $a_2 = 300^{-1}$.

ential diffusion. In the experiments with ethene, autoignition did not take place for values of $\phi_1 < 0.56$. Here, a faint emission of light is observed at the location of the reaction-zone, and its intensity is found to increase with increasing inert-gas temperature. This phenomena is further investigated numerically using the maximum value of the mass fraction of OH, $Y_{OH,max}$, as a measure for the overall reactivity of the premixed system.

The overall reactivity of the system depends on the strain rate, a_2, the temperature of the inert-gas stream, T_2, the equivalence ratio of the reactive mixture, ϕ_1, and the level of oxygen in the reactive mixture, $Y_{O_2,ox}$. For purposes of illustration the value of $Y_{O_2,ox}$ is held constant at 0.195 and changes in $Y_{OH,max}$ with ϕ_1, T_2, and a_2 are considered. Figure 4.8 shows numerically calculated values of $Y_{OH,max}$ as a function of T_2 for various values of ϕ_1. Here $a_2 = 300 \text{ s}^{-1}$. For $\phi_1 > 0.57$ the plots of $Y_{OH,max}$ versus T_2 at fixed ϕ_1 show two turning points where the derivative of T_2 with respect to $Y_{OH,max}$ vanishes. The turning point marked with E represents critical conditions of extinction and the turning point marked with I represents critical condition of autoignition. For fixed ϕ_1 the chemical system between E
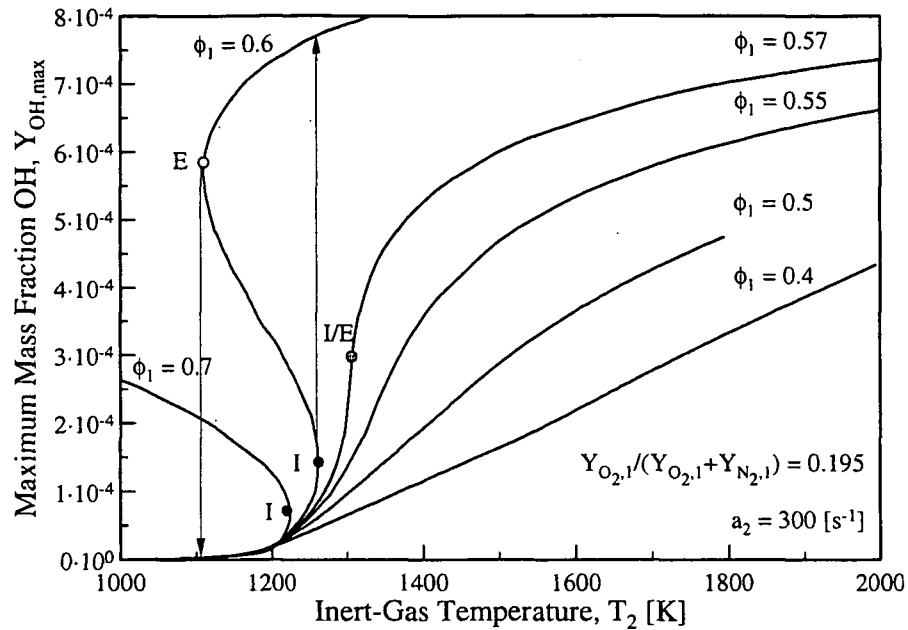
Figure 4.8: Numerically calculated peak values of the mass fraction of OH, $Y_{OH,max}$, as a function of the temperature of the inert-gas stream, T_2, for various values of ϕ_1. Results are shown for $Y_{O_2,ox} = Y_{O_2,1}/(Y_{O_2,1} + Y_{N_2,1}) = 0.195$ and for strain rate $a_2 = 300^{-1}$.

and I is physically unstable. For $\phi_1 = 0.57$, the turning points merges, and for $\phi_1 < 0.57$ the plots of $Y_{OH,max}$, versus T_2 at fixed ϕ_1 do not show any turning points anymore. Therefore the premixed system does not exhibit abrupt ignition or extinction for $\phi_1 < 0.57$. To evaluate the influence of strain rate on the critical value of ϕ_1 below which abrupt ignition or extinction do not take place, results similar to those shown in Fig. 4.8 were obtained for various values of strain rate. These calculations were performed for $Y_{O_2,ox} = 0.195$. For values of a_2 of 600 s^{-1}, 900 $^{-1}$, and 1200 $^{-1}$, the critical values of ϕ_1 were found to be 0.63, 0.67, and 0.7, respectively. The lean flammability limit of mixtures of ethene and air is reported to be $\phi_1 = 0.457$ [80]. Thus increasing strain rate increases the limiting value of ϕ_1.

Figure 4.9 shows $Y_{OH,max}$ as a function of the strain rate, a_2, for various values of ϕ_1. Here the temperature of the inert-gas stream, T_2, is held at constant value of 1350 K. For $\phi_1 > 0.63$ two turning points are observed and none for $\phi_1 < 0.63$. At $\phi_1 = 0.63$, the turning points merge. Thus at $T_2 = 1350$ K, the reactive system does not exhibit abrupt ignition or extinction for $\phi_1 < 0.63$. The third case where ϕ_1 is held constant was considered previously by Smooke et al. [81] in their exper-
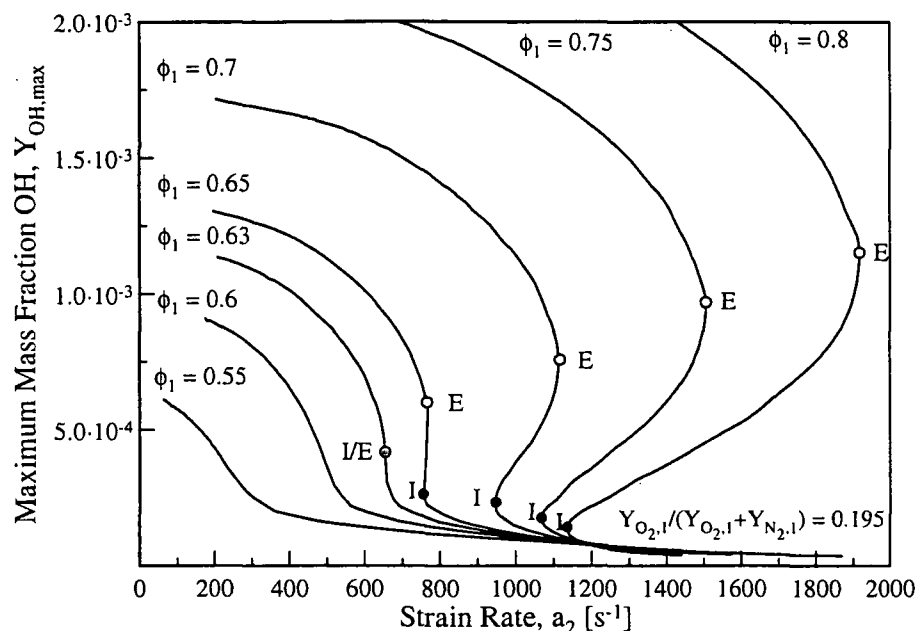
Figure 4.9: Numerically calculated peak values of the mass fraction of OH, $Y_{OH,max}$, as a function of the strain rate, a_2, for various values of ϕ_1. Results are shown for $Y_{O_2,ox} = Y_{O_2,1}/(Y_{O_2,1}+Y_{N_2,1}) = 0.195$ and for the temperature of the inert-gas stream, $T_2 = 1350$ K.

imental and numerical study of premixed methane flames. This study was limited to extinction. In this previous study the overall reactivity of the premixed system was characterized by the maximum temperature, T_{max}, in the reaction zone [81]. Numerically calculated values of T_{max} were plotted as a function of the strain rate for various values of the temperature of the inert-gas stream. It was found that for given values of ϕ_1, methane flames do not abruptly extinguish if the temperature of the inert-gas stream was above some critical value [81]. This observation was confirmed by comparing results of numerical calculations with experimental data.

4.3.3 Summary and Conclusion

Critical conditions of extinction and autoignition are measured for nonpremixed and premixed systems stabilized in the counterflow configuration. Numerical calculations are performed using the San Diego Mechanism [75] and results are compared with measurements. The present study gives influences of nonuniform flow-field on the critical conditions of extinction and autoignition of the reactive systems

considered here. It is of interest to compare the present study on premixed systems with previous studies carried out using shock tubes [64, 72, 73, 74] and on premixed flames stabilized in the so-called "back-to-back" configuration [69]. In the "back-to-back" configuration, two premixed streams are stabilized between two identical reactant streams. Studies on shock tubes give useful information concerning the chemical-kinetic mechanisms of autoignition. Studies on two premixed flames stabilized in the "back-to-back" configuration have significantly advanced the understanding of structure and dynamics of laminar premixed flames in nonuniform flow-field [69]. Studies on shock tubes and flames stabilized in the "back-to-back" configuration do not, however, give the influences of nonuniform flow-field on autoignition. A key observation of the present study is that for premixed systems abrupt extinction and autoignition does not take place if the value of the equivalence ratio is less than some critical value. This critical value of ϕ is found to depend on the strain rate.

Chapter 5

Liquid Pool Experiments

Turbulent nonpremixed flames are of interest in practical applications. They appear in jet engines[1], Diesel engines, steam boilers, furnaces, and hydrogen-oxygen rocket motors. Except or the turbulent premixed combustion in many spark-ignited engines (Otto-cycle), most combustion is turbulent nonpremixed. Nonpremixed flames are safer to handle than premixed flames, because fuel and oxidizer are mixed in the combustor itself. [82] In the combustion process of diesel engines and aviation turbines (jet engines) fuel gets sprayed into the combustion chamber. Figure 6.13 shows schematic the injection and ignition process in a diesel engine. It is also shown the ignition delay time in a diesel engine. To achieve a good mixture of reactants, the process is turbulent. In this case, nonpremixed flames burn in a turbulent flow field. For low turbulence intensity the so-called flamelet concept can be used. Figure 5.2 shows on the left side (1) a typical spray pattern of a dual orifice pressurized fuel injector used in Auxiliary Power Units (APU) in aviation, on the right side (2) a spray pattern of a six orifice fuel injector (by BOSCH) used in big diesel engines. Zoomed in on the liquid fuel spray single droplets are visible (see figure 5.2, (3)). Zoomed in further on the surface, it is somehow similar to an oxidizer flow over a liquid, evaporating surface - counterflow liquid pool.

5.1 Liquid Pool

The setup is similar to the one shown in section 3.1 on page 24 with the differences described here. Instead of the fuel duct a cup - the liquid pool - with a liquid fuel delivery system was installed. Figure 5.3 shows the setup for the liquid pool experiments including its fuel supply. Equation 3.1, which defines the strain rate,

---

[1]reverse flow combustion chamber (eg. APUs), straight flow combustion chamber are premixed

simplifies to

$$a_2 = \frac{2|V_2|}{L} \tag{5.1}$$

since $V_1=0$, with L the distance between the oxidizer duct and the liquid surface, and V_2 the flow velocity at the exit of the oxidizer duct.

5.1.1 Setup

An gaseous oxidizer stream flows over the surface of a liquid pool - an axis-symmetric stagnation point flow gets formed. In Figure 5.4 a schematic illustration of the counterflow configuration in the liquid pool setup is shown. Here, the oxidizer is injected from the upper duct, called the oxidizer duct, and it flows against the surface of a liquid pool from which fuel is evaporating. At the exit of the oxidizer duct several layer of screen are installed. The screen material is inconel 600 with a mesh of 200.

The liquid fuel flows into a small brass cup - the liquid pool. The cup has an diameter of 36mm and a depth of 11mm. Figure 5.4 shows on the right hand side the pool itself. The fuel flows against a small plate through 3 openings on the side to minimize the influence of movement in the pool. The surface level of the liquid pool is very important. To adjust the level the reservoir can be raised or lowered on a stage. The liquid surface is flush with its sidewalls. To ensure the
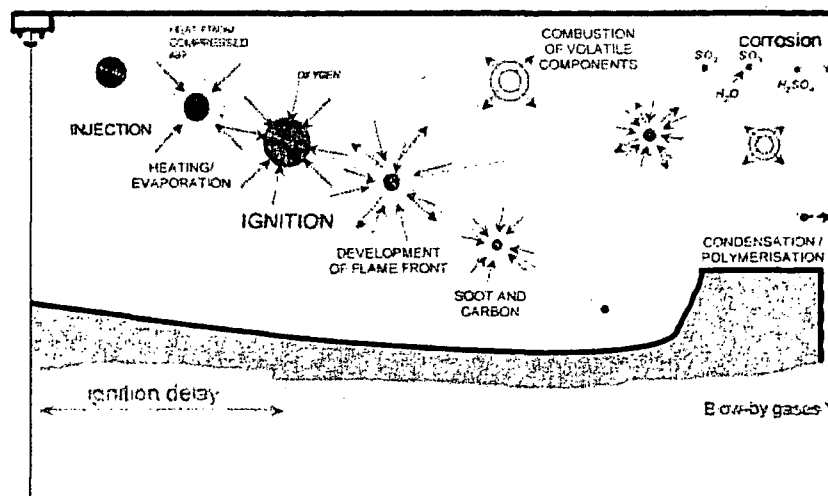
Figure 5.1: Schematic Illustration of Diesel Ignition and Ignition Delay time in a diesel engine. A section view of the combustion chamber is shown. Diesel fuel droplets are sprayed from the top against the piston.

Typical spray of dual orifice pressure atomized fuel injector (APU).

Typical spray of a diesel fuel injection (Bosch).

Zoomed in on the spray, single droplets get visible.

(3)

(4)
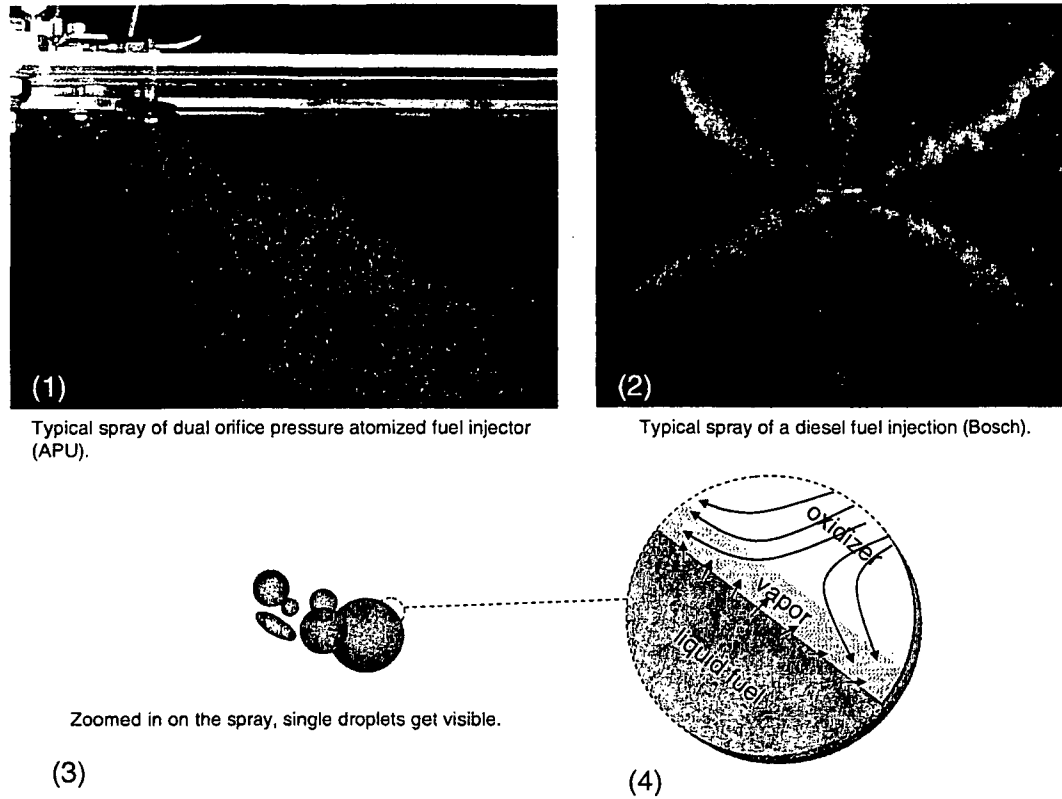
Figure 5.2: (1) shows a typical spray pattern of a dual orifice pressurized fuel injector used in Auxiliary Power Units (APU), (2) shows a diesel fuel injection of a six orifice fuel injector (by BOSCH), (3) and (4) are zoomed in on the spray droplet, that shows the similarity to a liquid pool.

liquid level, a needle is mounted to the bottom of the pool with its needle tip at exactly the hight of the pool rim. The liquid pool is cooled from the bottom with an adjustable water flow to avoid boiling of the fuel. A thermocouple is installed about 3mm below the liquid surface. By adjusting the water cooling flow, the temperature of the liquid is kept constant. The curtain duct is axis symmetrical around the liquid pool, similar to the design described in Chapter 3.1.

Fuel supply

It was found out that the level of the liquid surface has an influence on the results. This simple device described here (see Fig.5.3) is based on pressure equalization and keeps the level of the fuel constant. The fuel is stored in a glass reservoir and flows from there into the liquid pool. A tube inside the reservoir is aligned with the surface of the liquid pool. The reservoir can be vertically adjusted. Pressure
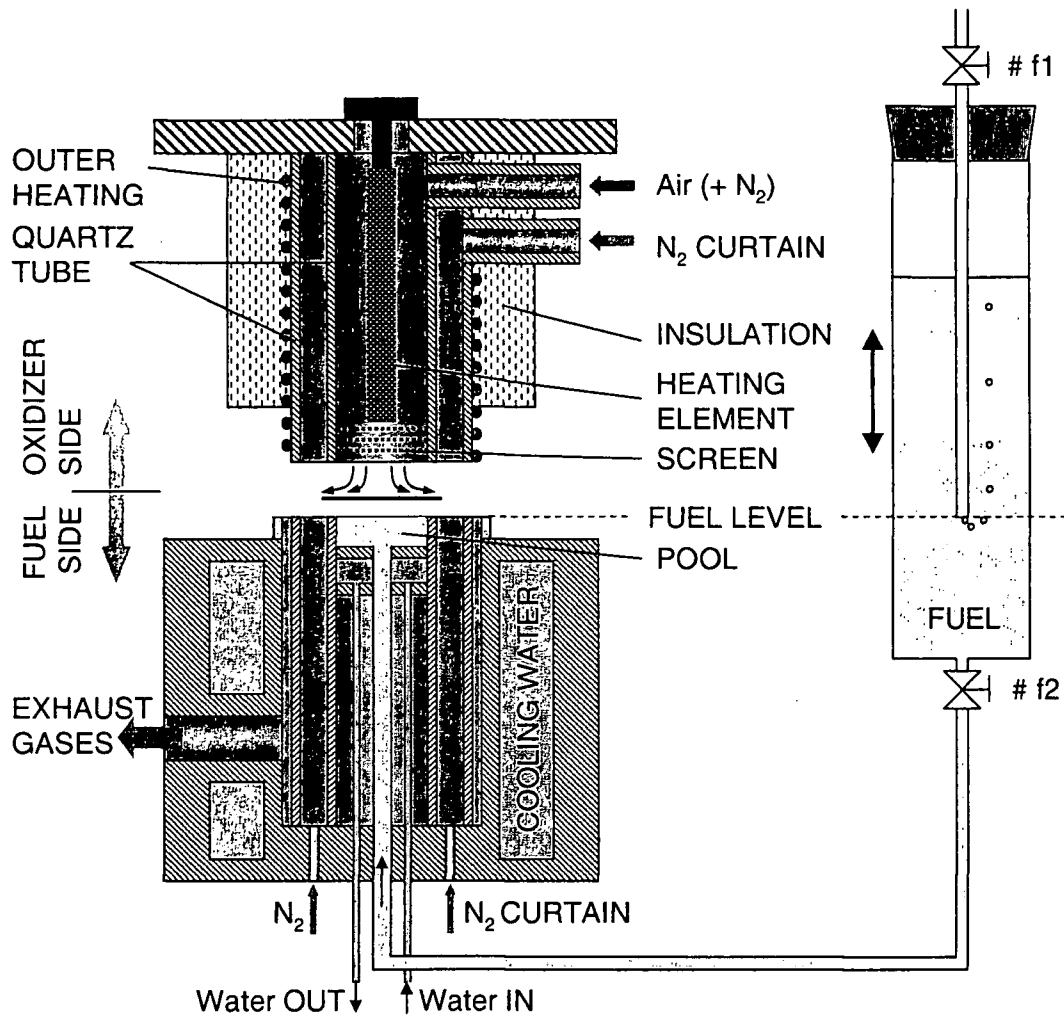
Figure 5.3: 2D illustration of the liquid pool with its fuel feeding system.

in the closed reservoir has to be equal to the pressure at the liquid pool surface - the level of the liquid surface in the pool is leveled with the exit of the tube inside the fuel reservoir. Since fuel is consumed by the flame or vaporization, the fuel level in the pool sinks and the pressure in the reservoir drops, the pressure is equalized through the tube. During running experiments the tube exit has to be actually slightly above the liquid surface since the oxidizer flow presses against the liquid surface and to overcome flow resistance of the fuel in the tube connecting the reservoir and the pool. A more detailed description is given by [51, 83].

(a) schematic illustration   (b) section view of liquid pool
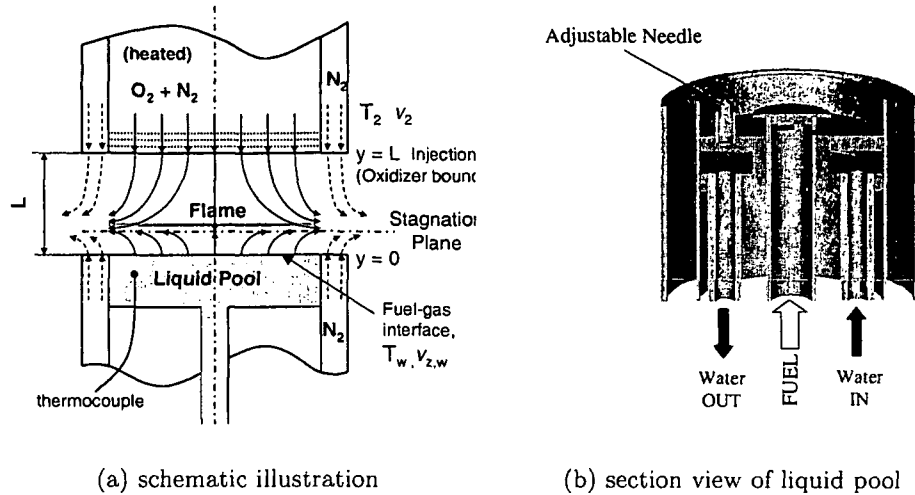
Figure 5.4: Schematic illustration of the counterflow configuration in the liquid pool setup. V_2 and $v_{z,w}$ are the velocities at the oxidizer-injection and the gas side of the liquid-gas interface planes, respectively. T_2 and T_w are the temperatures at the oxidizer-injection and liquid-gas interface planes, respectively. On the right side the water cooling of the pool can be seen to prevent boiling of the fuel.

5.1.2 Formulation

The distance between the surface of the liquid pool and the exit of the oxidizer duct is L. The oxidizer is a mixture of oxygen and nitrogen. At the exit of the oxidizer duct, the magnitude of the injected velocity is V_2, the temperature is T_2, the density is ρ_2, and the mass fraction of oxygen is $Y_{O_2,2}$. Here subscript 2 represents conditions at the exit of the oxidizer duct. On the gas side of the liquid gas interface the velocity is $v_{z,w}$, and the temperature is T_w. Here the subscript w represents conditions on the gas side of the liquide gas interface.

The chemical reaction between fuel and oxygen is represented by the one-step process

$$\nu_F \text{Fuel} + \nu_{O_2} \text{Oxygen} = \text{Products}.$$
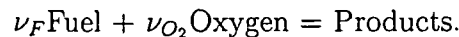
Here ν_F and ν_{O_2} are stoichiometric coefficients. The stoichiometric mass ratio of oxygen to fuel is $\nu = \nu_{O_2} W_{O2} / (\nu_F W_f)$, where W_F and W_{O_2} are molecular weights of fuel and oxygen, respectively. The reaction rate, ω, is given by

$$\omega = \rho^2 \left(\frac{Y_F Y_{O_2}}{W_F W_{O_2}} \right) B \exp\left(-\frac{T_a}{T}\right). \tag{5.2}$$

Here Y_F and Y_{O_2} are mass fractions of fuel and oxygen, respectively, ρ is the density, T the temperature, B the frequency factor, and T_a the activation temperature.

The average molecular weight of the mixture $\widehat{W}$, the heat capacity of the mixture c_p, and the product $\rho\mu$ are presumed to be constants. Here μ is the coefficient of viscosity. The Lewis number of fuel $L_F = \lambda/(\rho c_p D_F)$, and of oxygen $L_{O_2} = \lambda/(\rho c_p D_{O_2})$, the Prandtl number $Pr = \mu c_p/\lambda$ are presumed to be constant. In these equations λ is the thermal conductivity of the mixture and D_F and D_{O_2} are the coefficient of diffusion of gaseous fuel and oxygen respectively. Since $Pr, L_w, and c_p$ are constant, it follows by the ideal gas law that

$$\frac{T}{T_2} = \frac{\rho_2}{\rho} = \frac{\mu}{\mu_2} = \frac{\rho_2 D_F}{\rho_2 D_{F_2}} = \frac{\rho_2 D_{O_2}}{\rho_2 D_{O_2,2}} = \phi(z) \tag{5.3}$$

The origin is placed on the axis of symmetry at the surface of the liquid pool. The coordinates are nondimensionalized by division by L. The nondimensional radial coordinate is r and the nondimensional axial coordinate z. Velocities are nondimensionalized by division by the magnitude of the injection velocity at the duct exit, V_2, and the pressure by division by $\rho_2 V_2^2$. Other nondimensional quantities introduced in the analysis are normalized mass fraction of fuel, $y_F = Y_F/Y_{F,c}$, and normalized mass fraction of oxygen, $y_{O_2} = Y_{O_2}/(\nu Y_{F,c})$ where $Y_{F,c}$ is the mass fraction of fuel in the liquid pool. The nondimensional quantity $\theta = c_p(T_2 - T)/q_L$, where where q_L is the heat required to vaporize per unit mass of the liquid. The nondimensional quantity $q = q_L/(Y_{F,c}q_F)$, where q_F is the heat release per unit mass of gaseous fuel consumed. A Damköhler number, D is defined as

$$D = \frac{\nu_{O_2} Y_{F,c} B \rho_2 L}{V_2 W_F}. \tag{5.4}$$

There exists solutions for which the nondimensional radial velocity is $rU(z)$ where $U(z)$ is a function of the axial coordinate. All other quantities, except the nondimensional pressure, p, are functions only of the axial coordinate.

The equations describing the reactive flow field are [47, 84]

- Conservation of Mass

$$2U + \phi \frac{d}{dz}\left(\frac{v}{\phi}\right) = 0, \tag{5.5}$$

where v is the nondimensional axial component of the flow velocity.

- Equation of Motion—in the radial direction, which gives the pressure distribution

$$\frac{U^2}{\phi} + \frac{v}{\phi}\frac{dU}{dz} = -\frac{1}{r}\frac{\partial p}{\partial r} + \frac{1}{Re_2}\frac{d}{dz}\left(\phi\frac{dU}{dz}\right). \tag{5.6}$$

Here the Reynolds number $Re_2 = \rho V_2 L / \mu_2$. In view of Eqn. (5.6) the quantity $(1/r)(\partial p / \partial r)$ is a function of the axial coordinate. Thus, the pressure, p, is

$$p = P(z) - r^2 Q(z). \tag{5.7}$$

- Balance equation for the fuel is

$$\frac{v}{\phi} \frac{dy_F}{dz} = \frac{1}{Re_2 \, Pr \, L_F} \frac{d}{dz} \left(\phi \frac{dy_F}{dz} \right) - \frac{D}{\phi^2} y_F y_{O_2} \exp\left(-\frac{T_a}{T} \right) \tag{5.8}$$

- Balance Equation for oxygen is

$$\frac{v}{\phi} \frac{dy_{O_2}}{dz} = \frac{1}{Re_2 \, Pr \, L_{O_2}} \frac{d}{dz} \left(\phi \frac{dy_{O_2}}{dz} \right) - \frac{D}{\phi^2} y_F y_{O_2} \exp\left(-\frac{T_a}{T} \right) \tag{5.9}$$

- Energy equation for small Eckert number

$$\frac{v}{\phi} \frac{d\theta}{dz} = \frac{1}{Re_2 \, Pr} \frac{d}{dz} \left(\phi \frac{d\theta}{dz} \right) - \frac{D}{\phi^2} q^{-1} y_F y_{O_2} \exp\left(-\frac{T_a}{T} \right). \tag{5.10}$$

Equations (5.5), (5.6), (5.8), (5.9), and (5.10) are required to satisfy boundary conditions at the exit of the oxidizer duct at $z = 1$, and on the gas side of the liquid-gas interface at $z = 0$. At $z = 1$ the boundary conditions are

$$\begin{aligned} &U = 0; \quad v = -1; \quad ; \phi = 1; \quad y_F = 0; \\ &y_{O_2} = \alpha = Y_{O_2,2} / (\nu Y_{F,c}); \quad \theta = 0. \end{aligned} \tag{5.11}$$

At $z = 0$, the radial component of flow velocity is zero (no slip). Thus

$$U = 0. \tag{5.12}$$

Mass and energy balance at the liquid gas interface gives at $z = 0$

$$\begin{aligned} &\frac{v_w}{\phi_w}(1 - y_{F,w}) + \frac{1}{Re_2 \, Pr \, L_F} \phi_w \left(\frac{dy_F}{dz} \right)_w = 0, \\ &\frac{v_w}{\phi_w} y_{O_2,w} - \frac{1}{Re_2 \, Pr \, L_{O_2}} \phi_w \left(\frac{dy_{O_2}}{dz} \right)_w = 0, \\ &\frac{v_w}{\phi_w} + \frac{1}{Re_2 \, Pr} \phi_w \left(\frac{d\theta}{dz} \right)_w = 0. \end{aligned} \tag{5.13}$$

The first equation in Eqn. 5.13 describes the mass flux of fuel, the second equation the mass flux of oxygen into the liquid pool, which is zero, and the third equation the heat flux from the gas phase which balances the heat of vaporization. Here subscript w represents conditions on the gas side of the liquid gas interface. On

the gas side of this interface, the nondimensional burning rate v_w/ϕ_w, the mass fraction of fuel, $y_{F,w}$, and the mass fraction of oxygen, y_{O_2}, are not known and they can be obtained from integration of the governing equations. At the surface of the liquid pool the temperature T_w can be obtained from equations describing vapor-liquid equilibrium. For simplicity, T_w is presumed to be equal to the normal boiling point. The level of blowing at the surface of the liquid pool is characterized by the Reynolds number $Re_w = \rho_w V_w L/\mu_w$, where V_w is the magnitude of the blowing velocity on the gas side of the liquid gas interface.

The analysis is carried out for large values of Re_2. The quantities Pr, L_F, and L_{O_2} are presumed to be of the order of unity. The value of Re_w is presumed to be small. For large Re_w and small Re_w, a thin viscous boundary layer will develop close to the surface of the liquid pool at $z = 0$. Chemical reactions take place in this viscous boundary layer. The flow outside this viscous boundary layer is unreactive, inviscid and rotational.

Inviscid Flow

In the unreactive inviscid region to the leading order $y_F = 0$, $y_{O_2} = \alpha$, $\theta = 0$, and $\phi = 1$. The velocities are given by

$$U = 1 - z, \quad v = z^2 - 2z. \tag{5.14}$$

The components of the flow velocity given by Eqn. (5.14) satisfy Eqn. (5.5) and the boundary conditions at $z = 1$, given by Eqn. (5.11). Equation (5.5) does not satisfy the no-slip boundary condition given by Eqn. (5.12). The pressure gradient obtained from Eqn. (5.12) and (5.14) is $\partial p/\partial r = -r$. In view of Eqn. (5.7), $Q = 0.5$. The strain rate is defined as the axial gradient of the axial component of the flow velocity. The value of the strain rate in the inviscid flow, obtained from Eqn. (5.14), is 2z - 2. At $z = 0$, the magnitude of the strain rate, represented by a is

$$a = 2V_2/L. \tag{5.15}$$

Viscous Boundary Layer

To analyze the structure of the reactive and viscous boundary layer the expansions

$$\eta = \int_0^z \frac{\sqrt{2\,Re_2\,Pr}}{\phi}dz, \quad \frac{v}{\phi} = -\sqrt{\frac{2}{Re_2\,Pr}}f(\eta), \tag{5.16}$$

are introduced. Here η, and $f(\eta)$ are presumed to be of the order of unity. Introducing the expansions given by Eqn.(5.16) into Eqn.(5.5) gives $U = df/d\eta$.

Introducing Eqn. (5.16) into (5.6), (5.8), (5.9), and (5.10) gives

$$
\begin{aligned}
2Pr\frac{d^3f}{d\eta^3} + 2f\frac{d^2f}{d\eta^2} - \left(\frac{df}{d\eta}\right)^2 + \phi &= 0, \\
\frac{1}{L_F}\frac{d^2y_F}{d\eta^2} + f\frac{dy_F}{d\eta} &= \frac{D}{2\phi}y_F y_{O_2}\exp\left(-\frac{T_a}{T}\right), \\
\frac{1}{L_{O_2}}\frac{d^2y_{O_2}}{d\eta^2} + f\frac{dy_{O_2}}{d\eta} &= \frac{D}{2\phi}y_F y_{O_2}\exp\left(-\frac{T_a}{T}\right), \\
\frac{d^2\theta}{d\eta^2} + f\frac{d\theta}{d\eta} &= \frac{D}{2\phi q}y_F y_{O_2}\exp\left(-\frac{T_a}{T}\right).
\end{aligned}
\tag{5.17}
$$

The boundary layer approximation $(1/r)\partial p/\partial r = -1$ is employed. The quantity $\phi = 1 - \gamma\theta$, where $\gamma = q_L/(c_p T_2)$.

Introducing the expansions given by Eqn.5.16 into Eqn. 5.12 and 5.13 gives at $\eta = 0$ the boundary conditions

$$
\begin{aligned}
\left(\frac{df}{d\eta}\right)_w &= 0, \\
f_w y_{F,w} + \frac{1}{L_F}\left(\frac{dy_F}{d\eta}\right)_w &= f_w, \\
f_w y_{O_2} + \frac{1}{L_{O_2}}\left(\frac{dy_{O_2}}{d\eta}\right)_w &= 0, \\
f_w - \left(\frac{d\theta}{d\eta}\right)_w &= 0.
\end{aligned}
\tag{5.18}
$$

The temperature at the surface of the liquid pool is presumed to be equal to the normal boiling point. Thus, the value of θ at $\eta = 0$ is known. Matching the solutions in the viscous layer with those in the inviscid rotational flow at $z = 0$, gives at $\eta\to\infty$ the boundary conditions

$$
\eta\to\infty: \quad df/d\eta = 1, \quad y_F = 0, \quad y_{O_2} = \alpha, \quad \theta = 0.
\tag{5.19}
$$

At $\eta\to\infty$, $d^2f/d\eta^2 = d^3f/d\eta^3 = 0$.

5.2   Asymptotic Theory of Autoignition

Critical conditions of autoignition are obtained from a regular perturbation analysis starting from the structure of the non-reactive viscous layer (frozen flow solution).

Structure of the Non-reactive Viscous Layer

In the non-reactive viscous layer the profiles of velocity, mass fraction of fuel and oxygen, and temperature can be obtained by integrating Eqn. 5.17 after neglecting the chemical source term. The mass fraction of fuel, mass fraction of oxygen and temperature in the non-reactive viscous layer are presented by $y_{F,f}$, $y_{O_2,f}$ and θ_f respectively. These quantities are given by

$$\frac{1}{L_F}\frac{d^2y_{F,f}}{d\eta^2} + f\frac{dy_{F,f}}{d\eta} = \frac{1}{L_{O_2}}\frac{d^2y_{O_2,f}}{d\eta^2} + f\frac{dy_{O_2,f}}{d\eta}$$
$$= q\frac{d^2\theta_f}{d\eta^2} + qf\frac{d\theta_f}{d\eta} = 0. \qquad (5.20)$$

The asymptotic analysis requires values of $y_{F,f}$, $y_{O_2,f}$, and θ_f close to the oxidizer-boundary, when η is large. The leading order value of f in the limit $\eta \to \infty$ is

$$f \approx (\eta - B_2) \qquad (5.21)$$

where B_2 is an arbitrary constant of the order of unity. Introducing the asymptotic value of f given in Eqn. 5.21 into Eqn. 5.20, neglecting the constant B_2 and integrating, the result

$$y_{F,f} = \frac{F_2}{\sqrt{2\pi}\sqrt{L_F}\eta}exp\left[-\frac{L_F\eta^2}{2}\right],$$
$$y_{O_2,f} = \frac{Y_{O_2,2}}{\nu Y_{F,c}} = \alpha, \qquad (5.22)$$
$$\theta_f = \frac{C_2}{\sqrt{2\pi}\eta}exp\left[-\frac{\eta^2}{2}\right]$$

are obtained to the leading order. C_2 and F_2 are constants of the order of unity. The asymptotic values of $y_{F,f}$, $y_{O_2,f}$, and θ_f in Eqn. 5.22 satisfy the boundary conditions given by Eqn. 5.19. The values of C_2 and F_2 are required in the asymptotic analysis. C_2 depends on Pr and γ, and F_2 on Pr, γ, and L_F. The values of C_2 and F_2 are obtained from numerical integration of Eqn. 5.20.

The structure of the non-reactive flow-field are calculated for $Pr = 0.7$, $L_F = 2$. Results obtained using properties for n-heptane are shown in Figure 5.5 and Figure 5.6. As it can be seen in these two Figures, f, f', f'', θ, and y_f satisfy the boundary conditions specified in Eqn. 5.19. The position of the stagnation plane can be seen in Figure 5.5 and is about 1.7 mm from the liquid surface. The velocity f is 0 on this position. At $\eta = 0$ in Figure 5.6 the amount of fuel Y_F evaporation from the surface of the liquid pool and the temperature T_w at the surface of the pool can be seen.
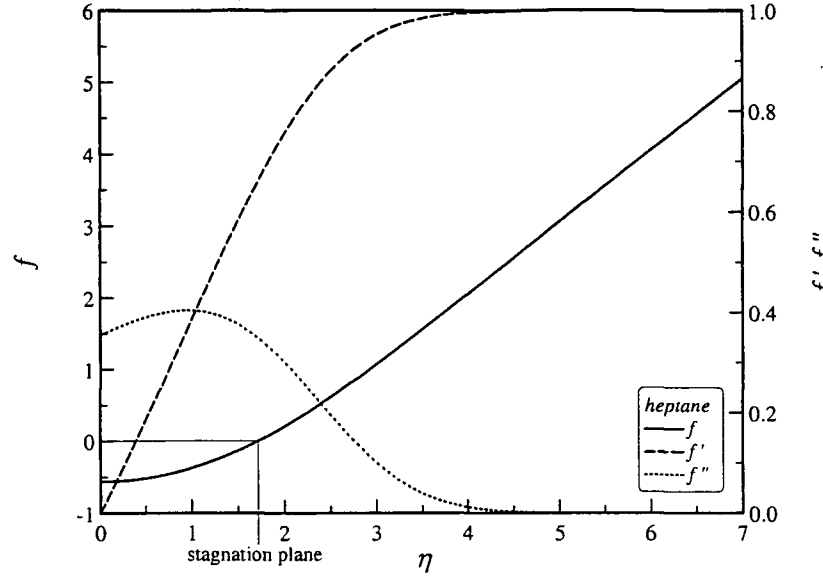
Figure 5.5: Profiles of f (normal compound of velocity), $f' = df/d\eta$ (radial compound of velocity), and $f'' = d^2f/d\eta^2$ in the non-reactive viscous layer as a function of η. The liquid gas interface is at $\eta = 0$. Results obtained using properties for n-heptane.

Analysis of the Reactive Viscous Layer

The analysis given here follows that of Liñàn and Williams [85]. In the "ignition regime" [86], the increase in temperature above that in the non-reactive viscous layer is of the order of β^{-1}. To obtain the critical conditions of autoignition the expansions

$$\theta = \theta_f - \beta^{-1}\varphi + \cdots$$
$$y_F = y_{F,f} - q\beta^{-1}\alpha_F + \cdots \qquad (5.23)$$
$$y_{O_2} = y_{O_2,f} - q\beta^{-1}\alpha_{O_2} + \cdots$$

are introduced where φ, α_F, and α_{O_2} are presumed to be of the order of unity. The quantity β is the Zel'dovich number. It is defined as

$$\beta = \frac{q_L T_a}{c_p T_2^2}. \qquad (5.24)$$

The Zel'dovich number is presumed to be large. Using the definition of θ and the expansion in Eqn. 5.23 the temperature distribution $T = T_2 - (q_L/c_p)\theta_f + \beta^{-1}(q_L/c_p)\varphi$ is obtained. Introducing this expansion for T, and those given in Eqn.
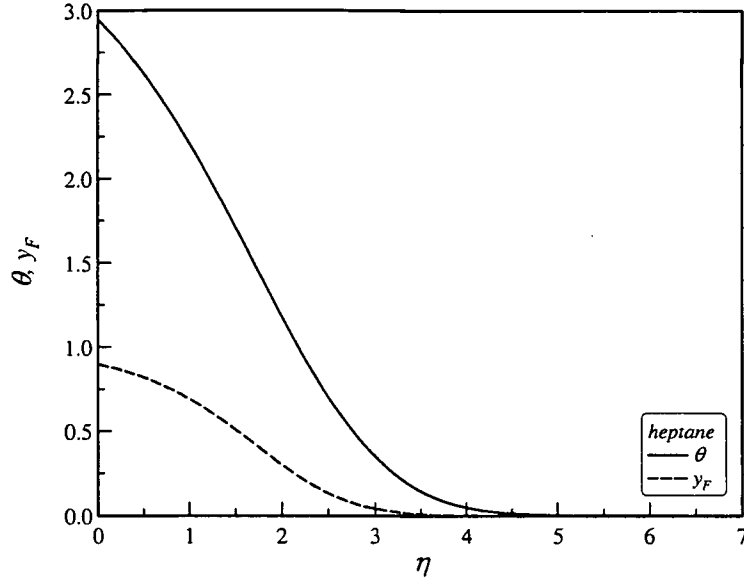
Figure 5.6: Profiles of θ_f and $y_{F,f}$ in the non-reactive viscous layer as a function of η. The liquid gas interface is at $\eta = 0$. Results obtained using properties for n-heptane.

5.23 into Eqn. 5.17, the equations

$$
\begin{aligned}
-\frac{1}{L_F}\frac{d^2\alpha_F}{d\eta^2} - f\frac{d\alpha_F}{d\eta} &= -\frac{1}{L_{O_2}}\frac{d^2\alpha_{O_2}}{d\eta^2} - f\frac{d\alpha_{O_2}}{d\eta} \\
&= -\frac{d^2\varphi}{d\eta^2} - f\frac{d\varphi}{d\eta} \\
&= \frac{D\beta}{2\phi q}exp(-\frac{T_a}{T_2})(y_{F,f}\ y_{O_2,f})exp(\varphi - \beta\theta_f),
\end{aligned}
\tag{5.25}
$$

are obtained. For large β, chemical reaction will be negligibly small except where $\beta\theta_f$ is of the order of unity. Autoignition would take place close to the edge of the boundary layer where the value of θ_f is small. Following the analysis in Reference [85], chemical reaction is presumed to take place in a region around η_r, where $\beta\theta_f = 1$. Using Eqn. 5.22, η_r is given by

$$
\frac{\beta C_2}{\sqrt{2\pi}\eta_r}exp(-frac\eta_r^2 2) = 1.
\tag{5.26}
$$

The value of η_r is expected to be large. To analyze the structure of the reaction layer it is convenient to introduce the independent variable ζ, given by the equation

$$
\zeta = \eta - \eta_r.
\tag{5.27}
$$

Using Eqns. 5.22 and 5.26, a quantity $\xi = \beta\theta_f$ is defined by following equation

$$\xi = \beta\theta_f = exp(-\zeta\eta_r),\tag{5.28}$$

where the approximation $\eta \approx \eta_r^2 + 2\zeta\eta_r$ is employed. Using Eqns. 5.22, 5.26, 5.27, and 5.28, $y_{F,f}$ is given by [85]

$$y_{F,f} = F_2(C_2\beta)^{L_F}(\eta_r\sqrt{2\pi})^{L_F-1}L_F^{-0.5}\xi^{L_F}.\tag{5.29}$$

Introducing the asymptotic value $f = \eta$ for large η, and Eqns. 5.15, 5.22, 5.27, 5.28, and 5.29 into Eqn. 5.25, using the approximation $\phi = 1$ for large η, the differential equation

$$\frac{d^2\varphi}{d\zeta^2} + \eta_r\frac{d\varphi}{d\zeta} + D_m\xi^{L_F}exp(\varphi - \xi) = 0\tag{5.30}$$

is obtained [85]. Here the Damköhler number, D_m is given by

$$D_m = \frac{F_2\nu_F Y_{O_2,2}\rho_2 B}{C_2^{L_F}qW_{O_2}a_2 L_F^{0.5}}\left(\frac{\eta_r\sqrt{2\pi}}{\beta}\right)^{L_F-1}exp\left(-\frac{T_a}{T_2}\right).\tag{5.31}$$

Boundary conditions to Eqn. 5.30 are $\varphi \to \varphi_m$ for $\zeta \to -\infty$, and $\varphi \to \infty$, where φ_m is an eigenvalue to be determined by matching with the solution in the reaction layer [85]. Using Eqn. 5.28, Eqn. 5.30 can be written as [85]

$$\frac{d^2\varphi}{d\xi^2} + \Delta\xi^{L_F-2}exp(\varphi - \xi) = 0,\tag{5.32}$$

where the modified Damköhler number Δ is given by

$$\Delta = D_m\eta_r^{-2}.\tag{5.33}$$

Boundary conditions to Eqn. 5.32 are $\varphi \to \varphi_m$ for $\xi \to \infty$, and $\varphi \to 0$ for $\xi \to 0$. Equation 5.32 is identically to Eqn. A22 in Liñán and Williams [85]. The value of Δ at the ignition is denoted by Δ_i is plotted in Figure 5.7 of reference as a function of L_F. For $L_F = 2$, $\Delta_i = 0.5$.

The values of a_2 and T_2 at autoignition are $a_{2,I}$ and $T_{2,I}$ respectively. The results of the asymptotic analysis are used to analyze experimental data on autoignition obtained in the counterflow configuration.

Experiments on Autoignition

The asymptotic analysis developed in the previous section is used to deduce overall chemical kinetic rate parameters from experimental data on autoignition of various fuels. The fuels teste are paraffin fuels n-heptane C_7H_{16}, iso-octane C_8H_{18},
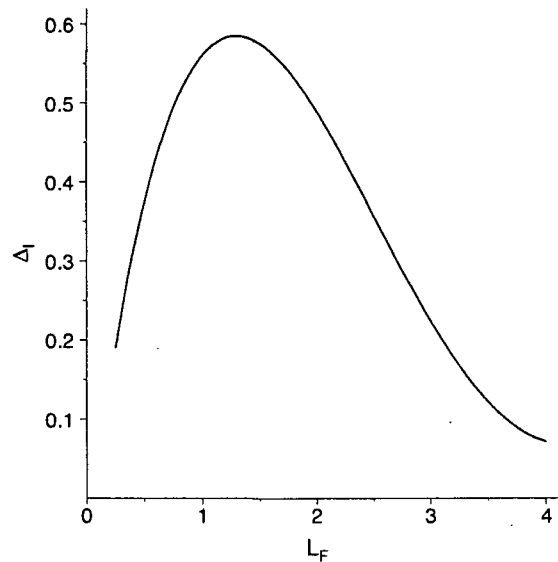
Figure 5.7: Lewis Number of reference [85]

n-octane C_8H_{18}, n-decane $C_{10}H_{22}$, n-dodecane $C_{12}H_{26}$, and n-hexadecane, the cycloparaffin fuels cyclohexane C_6H_{12}, and methylcyclohexane C_7H_{14}, and aromatic fuel is o-xylene C_8H_{10}, and multicomponent fuels diesel, and JP-8.
The autoignition experiments are carried out with a distance between the exit of the oxidizer and fuel duct of L = 12 mm and are performed at ambient pressure of 1.013 bar. In all experiments the oxidizer stream is pure air with mass fraction of oxygen $Y_{O_2,2} = 0.233$. At a given strain rate and oxidizer temperature T_2 ¡ $T_{2,I}$ the flow field is established. At this selected strain rate, the oxidizer temperature is gradually increased until autoignition takes place. The critical values $T_{2,I}$ and $a_{2,I}$ are recorded. Figure 5.9 shows the experimental data of $T_{2,I}$ as a function of $a_{2,I}$. These data represent the critical conditions of autoignition for liquid fuels. Symbols indicate experimental data points, the line are for better distinctiveness between each fuel. At a given value of strain rate, autoignition will take place if the temperature of the oxidizer stream reached a value bigger then $T_{2,I}$. Experimental data show that the value for $T_{2,I}$ increases with increasing $a_{2,I}$. The fuel with the highest value of $T_{2,I}$ is o-xylene followed by iso-octane. The lowest autoignition temperature is necessary for hexadecane. That means that hexadecane is easier to ignite than o-xylene and applies also for te order of fuels in between. Noteworthy is the crossover between n-decane and n-dodecane among the other tested fuels. The gradient of both fuels is less compared to the other tested fuels. That means that n-decane and n-dodecane ignite easier a low strain rate than at high strain rate compared to the other fuel types. Also diesel and n-octane show a faster decrease in reactivity over the strain rate compared to the other investigated fuels.
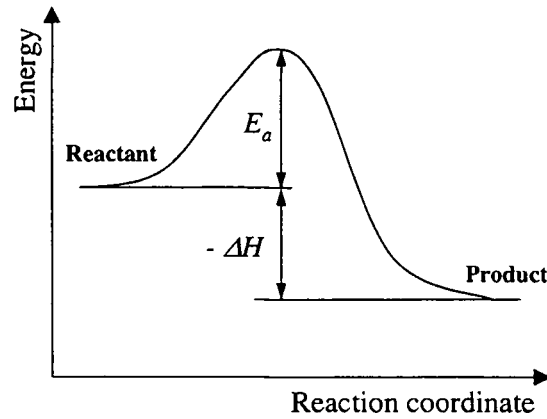
Figure 5.8: Energies in a reaction as a function of the reaction coordinate, where E_a stands for the activation energy, and ΔH for the reaction enthalpy.

This shows the influence of the strain rate.

Overall Chemical-Kinetic Rate Parameters

The chemical reaction between fuel and oxygen is represented the the following one-step, irreversible process

$$C_m H_n + (m + n/4)O_2 \rightarrow mCO_2 + (n/2)H_2O$$
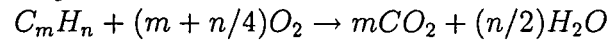
The stoichiometric coefficients $\nu_F = 1$, and $\nu_{O_2} = (m + n/4)$. The reaction rate is presumed to be given by Eqn. 5.2. For diesel the proportion of carbon and hydrogen is presumed to be $C_{14.7}H_{26.8}$, and for JP-8 it is presumed to be $C_{12}H_{23.3}$. For convenience, a quantity of G is defined as

$$G^{-1} = \frac{1}{\Delta_i \eta_r^2} \frac{F_2 \nu_F Y_{O_2,2} Y_{F,c} q_F p \hat{W}}{C_2{}^{L_F} W_{O_2} R^0 q_L a_{2,I} L_F{}^{0.5} T_{2,I}} \left(\frac{\eta_r \sqrt{2\pi}}{\beta} \right)^{L_F - 1} \tag{5.34}$$

The value of β in Eqn. 5.34 is evaluated using Eqn. 5.24 with T_2 replaced by $T_{2,I}$ and η_r is evaluated using Eqn. 5.26. The equation

$$lnG = lnB - \frac{T_a}{T_{2,I}}, \tag{5.35}$$

where T_a is the activation temperature and B is the frequency factor, obtained from Eqns. 5.31, 5.33 ,and 5.34 applies at autoignition. Here $\rho_2 = p\hat{W}/(R^0 T_2)$, where $\hat{W}$ is the average molecular weight and R^0 the universal gas constant. The overall chemical kinetic parameters can be obtained from an "Arrhenius" plot of lnG as a linear function of $1/T_{2,I}$. For this purpose the linear approximation of
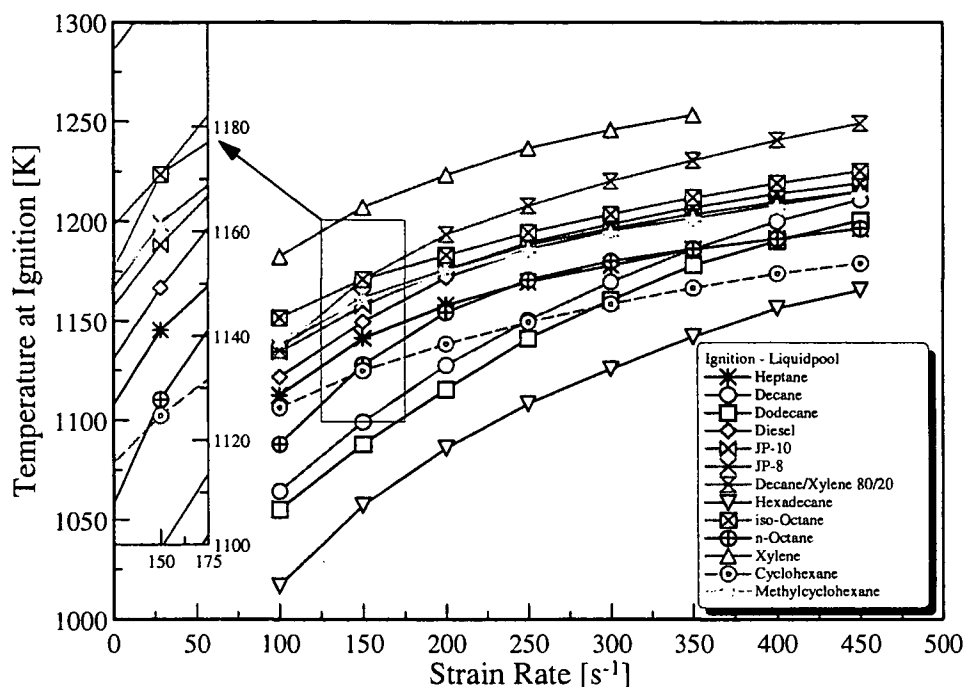
Figure 5.9: Experimental data showing the oxidizer temperature, $T_{2,I}$, as a function of the strain rate, $a_{2,I}$, at autoignition. Symbols represent the experimental data, the lines are for better distinctiveness between different fuels.

the experimental data points were used. The activation energy E is obtained by simply multiplying the activation temperature T_a with universal gas constant R^0. For comparison it is assumed that $L_F = 2$ for all fuels. The values of E and B from the "Arrhenius" plot with $L_F = 2$, which gives a value of $\Delta_I = 0.5$ from Figure 5.7, are given in Table 5.1. Figure D.1 show "Arrhenius" plots of lnG as a function of $1/T_{2,I}$. The whole calculation can be seen in appendix D.1.3.

The values of E and B obtained from the "Arrhenius" plots for calculated lewis number are shown in Tabel 5.2. The gradient of the linear line is a degree of the activation energy. For diesel and JP-8 an average molecular mass of 197 g/mol ($C_{14.17}H_{26.8}$) and 167.65 g/mol ($C_{12}H_{23.3}$) was assumed. Figures 5.10 show "Arrhenius" plots of lnG as a function of $1/T_{2,I}$ with values of L_F from FlameMaster with its reduced Damköhler number,Δ_I. For o-xylene, diesel, and JP-8 no values of L_F were available in FlameMaster. For these fuels $L_F = 2.0$ was assumed.

5.2.1 Results of Extinction Experiments

For extinction experiments a distance between fuel duct and oxidizer duct exit $L = 10mm$ was selected. The temperature of the oxidizer stream at the exit of

Table 5.1: Activation Temperature T_a, Frequency Factor B, and Activation Energy E for one-step, irreversible reaction obtained from interpretation of experimental data using asymptotic analysis with $L_F = 2.0$ and $\Delta_I = 0.5$.

Fuel	T_a [K]	E_a [kJ/mol]	B [m^3/mol s]
hexadecane	1.1909E+04	9.9009E+01	1.2590E+05
n-dodecane	1.2738E+04	1.0591E+02	2.7208E+05
n-decane	1.3052E+04	1.0851E+02	3.8553E+05
n-octane	1.7650E+04	1.4674E+02	3.0730E+07
diesel	2.1829E+04	1.8148E+02	4.5323E+08
n-heptane	2.3967E+04	1.9926E+02	8.9332E+09
o-xylene	2.5936E+04	2.1563E+02	1.7963E+10
cyclohexane	2.6761E+04	2.2249E+02	1.6804E+11
JP-8	2.6831E+04	2.2308E+02	6.2334E+10
methylcyclohexane	2.7127E+04	2.2553E+02	1.1361E+11
iso-octane	2.8796E+04	2.3941E+02	4.0926E+11

the duct was at ambient temperature (298K). At a given mass fraction of oxygen and strain rate the flame was ignited by a torch and stabilized in the mixing layer between the surface of the liquid pool and the oxidizer duct. The velocity of the oxidizer stream gets slowly increased until the flame extinguishes. Figure 5.11 shows the oxygen mass fraction $Y_{O_2,2}$ at extinction as a function of the strain rate, $a_{2,E}$. For a given fuel type and oxygen mass fraction, the flame will extinguish if the strain rate is higher than $a_{2,E}$. That means that for a given value of oxygen mass fraction the region a_2 ¡ $a_{2,E}$ represents an area of flammable conditions. The line represents a boarder between flammable area and an area where no flame can exist. All fuels tested here show the same tendency. The strain rate $a_{2,E}$ increases with increase of the oxygen mass fraction. Also the investigated fuels show a regressive behavior. With increasing strain rate the mass fraction $Y_{O_2,2}$ also increases, but at higher strain rate, the smaller the oxygen mass fraction difference between two adjacent measurement point. The order of the reactivity of different fuels is nearly independent from the strain rate. Fuels with a smaller value of C-atoms are generally more reactive then fuels with long-chained carbons. Not surprisingly is that adding a less reactive fuel to another fuel decreases the overall reactivity of the fuel mixture as it was done here for n-decane mixing with o-xylene. Already with a simple mixture of two fuels it is possible to mimic similar characteristics of extinction as multicomponent fuels. With certain combinations it is possible to achieve a fuel mixture that shows similar characteristics of extinction behavior as multicomponent fuels like diesel and JP-8. That doesn't implement that a found mixture with the desired behaviors for extinction shows the same

Table 5.2: Activation Temperature T_a, Frequency Factor B, and Activation Energy E for one-step, irreversible reaction obtained from interpretation of experimental data using asymptotic analysis with calculated L_F.

Fuel	L_F [-]	Δ_I [-]	T_a [K]	E_a [kJ/mol]	B [m^3/mol s]
n-heptane	2.16675	0.4503	2.39E+04	198.5	9.06E+09
hexadecane	2.9692	0.2342	1.15E+04	96.0	8.76E+04
n-dodecane	2.63309	0.3228	1.25E+04	103.7	2.34E+05
n-decane	2.55652	0.344	1.28E+04	106.5	3.47E+05
n-octane	2.26712	0.4237	1.75E+04	145.6	2.88E+07
JP-10	2.64582	0.3193	2.38E+04	197.9	6.79E+09
o-xylene	2.32614	0.4077	2.57E+04	214.0	1.74E+10
cyclohexane	1.99563	0.4926	2.68E+04	222.5	1.62E+11
methylcyclo-hexane	2.17598	0.4479	2.70E+04	224.7	1.12E+11
iso-octane	2.37783	0.3936	2.86E+04	237.5	4.20E+11

behavior for autoignition.

5.2.2 Possible Surrogate of JP-8 and Diesel

Surprisingly JP-8 and Diesel have very similar autoignition and extinction behaviors in the liquid pool setup. Surrogate fuels that show similar chemical behaviors as diesel and JP-8 can be developed by mixing higher and lower reactive short chained fuels. Previous studies consider n-heptane as a surrogate diesel. It is shown here that n-heptane does not reproduce extinction and autoignition characteristics of diesel and JP-8. A mixture consisting of n-decane and o-xylene is a good approach to create a surrogate fuel for diesel and JP-8. In both experiments (extinction and autoignition) the mixture of n-decane 80% and o-xylene 20% shows slightly to high values compared to the results of diesel and JP-8. Especially at autoignition experiments the mixture shows a bigger reactivity increase at low strain rate compared to the "real" fuels. For extinction experiments the mixture of n-decane 80% and o-xylene 20% shows the same trendline but a little too high values, the mixture of n-decane 70% and o-xylene 30% fits better, but the difference in the data of autoignition would be even bigger.

5.2.3 Calculation

Chemical-kinetic mechanisms were available for n-decane and n-heptane. The used chemical kinetic mechanism for n-decane and n-heptane contained 67 species and
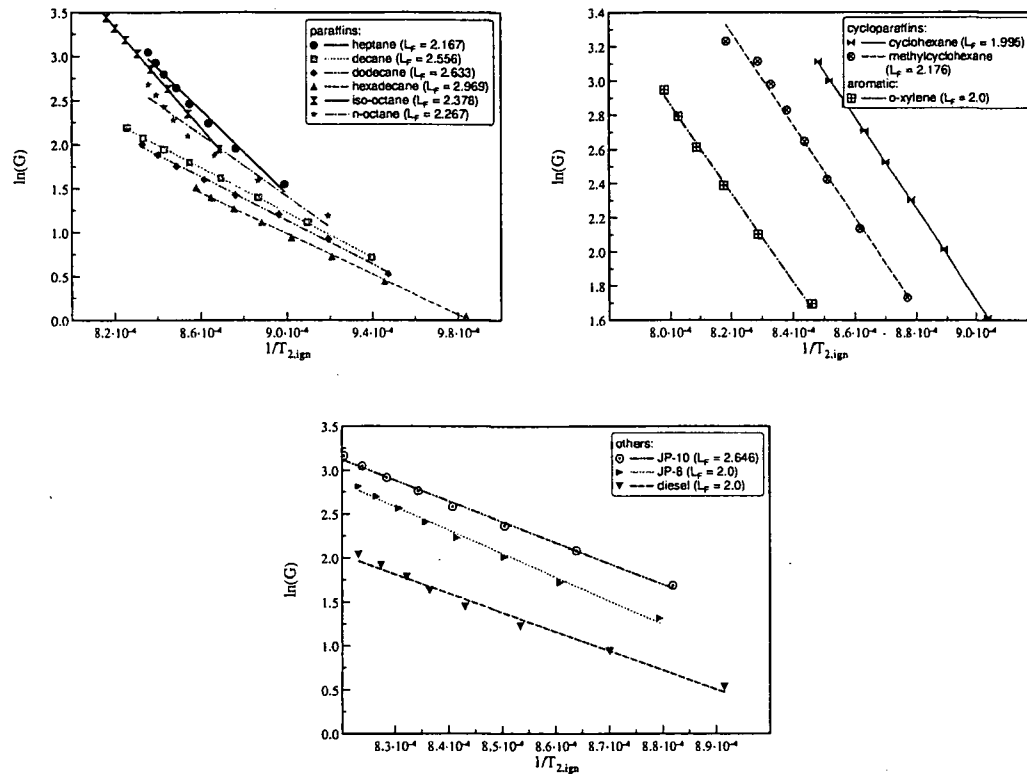
Figure 5.10: "Arrhenius" Plot with L_F obtained from FlameMaster for paraffins, cycloparafins, aromatics, and others. To obtain the kinetic parameters the linear approximation of the experimental data points was used. The symbols represent the data calculated from the experimental points.

180 respectively. Figure 5.12 shows a comparison for extinction between experimental data, represented by symbols and of the calculation, represented by lines. The calculation show the same trend and the order of reactivity as the experimental data, but predicts too high values of strain rate at excitation. In Figure 5.13 are the experimental data of n-decane with its appropriate calculation of autoignition shown. The calculation for n-heptane over-predicted the experimental results so far, that it's not shown. An interesting issue is that the calculation for autoignition over-predicts the experimental results at low strain rate, but show too low values at a high strain rate. That means that the overall gradient of the calculation is less compared to the experimental data. The slope of the calculation levels out stronger at high strain rate compared to the experimental data. The big difference between numerical calculation and experimental data occur because it
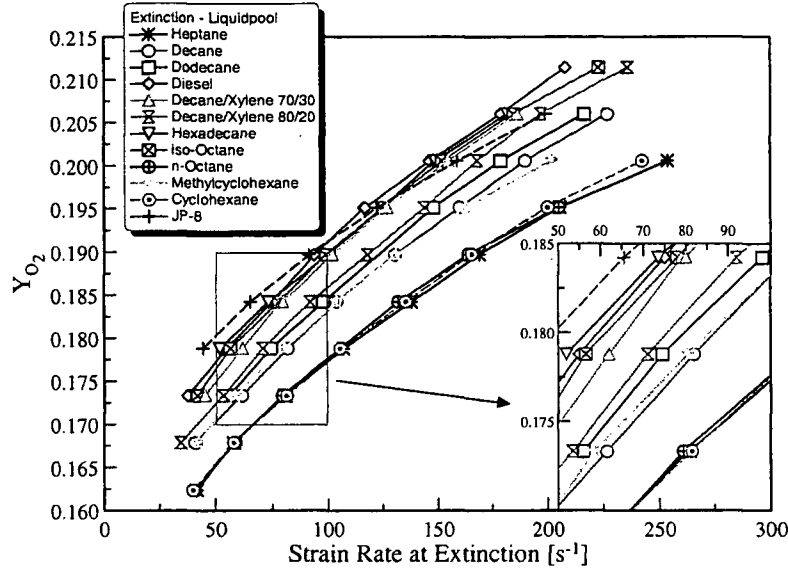
Figure 5.11: Experimental data showing oxygen mass fraction $Y_{O_2,2}$ as a function of the strain rate, $a_{2,E}$ at extinction. Symbols represent the experimental data, the lines are for better distinctiveness between different fuels.

is very difficult to find the correct boundary condition at the liquid surface. On the surface are non-slip boundaries assumed $(v_x(y = 0) = 0)$. In the experimental setup the air-flow above the surface forces the liquid to the side and introduces a flow in the liquid pool to the side. At the surface it is assumed that the liquid is close to boiling temperature. Measuring the temperature with a thermocouple a few mm below the surface is not accurate enough to find the actual temperature at the surface since there is a thermal gradient because the bottom of the liquid pool has to be cooled to avoid boiling. Not knowing the exact temperature makes a difference in how much fuel actually evaporates. Both assumptions change the result of the experiments compared with its calculations. By installing a second thermocouple located either below or above the first thermocouple the thermal gradient can be determined and with that the actual surface temperature and correct boundary condition. A decrease in the thermal gradient would also improve the result. This can be done by increasing the depth of the liquid pool. This improvement is recommended for future experiments using the liquid pool.
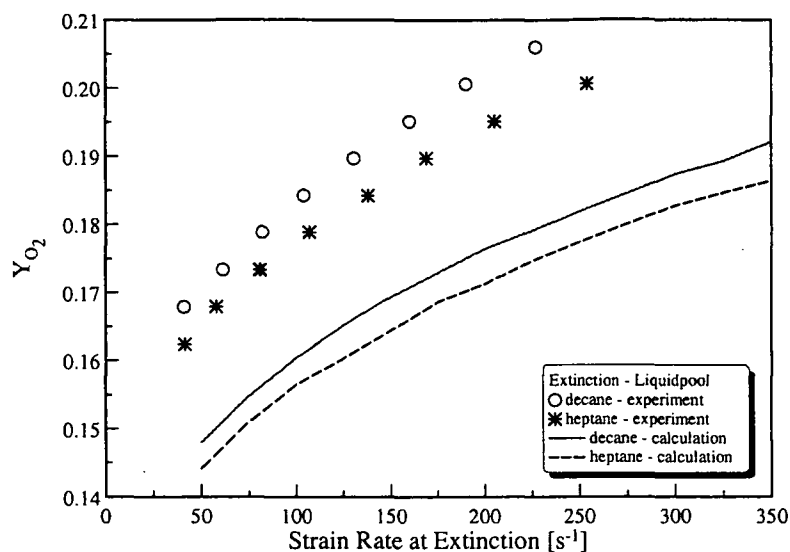
Figure 5.12: shows a comparison for extinction between experimental data of n-heptane and n-decane, represented by symbols, and calculation, represented by lines.
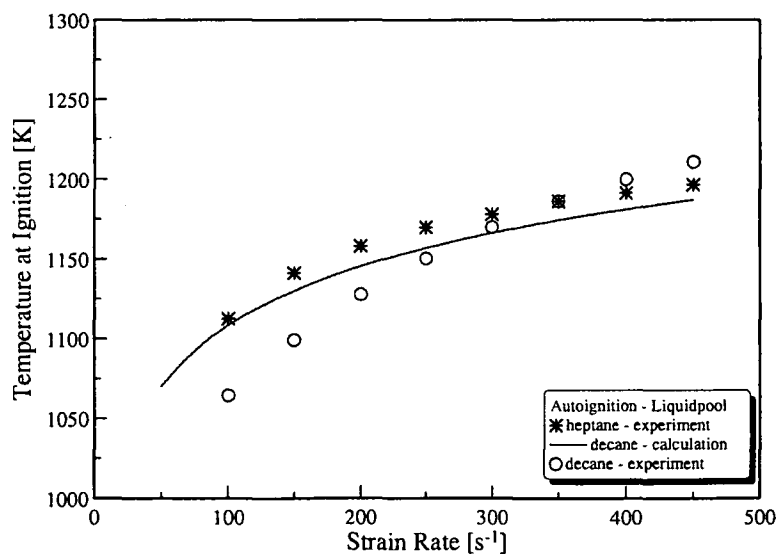
Figure 5.13: shows a comparison for autoignition between experimental data of n-decane and its appropriate calculation.

5.3 Conclusion

It was shown how to calculate the activation temperature, T_a, activation energy, E_a, and frequency factor, B, using asymptotics. This technique provides an accu-

rate and simple way to find the overall chemical-kinetic rate parameters by using experimental results of autoignition temperature and extinction strain rate.

Diesel and JP-8 had very similar results in autoignition and extinction experiments in the liquid pool setup. The mixture consisting of n-decane and o-xylene mimicked the autoignition and extinction behavior of JP-8 and diesel very well. This mixture is a good approach to be used as a surrogate for JP-8 and diesel. In both experiments (extinction and autoignition) the mixture of n-decane 80% and o-xylene 20% shows slightly to high values compared to the results of diesel and JP-8.

Using chemical kinetic mechanisms to calculate the strain rate at extinction, a_{ext}, gave a too high value as a result. The calculated results for autoignition fit fairly well for n-decane, but show much too high values for n-heptane. In both experiments, this can be attributed to different boundary conditions in the experiment and calculation. A non-slip boundary condition and a temperature close to the boiling temperature of the respective fuel is assumed on the surface of the liquid pool. The results of the calculation show the same trend as the experimental data. The temperature and flow in the liquid pool have an influence on the results. The temperature at the surface defines the fuel amount evaporating from the liquid pool surface.

Chapter 6

Multicomponent Experiments

Today's transportation systems depend nearly to 100 % on oil which is a liquid fuel, although lately some gaseous fuels like natural gas, LPG and hydrogen get some attention. These gaseous fuels are only a small percentage in the transportation section and have to be seen more as a research project for alternative fuels. Gaseous fuels are mostly used in truck or automobile fleets like public transportation in cities as Vienna, Austria, or San Diego, CA. In practise liquid fuels have the advantage that they are easy to store, handle and of a higher energy content per volume or mass. In the field of research it is a little bit different. Gaseous fuels have seen a much higher interest in research compared to liquid fuels. The main disadvantage of liquid fuel is that these fuels have to be vaporized. This can present quite some difficulties in the operation and in measuring the fuel flow.

Fuels like gasoline, diesel and aviation fuels are made up of thousands of components. Hence the simulation of these fuels is challenging. Gasoline, diesel and aviation fuels are mainly made up of straight chained and branched paraffins, cycloparaffins, aromatics and for a small amount alkenes. To model combustion of complex fuels such as gasoline, diesel, Jet A or JP-8, it is necessary to investigate all major components first. Chemical kinetic mechanisms do not exist for many compounds. A simple and fast (but not always accurate) approach is to use one-step chemistry and asymptotics as described further here.

Fundamental studies on extinction and autoignition of strained flames provide knowledge for modelling turbulent combustion. Previous studies on autoignition of reactant mixtures were focused on measuring ignition delay time in shock tubes [42] and rapid compression machines [87]. These studies do not characterize the influence of strain on autoignition. In this study the influence of strain on the critical conditions of autoignition of flames is investigated.

66

6.1 Introduction

Developing chemical kinetic models that describe combustion of commercial fuels is of practical importance [88, 89]. Availability of these models will permit reliable predictions of chemical-kinetics related issues in transportation systems. The predictive capability of these models have significant impact on operation, performance, and pollutant emissions from these systems. Practical fuels, for example, gasoline, diesel, and jet fuels comprise hundreds of aliphatic and aromatic hydrocarbon compounds. JP-8 is a "kerosene" fuel used by the U.S. Air Force. The major components of JP-8 are straight chain paraffins, branched chain paraffins, cycloparaffins, aromatics, and alkenes [13, 90]. In JP-8 the concentration of paraffins is on the average 60 % by volume, that of cycloparaffins 20 %, that of aromatics 18 %, and that of alkenes 2 % [13]. This is similar to hydrocarbon class distribution in Jet-A fuel [4]. Detailed chemical-kinetic mechanisms describing combustion for many of the components in JP-8 are not available. A useful approach in developing chemical-kinetic mechanisms for jet fuels is to first develop surrogates for these fuels. Surrogate fuels are defined as mixtures of few hydrocarbon compounds whose relative concentrations can be adjusted so that the physical and chemical properties pertinent to combustion approximate those of commercial fuels [89]. The physical properties include vapor-liquid-equilibrium, density and viscosity. The chemical properties include thermal stability, rates of heat release, autoignition and extinction characteristics in non premixed systems, ignition delay times and burning velocities in premixed systems, temperature and concentration histories in flow reactors, and rates of soot formation.

6.1.1 Tested Surrogates

Several surrogates developed in previous studies were tested. Since surrogates are usually designed for one certain experiment it was from interest to investigate also surrogate developed by previous studies if they are feasible to mimic extinction and autoignition characteristics of real jet fuel in a counterflow setup. The investigated surrogates are based on surrogates found in the literature (see Chapter 2.3) and the average chemical composition listed in Table 2.3. In Table 6.1 all investigated surrogates are listed with their components, composition, average mole weight, average density, and hydrogen to carbon ratio (H/C). For comparison reason, the mole weight, density, and H/C is shown for JP-8 at the bottom of the table. Surrogate (A), (B), and (C) are the base surrogates. Numerical calculations were performed for these surrogates. Surrogate B.1 and C.1 have an additional 5% of α-methylnapththalene to increase the soot formation. Surrogate D, E, and F investigate different amount of n-decane, n-butylcyclohexane, and n-butylbenzene. Surrogate G is a surrogate for a syntectic JP-8 (FT JP-8) fuel derived by Fischer-

Table 6.1: Composition of investigated surrogates for JP-8. This table is split across pages.

Surr.	Compounds	Formula	Vol.%	mass %	mol weight	Density	H/C
A[3]	n-decane	$C_{10}H_{22}$	60	56.56	123.43	0.7755	1.9347
	methylcyclohexane	C_7H_{14}	20	20.15			
	toluene	C_7H_9	20	23.29			
B[3]	n-decane	$C_{10}H_{22}$	60	56.50	126.24	0.7759	1.9267
	methylcyclohexane	C_7H_{14}	20	20.15			
	o-xylene	C_8H_{10}	20	23.35			
B.1	n-decane	$C_{10}H_{22}$	60	55.99	120.93	0.8337	1.9050
	methylcyclohexane	C_7H_{14}	20	19.97			
	o-xylene	C_8H_{10}	15	17.36			
	α-methylnaphthalene	$C_{11}H_{10}$	5	6.68			
C[3]	n-dodecane	$C_{12}H_{26}$	60	57.74	143.07	0.7882	1.9158
	methylcyclohexane	C_7H_{14}	20	19.57			
	o-xylene	C_8H_{10}	20	22.68			
C.1	n-dodecane	$C_{12}H_{26}$	60	57.24	144.87	0.8429	1.8847
	methylcyclohexane	C_7H_{14}	20	19.40			
	o-xylene	C8H10	15	16.86			
	α-methylnaphthalene	$C_{11}H_{10}$	5	6.49			
D	n-decane	$C_{10}H_{22}$	50	46.93	139.76	0.7653	1.9191
	n-butylcyclohexane	$C_{10}H_{20}$	25	25.33			
	n-butylbenzene	$C_{10}H_{14}$	25	27.73			
E	n-decane	$C_{10}H_{22}$	34	31.30	138.96	0.7654	1.8385
	n-butylcyclohexane	$C_{10}H_{20}$	33	32.79			
	n-butylbenzene	$C_{10}H_{14}$	33	35.90			

Continued on Next Page...

Table 6.1 – Continued

Surr.	Compounds	Formula	Vol.%	mass %	mol weight	Density	H/C
F	n-decane	$C_{10}H_{22}$	60	57.00	140.27	0.7651	1.9715
	n-butylcyclohexane	$C_{10}H_{20}$	20	20.53			
	n-butylbenzene	$C_{10}H_{14}$	20	22.47			
$G^{(1)}$	n-decane	$C_{10}H_{22}$	60	61.56	141.86	0.6875	2.2167
	iso-octane	C_8H_{18}	40	38.44			
Aachen	n-decane	$C_{10}H_{22}$	80	77.19	137.86	0.7883	1.9925
	mesitylene	C_9H_{12}	20	22.81			
mod. Aachen	n-dodecane	$C_{12}H_{26}$	80	77.61	160.30	0.7970	1.9711
	mesitylene	C_9H_{12}	20	22.39			
N1	n-decane	$C_{10}H_{22}$	80	77.03	137.86	0.7923	1.9910
	propylbenzene	C_9H_{12}	20	22.97			
N2	n-decane	$C_{10}H_{22}$	70	66.18	135.65	0.7924	1.8945
	propylbenzene	C_9H_{12}	30	33.82			
Drexel 1[2,3]	n-dodecane	$C_{12}H_{26}$	26	23.85	142.77	0.8318	1.8175
	iso-cetane	$C_{16}H_{34}$	36	33.92			
	methylcyclohexane	C_7H_{14}	14	13.05			
	decaline	$C_{10}H_{18}$	6	6.70			
	α-methylnaphthalene	$C_{11}H_{10}$	18	22.47			
Drexel 2	n-dodecane	$C_{12}H_{26}$	43	40.42	170.44	0.8147	1.8730
	iso-cetane	$C_{16}H_{34}$	27	26.07			
	methylcyclohexane	C_7H_{14}	15	14.33			
	α-methylnaphthalene	$C_{11}H_{10}$	15	21.85			
Montgomery[2]	n-decane	$C_{10}H_{22}$	32.6	30.78	143.36	0.7568	2.0054
	n-dodecane	$C_{12}H_{26}$	34.7	34.48			
	methylcyclohexane	C_7H_{14}	16.7	16.86			

Table 6.1 – Continued

Surr.	Compounds	Formula	Vol.%	mass %	mol weight	Density	H/C
	n-butylbenzene	$C_{10}H_{14}$	16	21.44			
Utah[3]	n-dodecane	$C_{12}H_{26}$	30	26.29	166.91	0.7924	1.9255
	n-tetradecane	$C_{14}H_{30}$	30	26.64			
	iso-octane	C_8H_{18}	10	8.10			
	methylcyclohexane	C_7H_{14}	20	17.82			
	o-xylene	C_8H_{10}	15	15.49			
	tetraline	$C_{10}H_{12}$	5	5.66			
JP-8		$C_{12}H_{23.2}$	100	100	167.65	0.8036	1.9417
JP-8[4]		$C_{11}H_{21}$	100	100	153.32	0.8036	1.9091
FT JP-8		NA	100	100	NA	NA	NA

[1] surrogate for Fisher-Tropsch JP-8, [2] not tested, [3] numerical calculation, [4] chemical formula more commonly used.

Tropsch process. Surrogate Aachen and modified Aachen were suggestions by collaborator Norbert Peters from the RWTH-Aachen.

The work is focused on extinction and autoignition in non premixed systems. The counterflow configuration is employed. The "reference" fuels tested are n-decane, n-dodecane, methylcyclohexane, o-xylene, and toluene. Surrogates are developed by mixing these reference fuels as shown in Table 2.6. The extinction and autoignition characteristics for these surrogates are measured and compared with those of JP-8 and Jet-A. Numerical calculations are performed employing a general semi-detailed chemical-kinetic model, both for the reference fuels and for the surrogates. The results of the calculations are compared with the experimental data.

6.1.2 Background and Review of Relevant Research

Numerous attempts have been made to develop surrogates for JP-8 and diesel. Guéret et al [91] studied oxidation of kerosene fuel and oxidation of a mixture of 79 % undecane, 10 % propylcyclohexane, and 11 % trimethylbenzene in a jet-stirred flow reactor in the temperature range 873-1033 K at atmospheric pressure. The reaction products formed during the oxidation of kerosene and the ternary mixture were similar [91]. Quasi-global chemical kinetic models were developed to reproduce experimental data. Dagaut et al [92] modeled kerosene combustion in jet-stirred reactor using n-decane. Lindstedt and Maurice [36] calculated the structure of premixed n-decane flames and compared their results with experimental data. Experimental data show that there exists similarities between the structure of n-decane flames and kerosene flames. Lindstedt and Maurice [36] modeled the structure of kerosene flames using a surrogate blend comprising 89-mol% n-decane and 11-mol% aromatic fuel. The aromatic component was represented by 1) benzene, 2) toluene, 3) ethylbenzene, and 4) ethylbenzene/naphthalene [36]. The calculated structure was compared with experimental data. Patterson et al [93] assumed that a mixture of 89 % n-decane and 11 % toluene as a surrogate for kerosene. They computed the structure of counterflow diffusion flames using this surrogate. Edwards and Maurice [13] report that a mixture of iso-octane, methyl cyclohexane, m-xylene, cyclooctane, decane, butyl benzene, 1,2,4,5 tetramethyl benzene, tetraline, dodecane, 1-methyl naphthalene, tetradecane, and hexadecane is a possible surrogate for JP-8. Montgomery et al [3] presumed that a mixture of 34.7 % n-dodecane, 32.6 % n-decane, 16.0 % butyl benzene, and 16.7 % methyl cyclohexane is a surrogate for JP-8. They developed a reduced chemical kinetic mechanism for the surrogate using CARM (Computer Assisted Reduction Method) [3, 37]. The reduced mechanism was tested by comparing profiles of temperature and concentration of various species obtained using this mechanism with those calculated using a detailed mechanism. Violi et al [4] modeled kerosene fuel by a surrogate blend composed of 73.5 mol% n-dodecane, 5.5 mol% i-octane, 10 mol% methylcyclohexane, and 11 mol% of aromatic fuel components. The aromatic com-

ponent was represented computationally by 9 mol% benzene, and 91 mol% toluene [4]. In a recent publication Edwards [90] has shown results of compositional analysis of kerosene fuels. The analysis suggest that a surrogate model for JP-8 should be made up of 18% aromatics, the aromatics should be a C_{10} alkyl benzene, the non aromatic component should be an isoparaffin and/or naphthene. The choice of the fuels to be tested in the present research is motivated by these previous studies.

Previous experimental studies on liquid hydrocarbon fuels were focused on measuring ignition delay times in shock tubes [42, 43] and rapid compression machines [87, 44, 94, 95]. Studies on liquid fuels in jet stirred flow reactors [91, 96, 97] and premixed flames stabilized on flat flame burners are available [98]. These experimental studies were conducted on premixed systems in the absence of fluid flow. Studies on counterflow non premixed flames [59, 48, 99, 100] and premixed flames [101] are also available. A comprehensive experimental, numerical, and analytical study of autoignition and extinction in non premixed systems are conducted here.

6.2 Experimental Apparatus and Procedures

Figure 6.1 shows a schematic illustration of the experimental setup. The figure
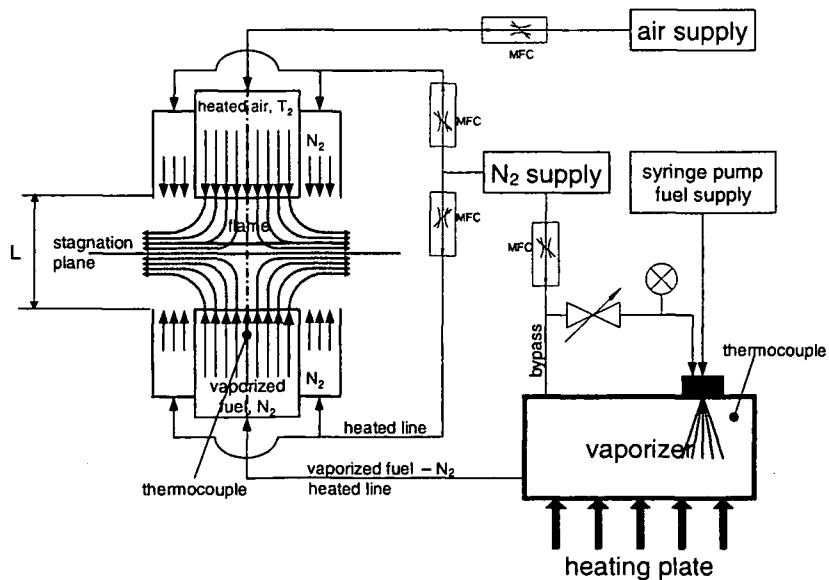
Figure 6.1: Schematic illustration of the experimental setup. The figure shows the counterflow flow field and the air, nitrogen, and fuel feed systems and the vaporizer.

shows the flow field in the counterflow burner and the air, nitrogen, and fuel feed systems. In the burner two streams flow toward a stagnation plane. The flows are steady, laminar and axisymmetric. The liquid fuels are vaporized in a device called the vaporizer. The walls of the vaporizer are heated. A syringe pump is used to introduce the liquid fuel into an "air"-blast injector attached to the vaporizer. Nitrogen is used to atomize the fuel. The atomized liquid is introduced as a fine mist into the heated mixing chamber where it is vaporized in hot nitrogen. A thermocouple is located close to the injector to monitor the temperature inside the vaporizer. The flow rates of gases are adjusted by computer-regulated mass flow controllers. The flow lines were heated to prevent condensation.

In the burner a fuel stream made up of prevaporized fuel and nitrogen is injected from the fuel-duct, and an oxidizer stream of air is injected from the oxidizer-duct. These jets flow into the mixing layer between the two ducts. The exit of the fuel-duct is called the fuel boundary, and the exit of the oxidizer-duct the oxidizer boundary. The mass fraction of fuel, the temperature, and the component of the flow velocity normal to the stagnation plane at the fuel boundary are represented by $Y_{F,1}$, T_1, and V_1, respectively. The mass fraction of oxygen, the temperature, and the component of the flow velocity normal to the stagnation plane at the oxidizer boundary are represented by $Y_{O_2,2}$, T_2, and V_2, respectively. The tangential components of the flow velocities at the boundaries are presumed to be equal to zero. The distance between the fuel boundary and the oxidizer boundary is represented by L. The velocities of the reactants at the boundaries of the counterflow burner are presumed to be equal to the ratio of their volumetric flowrates to the cross-section area of the ducts. The temperature of the fuel stream and the temperature of the oxidizer stream at the boundaries are measured using thermocouple.

In the experiments the momenta of the counterflowing reactant streams $\rho_i V_i^2$, $i = 1$, 2 at the boundaries are kept equal to each other. Here ρ_1 and ρ_2 represent the density of the mixture at the fuel boundary and at the oxidizer boundary, respectively. This condition ensures that the stagnation plane formed by the two streams is approximately in the middle of the region between the two boundaries. The value of the strain rate, defined as the normal gradient of the normal component of the flow velocity, changes from the fuel boundary to the oxidizer boundary [47]. The characteristic strain rate on the oxidizer side of the stagnation plane a_2 is presumed to be given by [47]

$$a_2 = \frac{2|V_2|}{L}\left(1 + \frac{|V_1|\sqrt{\rho_1}}{|V_2|\sqrt{\rho_2}}\right). \tag{6.1}$$

Equation 6.1 is obtained from an asymptotic theory where the Reynolds numbers of the laminar flow at the boundaries are presumed to be large [47]. Critical condi-

tions of extinction are presumed to be given by the strain rate, $a_{2,e}$, and the mass fraction of fuel at the fuel boundary. Critical conditions of autoignition are presumed to be given by the strain rate, $a_{2,I}$, the temperature of the oxidizer stream, $T_{2,I}$, and the mass fraction of fuel at the fuel boundary.

Experiments are carried out at a pressure of 1.013 bar. In the extinction experiments the temperature of the fuel stream is $T_1 = 503 \, (\pm 10) \, \text{K}$, and the temperature of the oxidizer stream, $T_2 = 298 \, \text{K}$. The distance between the fuel boundary and the oxidizer boundary is $L = 10 \, \text{mm}$. At some selected value of $Y_{F,1}$ the flame is stabilized at $a_2 < a_{2,e}$. The strain rate is increased by increasing V_1 and V_2 until extinction is observed. The accuracy of the strain rate is $\pm 10 \%$ of recorded value and that of the fuel mass fraction $\pm 3 \%$ of recorded value. The experimental repeatability on reported strain rate is $\pm 5 \%$ of recorded value. Experimental results are shown later.

In the autoignition experiments the distance between the fuel boundary and the oxidizer boundary was $L = 12 \, \text{mm}$. In these experiments the temperature of prevaporized fuel and nitrogen at the fuel boundary was maintained at 503 K. At chosen values of strain rate and mass fraction of fuel in the fuel stream, $Y_{F,1}$, the flow field was established. The temperature of air was increased until autoignition takes place. The onset of autoignition was observed using a high-speed camera to make sure that ignition takes place close to the axis of symmetry. At a fixed value of $Y_{F,1} = 0.3$, the temperature of the oxidizer stream was recorded as a function of the strain rate. The accuracy of the measurement of the temperature of air at autoignition is expected to be $\pm 30 \, \text{K}$, the strain rate $\pm 10 \%$, and fuel mass fraction $\pm 3 \%$ of recorded value. The experimental repeatability in the measurement of the temperature of air at autoignition is expected to be $\pm 6 \, \text{K}$. The results are shown later.

A temperature profile was compiled by measuring the temperature in the flow field along the y-axis and along the radial axis at a distance from the stagnation plane of z = 5.5 mm (close to oxidizer duct), z = 4.0 mm, and z = 2.4 mm (close to stagnation plane). Figure 6.2 shows the temperature profile along the radial- and z-axis. There is a strong temperature gradient along the radial axis at the measurement closest to the oxidizer duct (z = 5.5 mm). This is caused by the heat loss to the curtain flow that is not heated. The temperature profile gets more and more flat towards to the stagnation plane.
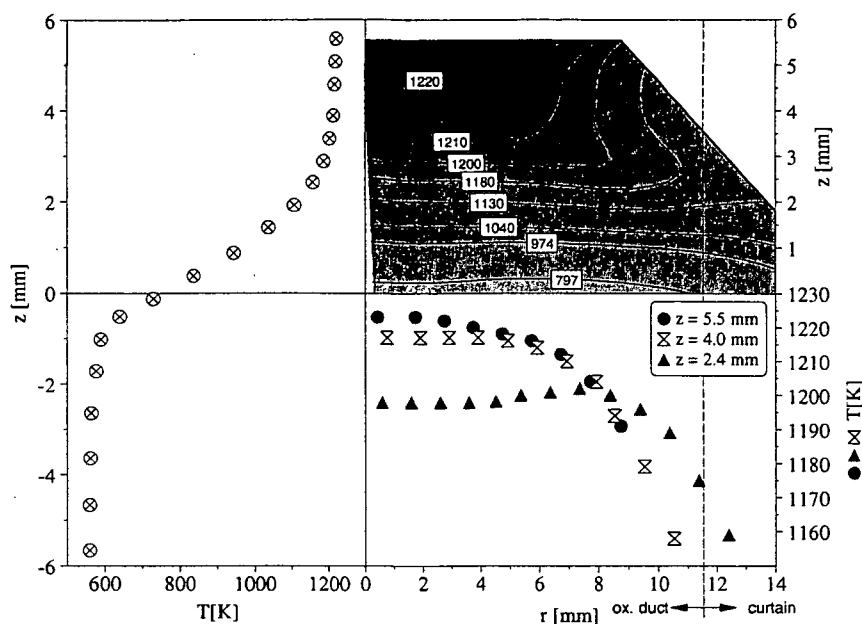
Figure 6.2: Temperature profile close to autoignition of JP-8 along the radial-, and z-axis.

6.3 Chemical-Kinetic Mechanism

The high molecular weight compounds, used as reference fuels here, undergo a sequential reduction to lower molecular weight hydrocarbons during combustion. Therefore chemical-kinetic mechanisms for these fuels include those for lower molecular weight compounds. In these chemical-kinetic mechanisms, in addition to pyrolysis and oxidation reactions that convert large molecules to smaller molecules and radicals, it is also necessary to include several classes of condensation and dealkylation reactions that govern the growth of polycyclic aromatic hydrocarbons (PAHs) and soot [88, 102]. The large number of reactions that are required to describe the combustion of each reference fuel precludes a reliable extension to complete detailed chemical-kinetic models for jet fuels or mixtures of high molecular weight hydrocarbon compounds. The semi-detailed or lumped approach reduces the overall complexity of the resulting chemical-kinetic scheme both in terms of equivalent species and lumped or equivalent reactions. In fact, the scheme uses a lumped description of the primary propagation reactions for the large species to smaller species, and then treats the successive reactions of smaller species with a detailed chemical-kinetic scheme. For any new reference species it is only necessary to include all the primary oxidation and decomposition reactions in the chemical-kinetic model. The pyrolysis and oxidation of high molecular weight n-alkanes has been analyzed recently, and lumped chemical-kinetic models have been proposed

and validated for different n-alkanes up to n-hexadecane [89]. Similarly, primary reactions of cyclohexane and methylcyclohexane have been studied and validated in a wide range of conditions [103]. Also chemical-kinetic modeling of low temperature ignition of JP-8 surrogates and of the structure of diffusion flames have been carried out previously [4, 2, 104].

To illustrate the approach described above, it is useful to discuss the similarities between primary reactions of toluene and xylene, where typical features of the modeling of aromatic fuels are apparent. Figure 6.3 shows that the major reaction
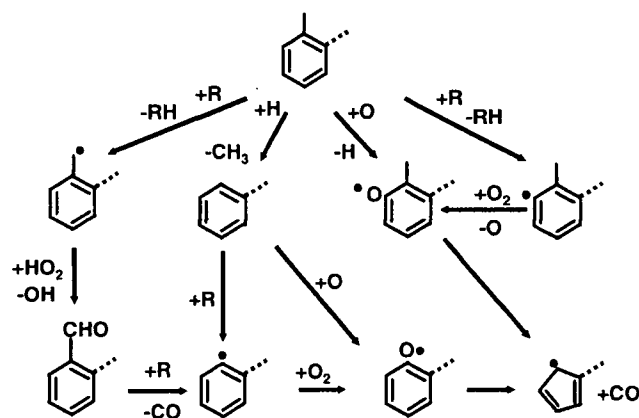
Figure 6.3: Principal path for oxidation of toluene and o-xylene. Dotted lines refer to methyl group of o-xylene.

paths are similar for these fuels. The reaction path without the dotted lines in Fig. 6.3 refers to toluene. The dotted lines indicate the methyl substitution that converts the reaction path for toluene into that for o-xylene. The H-abstraction reactions both on toluene and xylene, each lead to the formation of two different radicals of benzyl ($CH_2C_6H_5$ and $CH_2C_6H_4CH_3$) and phenyl type ($CH_3C_6H_4$ and $(CH_3)_2C_6H_3$). Only one phenyl radical has been considered for each fuel: it lumps two or three isomers, respectively. The stable and resonant benzyl like radicals explain the lower reactivity of aromatic fuels and contribute to PAH formation in pyrolytic conditions. The sensitivity analysis shows that other important pathways for breakdown of toluene and xylene are the reactions with both O and H radicals. The direct addition of O radical to the fuels forms the cresoxy and methyl-cresoxy radicals. Substitutive addition of H radical to form methyl radical and benzene or toluene, respectively, are also very important steps. The stable benzyl type radicals react with O to form (methyl-)benzaldehyde, rapidly consumed through successive H-abstraction and CO elimination. The phenyl like radicals preferably react with molecular oxygen to form the cresoxy radicals. These radicals are

analogous to phenoxy radical (C_6H_5O) and they are important intermediates to explain the aromatic ring degradation into cyclopentadiene structures. Successive reactions of different intermediates are included in the chemical-kinetic model and consistent with literature parameters [105]. Experimental measurements obtained in flow [106, 107, 108] and jet stirred reactors [109] as well as in shock tubes and rapid compression machines [110, 111] provide useful comparisons for the validation of the chemical-kinetic model. Other experimental data also refer to mixtures of toluene with n-butane [112], and even methylcyclohexane [113].

The overall chemical-kinetic scheme for the simulation of pyrolysis and combustion of high molecular weight hydrocarbon fuels, including those for the reference fuels considered here, is made up of 7878 reactions among 283 species. This chemical-kinetic model includes both low and high temperature mechanisms. The reduced high temperature mechanism is made up of 4890 reactions and 173 species. Both these chemical-kinetic models are used. They are available at Ref. [114].

Numerical calculations are performed using the chemical-kinetic in Ref. [114]. The computational model used here is a modified version of the opposed-flow diffusion flame code (OPPDIF [115]) with proper modifications in order to use H abstraction reactions described in a simplified form and with a greater flexibility with respect to equivalent or lumped reactions with several products. The boundary conditions employed in the calculations are identical to those in the experiments. Flame structures and critical conditions of extinction and autoignition are obtained.

6.3.1 Autoignition and Extinction of JP-8 and Jet A

As described in Chapter 2.2.1, real fuel consist of thousands of components. The composition of these fuels is not known and depends on the crude oil and production process. To investigate the influence of different batches of JP-8 and Jet A, several fuels of different batches were tested. Three different batches of JP-8 are available - JP-8 from Patterson Air Force Base (WPAFB), JP-8 02POSF 4177, and JP-8 00POSF 3773. Also three batches of Jet A fuel were tested - Jet A purchased at the local airport, Jet A 99POSF 3602, and Jet A 99POSF 3638. Additionally a composite blend of several batches was investigated - 04 POSF4658. For all fuels except JP-8 from EAFB, 02POSF 4177 and the Jet A fuel purchased at the locale airport material safety sheets are available that give the chemical and physical properties. The given physical and chemical properties agree with the data found in literature. The data are given in Appendix A.1.1, Table A.2.

Figure 6.4(a) shows autoignition data for different fuel batches of JP-8 at a constant fuel mass fraction, $Y_{fuel} = 0.4$ and Figure 6.4(b) shows a comparison of JP-8

(a) JP-8   (b) Jet A
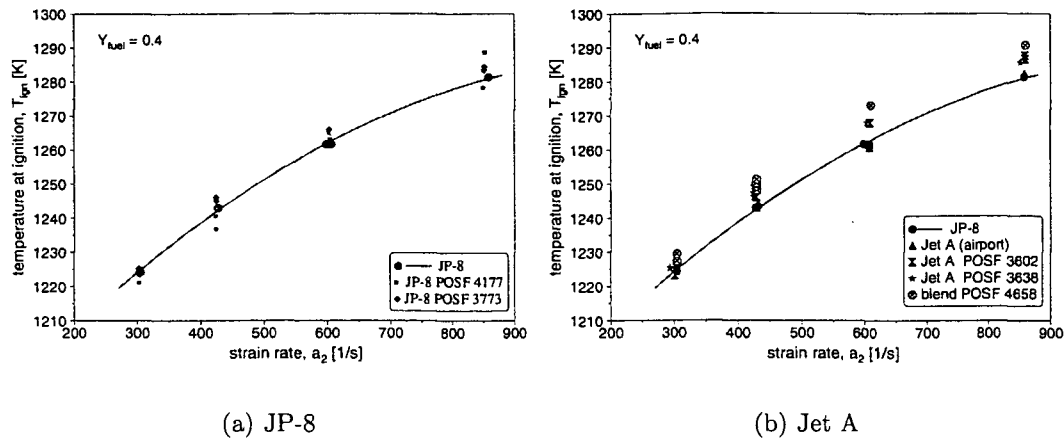
Figure 6.4: shows autoignition data for different batches of JP-8 (a) and Jet A (b) fuels. Symbols represent experimental data, lines represent best fit.

and different batches of Jet A fuels at a constant fuel mass fraction, $Y_{fuel} = 0.4$. As it can be seen from both figures, there is little influence between the different batches. 02POSF 4177 and 00POSF 3773 have a similar aromatic content. Even between JP-8 and Jet A fuel is only a slight difference. The aromatic content between 99POSF 3602 (24Vol.%) and 99POSF 3638 (12Vol.%) is quit different. Even with this big difference of aromatics, the results of both fuels are nearly the same. There is a slight shift towards higher autoignition temperatures with increasing aromatic content. A second set of data was conducted with keeping the strain rate a_2 at a constant value of 550 s^{-1} show the same behavior. These results are shown in the Appendix D.1.4.

Figure 6.5 shows a comparison extinction strain rate data of JP-8 and Jet A fuels of different batches. The difference between different fuel types and batches account for less then 6%. There is only a very small shift to higher strain rates at extinction the lower the aromatic content. Therefor we conclude that either JP-8 or Jet A fuel can be used as a representative fuel to compare it with its surrogate. Due to the high dilution of the fuel (3-5% fuel in the reactant stream) the influence on the autoignition and extinction data of the composition itself is fairly small.

6.4   Results and Discussion

First, numerically calculated values of the critical conditions of extinction and autoignition of the reference single component fuels are compared with measure-
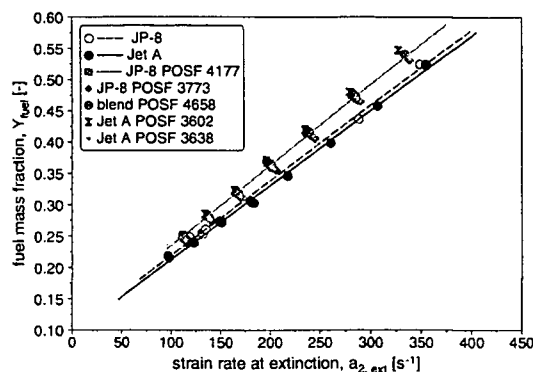
Figure 6.5: shows extinction data for different batches of JP-8 and Jet A fuel. Symbols represent experimental data, lines represent linear fit.

ments. Next, similar comparisons are made for the surrogates (A), (B), and (C) shown in Table 2.6. The results are shown in Figs. 6.6, 6.7, 6.9, and 6.10. The symbols in these figures represent experimental data, and the lines are results of numerical calculations.

6.4.1 Extinction and Autoignition of Reference Fuels

Figure 6.6 shows the mass fraction of fuel as a function of the strain rate at extinction. This figure shows extinction data for n-decane ($C_{10}H_{22}$), n-dodecane ($C_{12}H_{26}$), methylcyclohexane (C_7H_{14}), toluene (C_7H_8), o-xylene (C_8H_{10}), and trimethyl-benzene (C_9H_{12}). The lines in Fig. 6.6 represent boundaries separating a flammable region above the lines from extinguished states below the lines. Experimental data and numerical calculations show that aromatic fuels are easier to extinguish in comparison to alkanes. For alkanes, the numerically calculated values of the critical conditions of extinction agree well with experimental data. Experimental data show that extinction characteristics of the aromatic fuels are nearly the same. Calculated values of the critical conditions of extinction of toluene agree well with experimental data. For a given strain rate, the calculated values of $Y_{F,1}$ for o-xylene are higher than the measurements.

Figure 6.7 shows the temperature of the oxidizer stream at autoignition as a function of the strain rate for n-decane, n-dodecane, methylcyclohexane, and toluene. This figure shows data obtained at a fixed value of the mass fraction of fuel in the fuel stream $Y_{F,1} = 0.3$. The lines in Fig. 6.7 represent boundaries separating a region above where autoignition takes place from a region below where autoignition cannot take place. The numerically calculated values of the critical conditions of autoignition for n-decane, n-dodecane, and methylcyclohexane agree

well with experimental data. Experimental data and calculated values of critical conditions of autoignition show that methylcyclohexane is easiest to ignite followed by n-decane, n-dodecane, and toluene. At a given value of the strain rate the calculated value of T_2 at autoignition of toluene is higher than the measurements. Numerical calculations show that the critical conditions of autoignition for o-xylene is similar to those for toluene. Experimental data for autoignition for o-xylene are not available because the temperature of the oxidizer stream required for autoignition is higher than what can be attained in the current experimental apparatus. A significant observation concerning the extinction and autoignition characteristics of the aromatic fuels is made by comparing Figs. 6.6 and 6.7. Experimental data for extinction show that reactivity for toluene and o-xylene are nearly the same. The numerical calculated values of critical conditions of extinction of toluene agree well with experimental data, while the overall reactivity of o-xylene predicted by the chemical-kinetic mechanism is less than that observed. The calculated values of critical conditions of autoignition show toluene to be less reactive than o-xylene. Thus the calculated relative order of reactivities of toluene and o-xylene at extinction is not the same at autoignition. Further detailed studies are required to obtain an improved understanding of the reason for these differences.
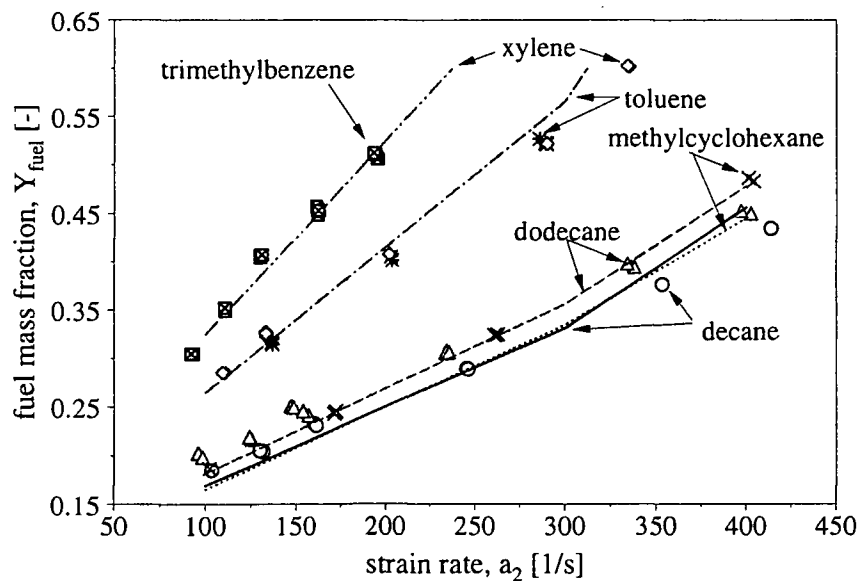
Figure 6.6: The mass fraction of fuel as a function of the strain rate at extinction. The symbols represent experimental data. The lines are results of numerical calculations.
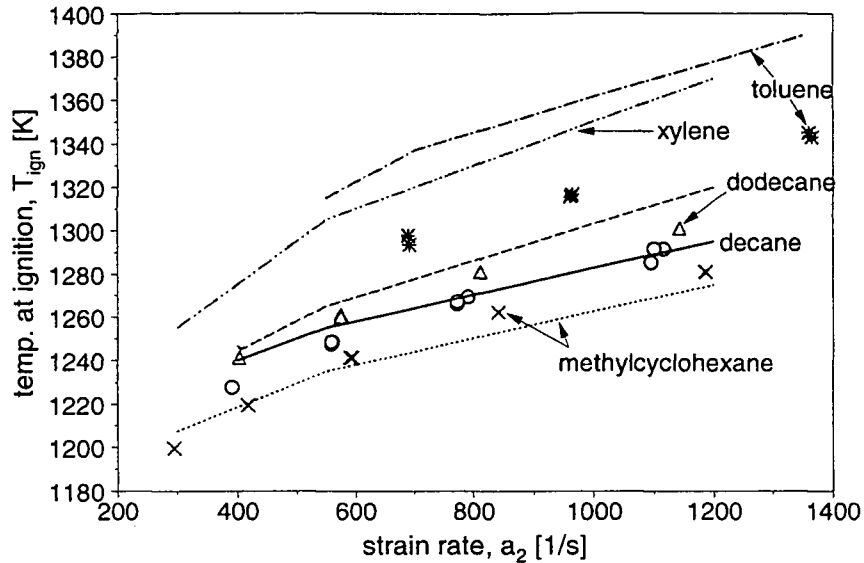
Figure 6.7: The temperature of the oxidizer stream at autoignition as a function of the strain rate. The figure shows experimental data obtained at fixed values of the mass fraction of fuel in the fuel stream $Y_{F,1} = 0.3$. The symbols represent experimental data. The lines are results of numerical calculations.

Extinction and Autoignition of Aromatics

Aromatics are very hard to autoignite because their ring structure is very stable and needs a lot of energy to be broken up. That means that the autoignition temperature is very high. As mentioned in the previous chapter it was not possible to ignite o-xylene and trimethylbenzene since the experimental setup is limited to a maximum temperature of about 1050 °C. To provide data for the development and improvement of those very difficult to ignite aromatic fuels, both fuels were mixed with n-decane to lower the ignition point. Figure 6.8(a) shows the measured temperatures at autoignition, T_{ign} as a function of the strain rate, a_2, at a constant fuel mass fraction, $Y_{fuel} = 0.4$. Figure 6.8(b) shows for the same mixtures the temperature of autoignition as a function of the fuel mass fraction, Y_{fuel} at a constant strain rate, $a_2 = 550$ s^{-1} and in Figure 6.8(c) is the extinction strain rate as a function of the fuel mass fraction shown. The symbols represent experimental data, and the lines represent best fit curves. Adding a less reactive fuel to the "base" fuel (n-decane) decreases of course the reactivity of the mixture. Unfortunately the data can't be extrapolated to a pure component. We can only speculate on autoignition temperatures for pure o-xylene or trimethylbenzene since there are interactive reactions between n-decane and the added aromatic component.

(a)   (b)

(c)
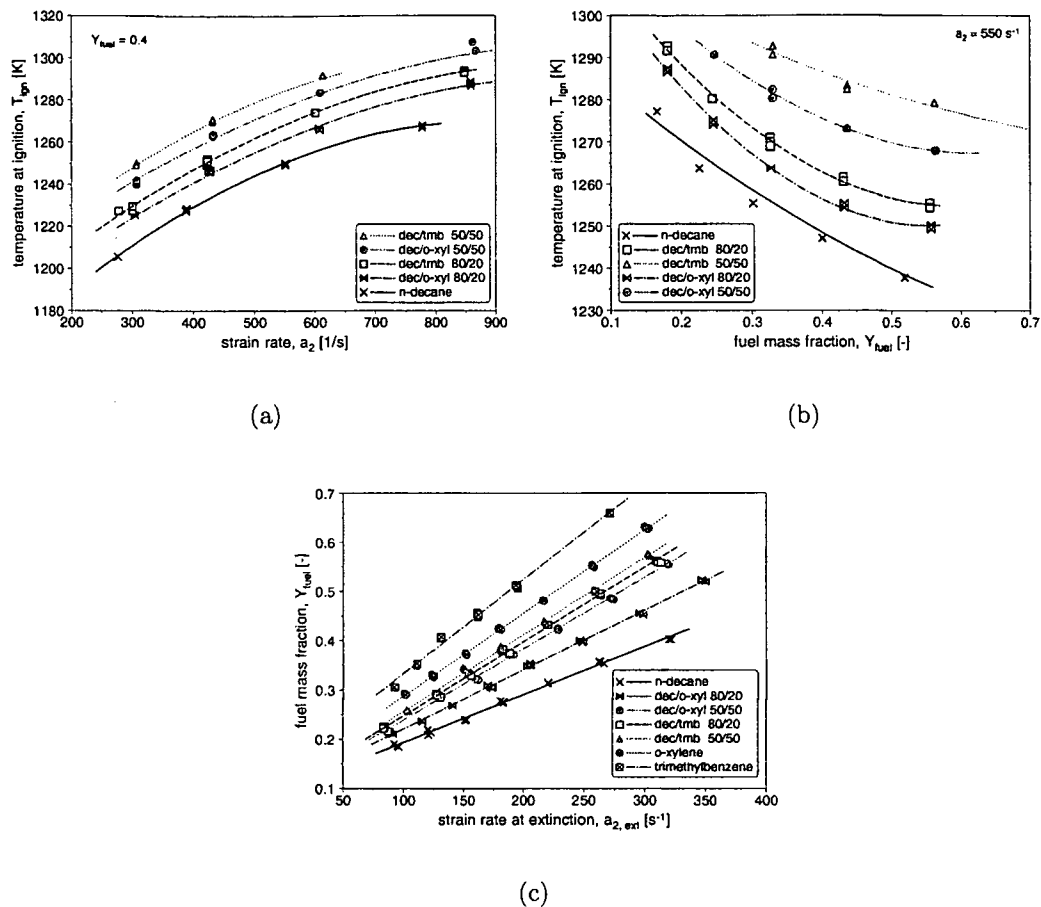
Figure 6.8: Autoignition and extinction of aromatic mixtures. Symbols represent experimental data, lines represent best fit curves.

6.4.2   Extinction and Autoignition of JP-8, Jet-A, and Surrogates

Three possible surrogates for the jet fuels were prepared. They are mixtures of the following hydrocarbon compounds by volume (A) n-decane (60%), methylcyclohexane (20%), toluene (20%) (B) n-decane (60%), methylcyclohexane (20%), o-xylene (20%), and (C) n-dodecane (60%), methylcyclohexane (20%), o-xylene (20%). The critical conditions of extinction of these fuels were compared with those for JP-8 and Jet-A. The jet fuels were obtained from Wright Patterson Air Force Base (WPAFB). Figure 6.9 shows the mass fraction of fuel as a function of the strain rate at extinction. The experimental data for the critical conditions
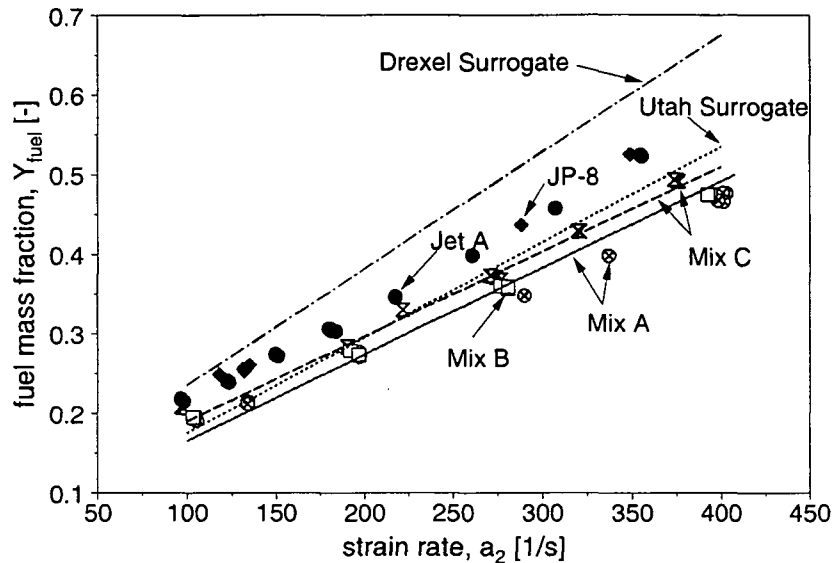
Figure 6.9: The mass fraction of fuel as a function of the strain rate at extinction. The figure shows extinction data for fuel mixtures shown in Table 6.1. The symbols represent measurements. The lines are results of numerical calculations. The critical conditions of extinction of surrogates are compared with those for JP-8 and Jet-A.

of extinction of these fuel mixtures are compared with those for JP-8 and Jet-A. Figure 6.9 shows that the extinction characteristics of JP-8 and Jet-A are similar. Moreover the extinction characteristics of the mixture (C) are close to those for JP-8 and Jet-A. In mixture (A) the aromatic component is toluene, while in mixture (B) the aromatic component is o-xylene. Figure 6.9 shows that the extinction characteristics of mixture (A) and (B) are similar. Therefore, replacing toluene with o-xylene has very little influence on critical conditions of extinction. The differences between extinction characteristics of mixture (A) and mixture (C) is attributed to replacing n-decane in mixture (A) with n-dodecane in mixture (C). Numerical calculations were performed only for mixture (A) and mixture (C), because the extinction characteristics of mixture (A) and mixture (B) are similar. The numerical results agree well with experimental data. It is of interest to test the performance of surrogates developed by other investigators. The Utah surrogate shown in Table 2.6 is made up of six components, so chosen that they match the composition and distillation characteristics JP-8. The Drexel surrogate shown in Table 2.6 is mainly designed to reproduce the autoignition characteristics of JP-8 at low temperatures. Figure 6.9 shows that the critical conditions of extinction calculated using the Utah and the Drexel surrogates agree well with those for the
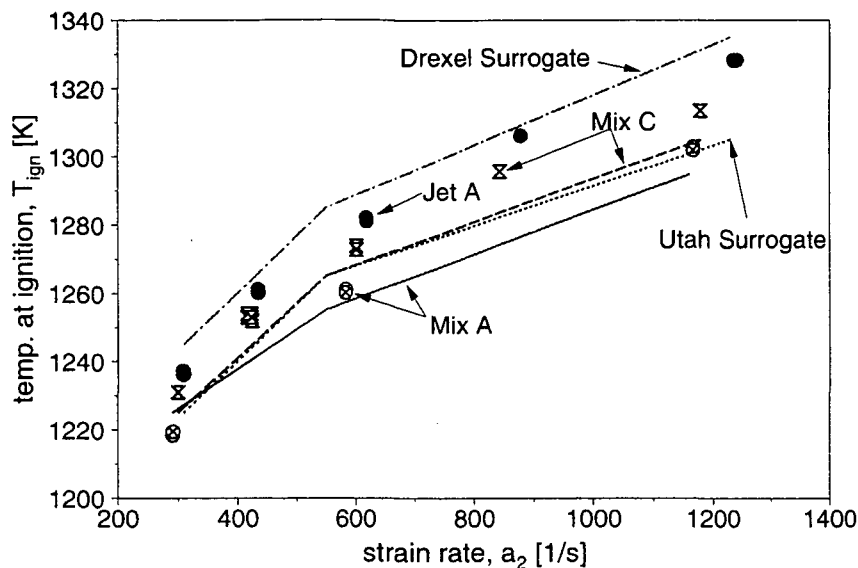
Figure 6.10: The temperature of the oxidizer stream at autoignition as a function of the strain rate. The figure shows data for fuel mixtures shown in Table 6.1. The symbols represent experimental data and the lines are results of numerical calculations. The critical conditions of autoignition of surrogates are compared with those for Jet-A.

jet fuels. The Utah surrogate is slightly more reactive than the jet fuels while the Drexel surrogate is slightly less reactive.

Figure 6.10 shows the temperature of the oxidizer stream at autoignition as a function of the strain rate for mixtures of (A) n-decane (60%), methylcyclohexane (20%), toluene (20%) and (C) n-dodecane (60%), methylcyclohexane (20%), o-xylene (20%). The critical conditions of autoignition of these fuel mixtures are compared with those for Jet-A. Figure 6.10 shows that the fuel mixtures are slightly more reactive than Jet-A. The autoignition characteristics of mixture (C) are closest to those for Jet-A. The predictions of the Utah surrogate and Drexel surrogate were also compared with experimental data. Figure 6.10 shows that both surrogates agree well with experimental data. Among all the surrogates tested the predictions of the Drexel surrogate agrees best with experimental data.

Critical conditions of autoignition were also measured at fixed value of the strain rate $a_2 = 550\,\text{s}^{-1}$. In this set of experiments the temperature of the oxidizer stream was recorded as a function of $Y_{F,1}$. The results are shown in Fig. 6.11. In this figure the symbols represent experimental data. The lines are best fit to
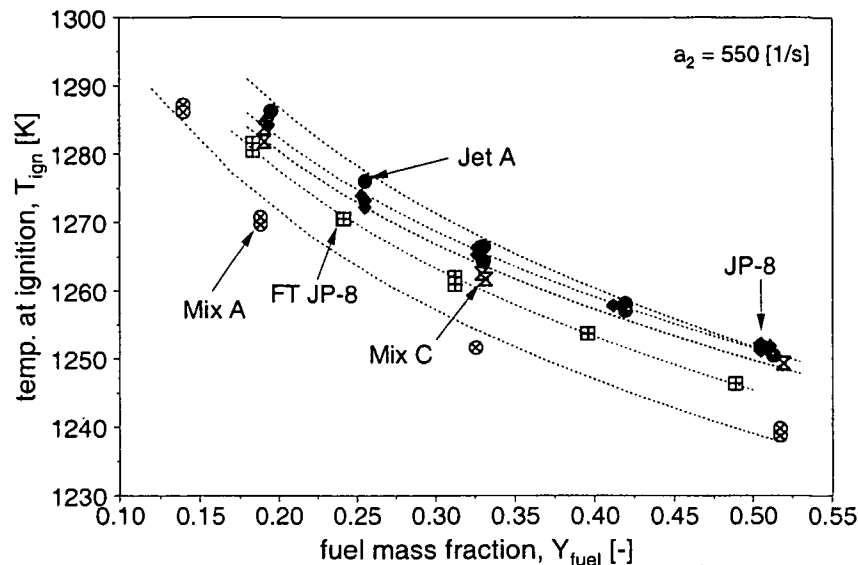
Figure 6.11: Measured values of the temperature of the oxidizer stream at autoignition as a function of the mass fraction of fuel in the fuel stream, $Y_{F,1}$. The data was obtained at a constant value of the strain rate $a_2 = 550\,s^{-1}$ The symbols represent experimental data. The lines are best fit to the experimental data. The figure compares critical conditions of autoignition of JP-8, Jet-A, Fischer-Tropsch JP-8, and mixture C shown in Table 6.1.

the experimental data. Figure 6.11 compares critical conditions of autoignition of JP-8, Jet-A, Fischer-Tropsch JP-8 (FT-JP-8), and mixtures (A) and (C) shown in Table 6.1. Figure 6.11 shows that the autoignition characteristics of Jet-A and JP-8 are similar. FT-JP-8 is easier to ignite when compared to Jet-A and JP-8.

In Appendix D.1.4 results are shown for autoignition and extinction for surrogates listed in Table 6.1. Figure D.1.4 shows autoignition data for Fischer-Tropsch JP-8 (FT JP-8) and its surrogate G. The FT JP-8 has a autoignition temperature about 10-15 K lower compared to regular JP-8. The surrogate for FT JP-8 fits the behavior in both autoignition and extinction very well.

Adding 5 % of α-methylnaphthalene to either surrogate B or C changes the autoignition temperature, T_{ign}, to a slightly higher value and extinction strain rate, a_{ext}, to a slightly lower value (Fig.D.1.4). The influence becomes more visible at a higher fuel mass fraction. Surrogate C fits the data of extinction and autoignition of JP-8 very well. Surrogate B.1 shows slightly lower autoignition temperatures compared to JP-8. Surrogate B.1 and C have a hydrogen to carbon ration of $H/C = 1.905$ and 1.915, respectively. These two surrogates have the closest H/C

to jet fuel, which has a H/C of 1.909.

Surprisingly surrogates composed with only two components (Aachen, N1, and N2) agree relative well on extinction and autoignition data. But surrogate C or C.1 are to favor since it is expected that they will have better agreement on soot formation.

The tested surrogates from previous studies, Drexel 2 and Utah, have a (slightly) too low and too high autoignition temperature, respectively.

6.5 Sensitivity Analysis

Figure 6.12 shows sensitivity analysis under autoignition conditions for n-dodecane and toluene. These fuels are selected because they illustrate key steps responsible for autoignition in alkane and aromatic fuels. This figure has three parts. Part (a) shows calculated temperature profiles for n-dodecane at a strain rate $a_2 = 400\,s^{-1}$, and oxidizer temperature of $T_2 = 1240\,K$, and for toluene at $a_2 = 700\,s^{-1}$, $T_2 = 1325\,K$. These conditions are close to autoignition (see Fig. 6.7). The intermediate
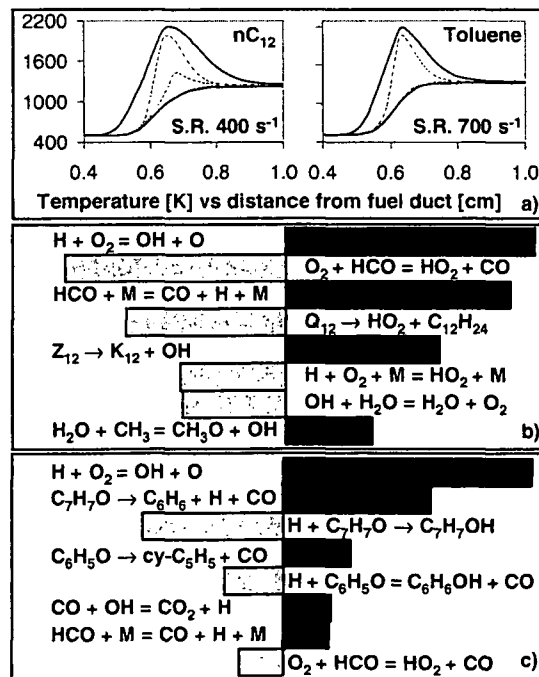
Figure 6.12: Sensitivity analysis at conditions close to autoignition for n-dodecane ($T_{air} = 1240\,K$, $a_2 = 400\,s^{-1}$, $YF, 1 = 0.3$) and toluene ($T_{air} = 1325\,K$, $a_2 = 700\,s^{-1}$, $YF, 1 = 0.3$). Part (a) Temperature profiles, Part (b) n-dodecane, Part (c) toluene.

dashed lines in part (a) of Fig. 6.12 represent the transient evolution of the temperature profile prior to autoignition. This behavior is similar to the time evolution of temperature profiles, as predicted by Im et al. [116] for the autoignition of CH_4. The results of sensitivity analysis for n-dodecane and toluene are shown in part (b) and part (c), respectively, of Fig. 6.12. Low temperature reactions, with the formation of peroxy-alkylhydroperoxy radicals (Z_{12}) and ketohydroperoxides (K_{12}), favor n-dodecane ignition, while the decomposition of the alkylhydroperoxy radical (Q_{12}) to form dodecene and hydroperoxy radical reduces the reactivity. The effect of the low temperature mechanism vanishes when increasing the strain rates. This behavior confirms previous analysis by Seiser et al. [99] for a n-heptane flame, showing that low temperature chemistry is important only at low strain rates ($a_2 <$ 350 s^{-1}). The typical branching reaction H+O_2 always plays the major role. This branching reaction is also the most sensitive one at conditions close to the critical conditions of autoignition of toluene, where phenoxy and methyl phenoxy radical decomposition are other critical steps in controlling the reactivity of toluene. The decomposition of phenoxy radical, to form CO and cyclopentadienyl radical, is assumed as a model reaction for similar decompositions of methyl- and dimethyl-phenoxy radicals. In the same way, the reaction [117]: $C_6H_5 + O_2 \rightarrow C_6H_5O + O$, with a rate constant, k given by $k = 2.6 \times 10^{10} \exp[-6.12/(RT)]$ (mol·s)$^{-1}$ is a model for the oxidation of methyl and dimethyl-phenyl radicals. Here R is the gas constant.

6.6 Concluding Remarks

The combustion characteristics of high molecular weight hydrocarbon fuels calculated using a semi-detailed chemical-kinetic mechanism is found to agree well with experimental data. The predictions of combustion characteristics of mixtures of these fuels using the semi-detailed mechanism also agrees with experimental data. The combustion characteristics of JP-8 and Jet-A are similar. The critical conditions of extinction and autoignition for the Surrogates (A), (B), and (C) tested here agree reasonably well with those for the jet fuels. The agreement between the computed results obtained using the Utah surrogate and the Drexel surrogate with experimental data for the jet fuels is even better. Surrogates (A), (B), and (C), however, are easier to model because they comprise fewer components in comparison to the Utah and Drexel surrogates. Modeling of aromatic fuels, in particular o-xylene, was found to be challenging. The calculated values of critical conditions of extinction in Fig. 6.6 show that o-xylene is less reactive than toluene, while calculated values of critical conditions of autoignition in Fig. 6.7 show that o-xylene is more reactive than toluene. More experiments and modeling are required to test this observation. Further experimental data are also needed elucidate the role of cresoxy radicals in combustion of aromatic fuels. The chemical-kinetic scheme that

describes the chemistry of xylene does not contain the low temperature mechanisms and the distinction among p-, m-, and o-xylenes. This distinction is expected to be more important at low and intermediate temperatures.

6.7 Diesel

It was not possible to run Diesel fuel in the current experimental setup. Diesel fuel contains larger molecules compared to jet fuel and needs therefore a higher temperature to vaporize the fuel. The setup has to be modified to achieve higher temperatures in the vaporizer and in the lines going from the vaporizer to the burner. Additionally the design of the burner has to be changed with an increased suction and heated ducts. Diesel fuel will have a higher autoignition temperature and a lower extinction strain rate. This assumption can be made by the fact that diesel fuel contains larger molecules compared to the tested jet fuels. It was possible to get one repeatable autoignition point for diesel fuel (although the result has to be observed with caution). The used fuel was a Chevron Diesel #2. Further experiments with Diesel were stopped because of safety reasons. Fuel condensing on the outside of the burner ignited, setting the whole burner in flames. Fig.6.13 shows a comparison of the autoignition temperature, T_{ign}, for a fuel mass frac-
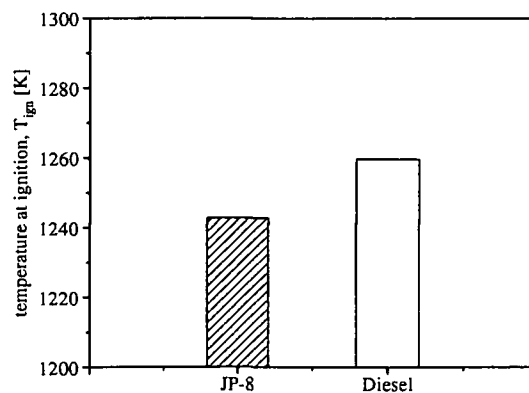
Figure 6.13: shows the temperature at ignition, T_{ign} at $Y_{fuel}= 0.4$ and $a_2= 444$ s^{-1}.

tion of $Y_{fuel}= 0.4$ at a strain rate of $a_2= 444$ s^{-1} between JP-8 (POSF 4177) and Diesel (Chevron Diesel #2). The diesel fuel ignited at $T_{ign}= 1259$ K, while the jet fuel ignited nearly 20 K lower at $T_{ign}= 1242$ K. This result was to be expected although there are still uncertainties about how much the ignition temperature differs. While running autoignition experiments, the radiation from the oxidizer duct heated up the screens and the duct of the fuel duct. The temperature in the fuel duct was sufficient high that no condensation occurred. In the extinction

experiments the radiation from the top heating was missing and fuel condensed on the screens of the fuel duct exit.

For developing a surrogate for diesel fuel following basic rules should be taken into account:

- average composition of fuel groups
- molecular weight of fuel
- hydrogen to carbon ratio

Following these three rules, the surrogate will (most likely) mimic the combustion behavior of extinction and autoignition. Of course if other behaviors of the real fuel should be simulated with a surrogate, some adjustments have to be made to these three basic rules.

Chapter 7

Conclusion

Studies on shock tubes give useful information concerning the chemical-kinetic mechanisms of autoignition. Studies on two premixed flames stabilized in the "back-to-back" configuration have significantly advanced the understanding of structure and dynamics of laminar premixed flames in nonuniform flow-field [69]. Studies on shock tubes and flames stabilized in the "back-to-back" configuration do not, however, give the influences of nonuniform flow-field on autoignition. A key observation of the present study is that for premixed systems abrupt extinction and autoignition does not take place if the value of the equivalence ratio is less than some critical value. This critical value of ϕ is found to depend on the strain rate. The strain rate is therefor an important value describing combustion behaviors of different fuels. It is also very suitable the compare different fuels or mixtures in their reactivity. In general the reactivity increases in following order: n-alkanes, olefins, cycloalaknes, and aromatics. In the same order the cetane number improves.

Studies on diesel and jet fuel were all performed in a nonpremixed environment, since this is the same environment these fuels are used in engines. The chemical structure of jet fuel and diesel is very similar although different in their exact composition. The results in the liquid pool setup show a similar behavior of jet fuel and diesel. The surrogate made up of n-decane 80 Vol.% and o-xylene 20 Vol.% shows the same autoignition and extinction behavior as JP-8 and diesel. It was shown how to calculate the activation temperature, T_a, activation energy, E_a, and frequency factor, B, using asymptotics. This technique provides an accurate and simple way to find the overall chemical-kinetic rate parameters by using experimental results of autoignition temperature and extinction strain rate.

The combustion characteristics of high molecular weight hydrocarbon fuels calculated using a semi-detailed chemical-kinetic mechanism developed by Ranzi et al. [114] is found to agree well with experimental data. The predictions of combustion characteristics of mixtures of these fuels using the semi-detailed mechanism also agrees with experimental data. The combustion characteristics of JP-8 and

90

Jet-A are similar. Surrogate C with a composition of n-dodecane 60%, methyl-cyclohexane 20%, and o-xylene 20% fits critical conditions of extinction and autoignition of JP-8 and Jet A very well. Since the percentage of the fuel in the dilution is very small (2-6%) the difference between slightly modified surrogates is also very small. The difference between surrogates that vary in one component by 5% is hard to distinguish. Surrogates that differ on one fuel with only 5% is insignificant. The results for autoignition temperatures and strain rate for extinction are in the error.

It was not possible to run Diesel fuel in the current experimental setup. Diesel will have a higher autoignition temperature and a lower extinction strain rate compared to jet fuel. The same rules to develop a surrogate fuel for diesel can be used as it was shown here for JP-8 and Jet A fuel.

Kerosene fuels as JP-8 or Jet-A can be used in reciprocal engines. Further research has to be done if kerosene fuel fulfill the lubrication requirements that are needed by the new injection systems since modern diesel fuel contains additives to increase lubrication, cleaning and so on. Studies on real engines should be conducted and both fuels compared with each other.

On the other and it is questionable if diesel could be used in turbines. Most likely diesel produces too much soot to be used in jet engines.

The fuels investigated in this work are designed to mimic the behavior of real fuel in a counterflow setup. The suggested surrogates have to be verified in different experimental setups or even real engines.

Bibliography

[1] W.D. Schulz. Oxidation products of a surrogate JP-8 fuel. *ACS Petroleum Chemistry Division Preprints*, 37(2):383–392, 1991.

[2] A. Agosta, N. P. Cernansky, D. L. Miller, T. Faravelli, and E. Ranzi. Reference components of jet fuels: Kinetic modeling and experimental results. *Experimental Thermal and Fluid Science*, 28:701–708, 2004.

[3] C. J. Montgomery, S. M. Cannon, M. A. Mawid, and B. Sekar. Reduced chemical kinetic mechanisms for JP-8 combustion. *40th AIAA Aerospace Sciences Meeting and Exhibit, Paper AIAA 2002-0036*, 2002.

[4] A. Violi, S. Yan, E. G. Eddings, A. F. Sarofim, S. Granata, T. Faravelli, and E. Ranzi. Experimental formulation and kinetic model for JP-8 surrogate mixtures. *Combustion Science and Technology*, 174:399–417, 2002.

[5] R. Edinger and S. Kaul. *Sustainable Mobility - Renewable Energies for Powering Fuel Cell Vehicles*. Praeger Publisher, 88 Post Road West, Westport, CT 06881, 2003.

[6] A. Liñán and F. A. Williams. *Fundamental Aspects of Combustion*, volume 34 of *Oxford Engineering Science Series*. Oxford University Press, New York, 1993.

[7] H.P. Lenz. *Verbrennungskraftmaschinen Grundzüge*. Institut für Verbrennungskraftmaschinen und Kraftfahrzeugbau, Vienna University of Technology, Austria, 1995.

[8] N. Peters and B. Rogg, editors. *Reduced Kinetic Mechanisms for Application in Combustion Systems*, volume m15 of *Lecture Notes in Physics*. Springer Verlag, Heidelberg, 1993.

[9] J. Bacha, L. Blondis, J. Freel, and et. all. Diesel fuels tecnical review (FTR-2). Technical Review 2, Chevron Products Company, 1998.

[10] J. Bacha, F. Barnes, M. Franklin, and et. all. Aviation fuels technical review (FTR-3). Technical Review 3, Chevron Products Company, 2000.

[11] T. Edwards. Liquid fuels and propellants for aerspace propulsion: 1903–2003. *Journal of Propulsion and Power*, 19(6), November–December 2003.

[12] TARDEC. JP-8 the single fuel forward: An information compemduim. Technical report, U.S. Army Tank-automotive and Armanents Command, May 2001.

[13] T. Edwards and L.Q. Maurice. Surrogate mixtures to represent complex aviation and rocket fuels. *Journal of Propulsion and Power*, 17(2):461–466, Jan.-Feb. 2001.

[14] C.R. Martel. Molecular weightand average composition of JP-4, JP-5, JP-8, and JET-A. *Chemical Propulsion Information Agency*, Sept. 2000.

[15] Handbook of aviation fuel properties. *Handbook of Aviation Fuel Properties*, 1983.

[16] Survery of fuels (1990-1997). June 1998.

[17] J. Yu and S. Eser. Determination of critical properties (t_c, p_c) of some jet fuels. *Industrial and Engineering Chemistry Research*, Vol. 34(No.1):404–409, 1995.

[18] D.R. Sobel and L.J. Spadaccini. Hyrdocarbon fuel cooling technologie for advanced technologoie. *American Society of Mechanical Engineers Journal of Engineering for Gas Turbines and Power*, Vol.119(No.2):344–351, April 1998.

[19] H. Wenck und C. Schneider. Dgmk-projekt 409: Chemisch-physikalische daten von otto- und dieselkraftstoffen. *DGMK Deutsche wissenschaftliche Gesellschaft fuer Erdoel, Erdgas und Kohle E.V.*, technical report, November 1993.

[20] Dipl. Ing. (FH) Horst Bauer, editor. *BOSCH, Automotive Handbook*. SAE, 5th edition, 2000.

[21] N. Ladommatos and J. Goacher. Equations for predicting the cetane number of diesel fuels from their physical properties. *Fuel*, 74(7):1083–1093, 1995.

[22] D. E. Steer. Development of the canadian general standards board (CGSB) cetane index. *SAE*, (841244), 1984.

[23] SAE Handbook. *Engines, Fuels, Lubricants, Emissions, and Noise*, volume 3. SAE, 1993.

[24] K. Owen and T. Coley. *Automotive Fuels Refernce Book*. Society of Automotive Engineers, Inc., 2nd edition, 1995.

[25] Y. Stein, R. A. Yetter, and F. L. Dryer. The autoignition behavior of surrogate diesel fuel mixtures and the chemical effects of 2-ethylhexyl nitrate (2-EHN) cetane improver. SAE Technical Paper Series 1999-01-1504, SAE, May 1999.

[26] J.A. Banard and B.A. Harwood. Slow combustion and cool flames behavior in iso-octane. *Combustion and Flame*, 21:345, 1973.

[27] J.A. Banard and B.A. Harwood. The sponteneous combustion of n-heptane. *Combustion and Flame*, 21:141, 1973.

[28] P.G. Lignola, E. Reverchon, and R. Piro. Dynamics of combustion processes of n-heptane and iso-octane and their mixtures and knocking. *Proceeding of the Combustion Institute*, 20:123, 1984.

[29] P.G. Lignola and E. Reverchon. Dynamics of n-heptane and iso-octane combustion process in a jet stirred flow reactor operating under pressure. *Combustion and Flame*, 64:177, 1986.

[30] A.R. Khan. Oxidation of industry standard fuels and blends of primary reference fuels in the low and negative temperature coefficient regions. M.s. thesis, Drexel University, Philadelphia, PA, 1998.

[31] W.R. Leppard. A comparison of olefin and paraffin autoignition chemistries: A motored engine study. *SAE Trans*, 98(892081), 1989.

[32] S. Kowalski. A study of the low and intermediate temperature oxidation chemistry of a primary reference fuel blend and two gasolines at high pressure. M.s. thesis, Princeton University, NJ, 1993.

[33] R.D. Wilk, D.N. Koert, and N.P. Cernansky. Low temperature carbon monoxide formation as a means of assessing the autoignition tendency of hydrocarbons and hydrocarbon blends. *Journal of Energy & Fuels*, 3:292, 1989.

[34] L.Q. Maurice and R.P. Lindstedt. Detailed chemical-kinetic model for aviation fuels. *Journal of Propulsion and Power*, 16(2):187–195, 2000.

[35] C.P. Wood, V.G. McDonnell, R.A. Smith, and G.S. Samuelsen. Development and application of a surrogate distillation fuel. *Journal of Propulsion and Power*, 5(4):399–405, 1989.

[36] R. P. Lindstedt and L. Q. Maurice. Detailed chemical-kinetic model for aviation fuels. *Journal of Propulsion and Power*, 16:187–195, 2000.

[37] C. J. Montgomery, M. A. Cremer, J. Y. Chen, C. K. Westbrook, and L. Q. Maurice. Reduced chemical kinetic mechanisms for hydrocarbon fuels. *Journal of Propulsion and Power*, 18:192–198, 2002.

[38] C.J. Montgomery, W. Zhao, C-J. Tam, D.R. Eklund, and J-Y. Chen. Cfd simulations of a 3-d scramjet flameholder using reduced chemical kinetic mechanisms. In *40th Joint Propulsion Conference 2004*, number AIAA 2004-3874, Florida, 2004.

[39] A.F. Sarofim, E.G. Eddings S., Yan, A. Violi, S. Granata, T. Faravelli, and E. Ranzi. Experimental formulation and kinetic modeling for jp-8 surrogate mixtures. 2nd Mediterranean Combustion Symposium, Sharm El Scheick, Egypt, 2002.

[40] F. A. Williams. *Combustion Theory*. Addison-Wesley Publishing Company, Redwood City, CA, 2 edition, 1985.

[41] R. Seiser. *Nonpremixed Combustion of Liquid Hydrocarbon Fuels*. Ph.D thesis, Technical University of Graz, 2000.

[42] H. K. Ciezki and G. Adomeit. Shock-tube investigation of self-ignition of *n*-heptane-air mixtures under engine relevant conditions. *Combustion and Flame*, 93:421–433, 1993.

[43] U. Pfahl, K. Fieweger, and G. Adomeit. Self-ignition of diesel-relevant hydrocarbon-air mixtures under engine conditions. In *Twenty-Sixth Symposium (International) on Combustion*, pages 781–789, Pittsburgh, Pennsylvanis, 1996. The Combustion Institute.

[44] J. F. Griffiths, P. A. Halford-Maw, and D. J. Rose. Fundamental features of hydrocarbon autoignition in a rapid compression machine. *Combustion and Flame*, 95:291–306, 1993.

[45] Reaction Design. *Theory Manual - Chemkin 4.0.2*, April 12 2005.

[46] T.P. Pandya and F.J. Weinberg. *Proc. Roy. Soc. London*, 279A:544, 1964.

[47] K. Seshadri and F. A. Williams. Laminar flow between parallel plates with injection of a reactant at high Reynolds number. *International Journal of Heat and Mass Transfer*, 21(2):251–253, 1978.

[48] R. Seiser, K. Seshadri, E. Piskernik, and A. Liñán. Ignition in the viscous layer between counterflowing streams: Asymptotic theory with comparison to experiments. *Combustion and Flame*, 122:339–349, 2000.

[49] H. Pitsch. Entwicklung eines Programmpaketes zur Berechnung eindimensionaler Flammen am Beispiel einer Gegenstromdiffusionsflamme. Master's thesis, RWTH Aachen, Germany, 1993.

[50] M. Bollig, H. Pitsch, J. C. Hewson, and K. Seshadri. Reduced *n*-heptane mechanism for non-premixed combustion with emphasis on pollutant-relevant intermediate species. *Proceedings of the Combustion Institute*, 26:729–737, 1996.

[51] W. Payer. Chemical-kinetic characterization of autoignition and combustion of liquid fuels. Diploma thesis, Technischen Universität Wien, Vienna, Austria, 2002.

[52] Verein Deutscher Ingenieure. *VDI-Wäermeatlas*, volume 7 erweiterte Auflage. 1994.

[53] W. Payer. Chemical-kinetic characterization of autoignition and combustion of liquid fuels. Diploma thesis, Vienna University of Technology, Austria, 2002.

[54] C. G. Fotache, T. G. Kreutz, and C. K. Law. Ignition of counterflowing methane versus heated air under reduced and elevated pressures. *Combustion and Flame*, 108:442–470, 1997.

[55] L. Q. Maurice. *Detailed Chemical Kinetic Models for Aviation Fuels*. Ph.D thesis, The University of London, 1996.

[56] R. P. Lindstedt. Modelling of the chemical complexities of flames. *Proceedings of the Combustion Institute*, 27:269–285, 1998.

[57] H. J. Curran, P. Gaffuri, W. J. Pitz, and C. K. Westbrook. A comprehensive modeling study of *n*-heptane oxidation. *Combustion and Flame*, 114:149–177, 1998.

[58] H. J. Curran, W. J. Pitz, C. K. Westbrook, C. V. Callahan, and F. L. Dryer. Oxidation of automotive primary reference fuels at elevated pressures. *Proceedings of the Combustion Institute*, 27:379–387, 1998.

[59] R. Seiser, L. Truett, D. Trees, and K. Seshadri. Structure and extinction of non-premixed *n*-heptane flames. *Proceedings of the Combustion Institute*, 27:649–657, 1998.

[60] R. Seiser, H. Pitsch, K. Seshadri, W.J. Pitz, and H.J. Curran. *Proceeding of the Combustion Institute, The Combustion Institute, Pittsburgh*, Vol.28:2029, 2000.

[61] S. P. Zeppieri, S. D. Klotz, and F. L. Dryer. Modeling concepts for large carbon number alkanes: A partially reduced skeletal mechanism for *n*-decane oxidation and pyrolysis. *Proceedings of the Combustion Institute*, 28:1587–1595, 2000.

[62] G. Bikas and N. Peters. Kinetic modelling of *n*-decane combustion and autoignition. *Combustion and Flame*, 126:1456–1475, 2001.

[63] A. Ristori, P. Dagaut, and M. Cathonnet. The oxidation of *n*-hexadecane: Experimental and detailed kinetic modeling. *Combustion and Flame*, 125:1128–1149, 2001.

[64] Z. Qin, V. V. Lissianski, H. Yang, W. C. Gardiner, S. G. Davis, and H. Wang. Combustion chemistry of propane: A case study of detailed reaction mechanism optimization. *Proceedings of the Combustion Institute*, 28:1663–1669, 2000.

[65] C. G. Fotache, H. Wang, and C. K. Law. Ignition of ethane, propane, and butane in counterflow jets of cold fuel versus hot air under variable pressures. *Combustion and Flame*, 117:777–794, 1999.

[66] M. M. Y. Waly, S. C. Li, and F. A. Williams. Experimental and numerical studies of two-stage ethane-air flames. *Journal of Engineering for gas Turbines and Power*, 122(4):651–658, 2000.

[67] H. Tsuji and I. Yamaoka. The structure of counterflow diffusion flames in the forward stagnation region of a porous cylinder. *Proceedings of the Combustion Institute*, 12:997–1005, 1969.

[68] C.K. Law. A compilation of experimental data on laminar burning velocities. In N. Peters and B. Rogg, editors, *Reduced kinetic mechanisms for applications in combustion systems*, volume m15 of *Lecture Notes in Physics*, pages 15–26. Springer Verlag, Heidelberg, 1993.

[69] C. K. Law and C. J. Sung. Structure, aerodynamics, and geometry of premixed flamelets. *Progress in Energy and Combustion Science*, 26:459–505, 2000.

[70] C. M. Vagelopoulos and E. N. Egolfopoulos. Direct experimental determination of laminar flame speeds. *Proceedings of the Combustion Institute*, 27:513–519, 1998.

[71] S. G. Davis, C. K. Law, and H. Wang. Propene pyrolysis and oxidation kinetics in a flow reactor and laminar flames. *Combustion and Flame*, 119:375–399, 1999.

[72] Y. Hidaka, T. Nishimori, K. Sato, Y. Henmi, R. Okuda, and K. Inami. Shock-tube and modeling study of ethylene pyrolysis and oxidation. *Combustion and Flame*, 117(4):755–776, 1999.

[73] C. J. Brown and G. O. Thomas. Experimental studies of shock induced ignition and transition to detonation in ethylene and propane mixtures. *Combustion and Flame*, 117(4):861–870, 1999.

[74] Z. Qin. *Shock Tube and Modeling Study of Propane Ignition.* Ph.D thesis, University of Texas at Austin, 1998.

[75] The San Diego Mechanism. http://www.mae.ucsd.edu/cecr/cermech.

[76] T. Weißweiler. Measurements of stable species and soot volume fraction in a propane-air counterflow diffusion flame. Diploma thesis, Institut für Allgemeine Mechanik, RWTH Aachen, Aachen, Germany, 1994.

[77] N. Peters. Laminar diffusion flamelet models in non-premixed turbulent combustion. *Progress in Energy and Combustion Science*, 10:319–339, 1984.

[78] B. Varatharajan and F. A. Williams. Ethylene ignition and detonation chemistry. *Journal of Propulsion and Power*, 17:624–645, 2001.

[79] B. Varatharajan and F. A. Williams. Ethylene ignition and detonation chemistry, part 2: Ignition histories and reduced mechanisms. *Journal of Propulsion and Power*, 18:352–362, 2002.

[80] H. F. Coward and G. W. Jones. Limits of flammability of gases and vapors. Technical Report Bulletin 503, U. S. Bureau of Mines, U. S. Government Printing Office, Washington, D. C., 1952.

[81] M. D. Smooke, J. Crump, K. Seshadri, and V. Giovangigli. Comparison between experimental measurements and numerical calculations of the structure of counterflow, diluted, methane-air, premixed flames. In *Twenty-Third Symposium (International) on Combustion*, pages 463–470. The Combustion Institute, Pittsburgh, PA, 1990.

[82] J. Warnatz, U. Maas, and R.W. Dibble. *Combustion - Physical and Chemical Fundamentals, Modeling and Simulation, Experiments, Pollutant Formation.* Springer Verlag, 2000.

[83] U. Niemann. The influence of cetane improvers on autoignition and extinction of nonpremixed flames burning high molecular weight hydrocarbon fuels and diesel. Diploma thesis, Technischen Universität Wien, Vienna, Austria, 2006.

[84] N. Peters. Flame calculations with reduced mechanisms - an outline. In N. Peters and B. Rogg, editors, *Reduced Kinetic Mechanisms for Applications in Combustion Systems*, volume m15 of *Lecture Notes in Physics*, chapter 1, pages 1–13. Springer-Verlag, Heidelberg, 1993.

[85] A. Liñán and F. A. Williams. Ignition in an unsteady mixing layer subject to strain and variable pressure. *Combustion and Flame*, 95:31–46, 1993.

[86] A. Liñán. The asymptotic structure of counterflow diffusion flames for large activation energies. *Acta Astronautica*, 1:1007–1039, July 1974.

[87] R. Minetti, M. Carlier, M. Ribaucour, E. Therssen, and L. R. Sochet. A rapid compression machine investigation of oxidation and auto-ignition of n-Heptane: Measurements and modeling. *Combustion and Flame*, 102:298–309, 1995.

[88] In J. W. Hudgens, editor, *Workshop on Combustion Simulation Databases for Real Transportation Fuels*. NIST Gaithersburg, Maryland, September 2003.

[89] E. Ranzi, T. Faravelli, A. Frassoldati, and S. Granata. Wide range kinetic modeling study of pyrolysis and combustion of heavy n-alkanes. *IEC*, 44:5170–5183, 2005.

[90] T. Edwards. "Real" kerosene aviation and rocket fuels: Compositions and surrogates. *2001 Fall Technical Meeting, Eastern States Section of the Combustion Institute*, 2001.

[91] C. Guéret, M. Cathonnet, J. C. Boettner, and F. Gaillard. Experimental study and modeling of kerosene oxidation in a jet-stirred flow reactor. In *Twenty-Third Symposium (International) on Combustion*, pages 211–216, Pittsburgh, Pennsylvania, 1990. The Combustion Institute.

[92] P. Dagaut, M. Reuillion, J. C. Boettner, and M. Cathonnet. Kerosene combustion at pressures up to 40 atm: Experimental study and detailed chemical kinetic modelling. *Proceedings of the Combustion Institute*, 25:919–926, 1994.

[93] P. M. Patterson, A. G. Kyne, M. Pourkashanian, and A. Williams. Combustion of kerosene in counterflow diffusion flames. *Journal of Propulsion and Power*, 16:453–460, 2000.

[94] A. Cox, J. F. Griffiths, C. Mohamed, H. J. Curran, W. J. Pitz, and C. K. Westbrook. Extents of alkane combustion during rapid compression leading to single- and two-stage ignition. In *Twenty-Sixth Symposium (International) on Combustion*, pages 2685–2692, Pittsburgh, Pennsylvania, 1996. The Combustion Institute.

[95] J. F. Griffiths, P. A. Halford-Maw, and C. Mohamed. Spontaneous ignition delays as a diagnostic of the propensity of alkanes to cause engine knock. *Combustion and Flame*, 111:327–337, 1997.

[96] P. G. Lignola, F. P. Di Maio, A. Marzocchella, R. Mercogliana, and E. Reverchon. JSFR combustion processes of *n*-heptane and isooctane. In *Twenty-Second Symposium (International) on Combustion*, pages 1625–1633, Pittsburgh, Pennsylvania, 1988. The Combustion Institute.

[97] A. E. Bakali, M. B. Unkhoff, P. Dagaut, P. Frank, and M. Cathonnet. Detailed kinetic reaction mechanism for cyclohexane oxidation at pressure up to ten atmospheres. *Proceedings of the Combustion Institute*, 28:1631–1638, 2000.

[98] C. Douté, J. L. Delfau, R. Akrich, and C. Vovelle. Experimental study of the chemical structure of low-pressure premixed *n*-heptane-O_2-Ar flames. *Combustion Science and Technology*, 124:249–276, 1997.

[99] R. Seiser, H. Pitsch, K. Seshadri, W. J. Pitz, and H. J. Curran. Extinction and autoignition of *n*-heptane in counterflow configuration. *Proceedings of the Combustion Institute*, 28:2029–2037, 2000.

[100] J. D. Blouch and C. K. Law. Non-premixed ignition of *n*-heptane and isooctane in a laminar counterflow. *Proceedings of the combustion Institute*, 28:1679–1686, 2000.

[101] S. G. Davis and C. K. Law. Laminar flame speeds and oxidation kinetics of *iso*-octane-air and *n*-heptane-air flames. *Proceedings of the Combustion Institute*, 27:521–527, 1998.

[102] W. Tsang. Progress in the development of combustion kinetics databases for liquid fuels. *Data Science Journal*, (2004) 3(1-9), 2004.

[103] S. Granata, T. Faravelli, and E. Ranzi. A wide range kinetic modeling study of the pyrolysis and combustion of naphthenes. *Combustion and Flame*, 132:533–544, 2003.

[104] A. Cooke, M. Bellucci, M. D. Smooke, A. Gomez, A. Violi, T. Faravelli, and E. Ranzi. Computational and experimental study of a jp-8 counterflow diffusion flame. *Proceedings of the Combustion Institute*, 30:439–446, 2005.

[105] Chemical Kinetics Database on the Web. http://kinetics.nist.gov/index.php.

[106] C. Venkat, K. Brezinsky, and I. Glassman. High temperature oxidation of aromatic hydrocarbons. *Proceedings of the Combustion Institute*, 19:143–152, 1982.

[107] J.L.Emdee, K. Brezinsky, and I. Glassman. Oxidation of o-xylene. *Twenty third Symposium (International) on Combustion, The Combustion Institute*, pages 77–84, 1990.

[108] K. Brezinsky. The high temperature oxidation of aromatic hydrocarbons. *Progr. Energy Combustion Science*, 12:1–24, 1986.

[109] S. Gail and P. Dagaut. Experimental kinetic study of p-xylene in a jsr and comprehensive detailed chemical modeling. *Combustion and Flame*, 141(3):281–297, 2005.

[110] D.F. Davidson, B.M. Gauthier, and R.K. Hanson. *Proceeding of the Combustion Institute*, 30:1175–1182, 2005.

[111] A. Roubaud, O. Lemaire, R. Minetti, and L. R. Sochet. High pressure auto-ignition and oxidation mechanisms of o-xylene, o-ethyltoluene, and n-butylbenzene between 600 and 900 K. *Combustion and Flame*, 123:561–571, 2000.

[112] S. D. Klotz, K. Brezinsky, and I. Glassman. Modeling the combustion of tolune-butane blends. *Proceedings of the Combustion Institute*, 27:337–344, 1998.

[113] S. Zeppieri, K. Brezinsky, and I. Glassman. Pyrolysis studies of methylcyclohexane and oxidation studies of methylcyclohexane and methylcyclohexane/tolune blends. *Combustion and Flame*, 108:266–286, 1997.

[114] http://www.chem.polimi.it/CRECKModeling.

[115] A.E. Lutz, R.J. Kee, J.F. Grcar, and F.M. Rupley. Technical Report SAND96-8243, Sandia National Laboratories, 1997.

[116] H.G. Im, L.L. Raja, R.J. Kee, and L.R. Petzold. A numerical study of transient ignition in a counterflow nonpremixed methane-air flame using adaptive time integration. *Combustion Science Technologies*, 158:341–364, 2000.

[117] P. Frank, J. Herzler, Th. Just, and C. Wahl. High-temperature reactions of phenyl oxidation. *Proceedings of the Combustion Institute*, 25:833–840, 1994.

[118] Department of Defense. *MIL-DTL-83122E - Detailed Specification - Turbine Fuels, Aviation, Kersosen Types, NATO F-34 (JP-8), NATO F-35, and JP-8+100*, April 1999.

[119] Ministry of Defence. *Defence Standard 91-87: Turbine Fuel, Aviation Kerosine Type: Containing Fuel System Icing Inhibitor, NATO Code: F-34, Joint Service Designation: AVTUR/FSII*, 5 edition, July 2005.

Appendix A

A.1 Fuels and Gases

The experiments reported in this work were performed using gas phase mixtures of air, nitrogen and fuel. The air was delivered by an in-house system with a pressure of 80 psi. All other gases were delivered in compressed 228 cubic feet bottles by Airgas, Inc. with a C.P. grade.

Table A.1: List of liquid fuels and suppliers

FUEL	GRADE	SUPPLIERS	CODE
cyclohexane	99+%	ACROS Organics [1]	NA
n-Decane	99+%	SigmaAldrich [2]	D90-1
Diesel	NA	Mobile	NA
n-Dodecane	99%	Fisher Scientific [3]	02666-500
Heptane	min. 98%	EM Science [4]	UN1206
Hexadecane	99.4%	Fisher Scientific [3]	03035-500
n-Octane	99+%	SigmaAldrich [2]	29,698-8
iso-Octane	99.9%	Fisher Scientific [3]	0296-4
Toluene	99.9%	Fisher Scientific [3]	T324-4
o-Xylene	NA	Fisher Scientific [3]	05081-4
2,2,4,4,6,8,8- heptamethylnonane	NA	SigmaAldrich [2]	

[1] ACROS Organics, ordered via Fisher Scientific
[2] Sigma-Aldrich, P.O. Box 2060, Milwakee, WI 53201
[3] Fisher Scientific International Inc., Liberty Lane, Hampton, NH 03842
[4] EM Science, a Div. of EM Industries Inc. 480 S. Democrat Rd.,Gibbstown, NJ 08027-1297

A.1.1   Physical and chemical Properties of tested Jet Fuels

Table A.2: Physical and chemical properties of tested
JP-8 and Jet A fuel given by the accompanied material
safety sheet.

00POSF 3773   JP-8

Manufaturer	Ashland Petroleum Company	
Components	Petroleum distillate	>95 %
	xylene mix	0.5-1.5 %
	napthalene	0.5-1.5 %
	biphenyl	0.4-1.2 %

Physical and chemical properties

	flash point	> 100.0 degF (37.8 degC)
	boiling range	350-360 degF @ 760 mmHg
	specific gravity	0.775-0.840 @ 60 degF (15.5 degC)

99POSF 3602 and 04POSF 4658   Jet A

Components	saturated hydrocarbons	70-80 weight %
	aromatic hydrocarbons	17-20 weight %
	unsaturated hydrocarbons	3-6 weight %

Physical and chemical properties

	flash point	120-190 degF
	autoignition temp.	489 degF
	appearance	clear to amber liquid
	molecular weight	180
	boiling range	360-550 degF
	specific gravity	0.8
	density	6.78 lbs/gal
	vapor pressure	1-10 mmHg at 100 degF
	viscocity	1.3-2.1 at 50 degC

99POSF 3638   Jet A

Manufaturer	Chevron Phillips Chemical Company Lp.	
Components	kerosene	100 weight%
	paraffinic hydrocarbons	> 50 weight%
	n-octane	> 1 weight%
	n-nonane	> 3 weight%
	naphthenes	< 33 weight%
	aromatic hydrocarbons	< 17 weight%
	benzene	< 0.8 weight%
	toluene	< 1.0 weight%

p-xylene			< 1.0 weight%
m-xylene			< 3 weight%
o-xylene			< 1.4 weight%
1,3,5-trimethylbenzene			< 1.4 weight%
1,2,4-trimethylbenzene			< 3.8 weight%
1,2,3-trimethylbenzene			< 1.2 weight%
sulfur compounds			< 0.3 weight%

Physical and chemical properties

appearance	colcoless liquid
boiling range	300-572 degF (149-300 degC)
vapor pressure	< 1
specific gravity	0.775-0.840
viscosity	8 cSt at -4 degF (-20 degC)
flash point	100-150 degF (38-66 degC)

Fuel		Jet A		JP-8		JP-8 average	
		99POSF 3602	99POSF 3638	02POSF 4177	00POSF 3773		
Aromatics	Vol.%	24	12	16.3	15.9	17.37	± 2.96
Alkenes	Vol.%	0.9	1.4	0.9	0.7	1.15	± 0.68
Naphthalenes	Vol.%			1.0		1.46	± 0.65
Hydrogen Content	mass%			13.7	13.9	13.8	± 0.22
API Gravity		41.1	46.1	42.4	45.8	44.07	± 2.10
Total Sulfur	mass%	0	0	0.14	0.07	0.058	± 0.049

A.2 Cetane Number, Cetane Index

The cetane number can be achieved by mixing hexadecane (aka. cetane, CN = 100) and 2,2,4,4,6,8,8-heptamethylnonane (CN = 15). A linear mixing was assumed as described in equation 2.1.
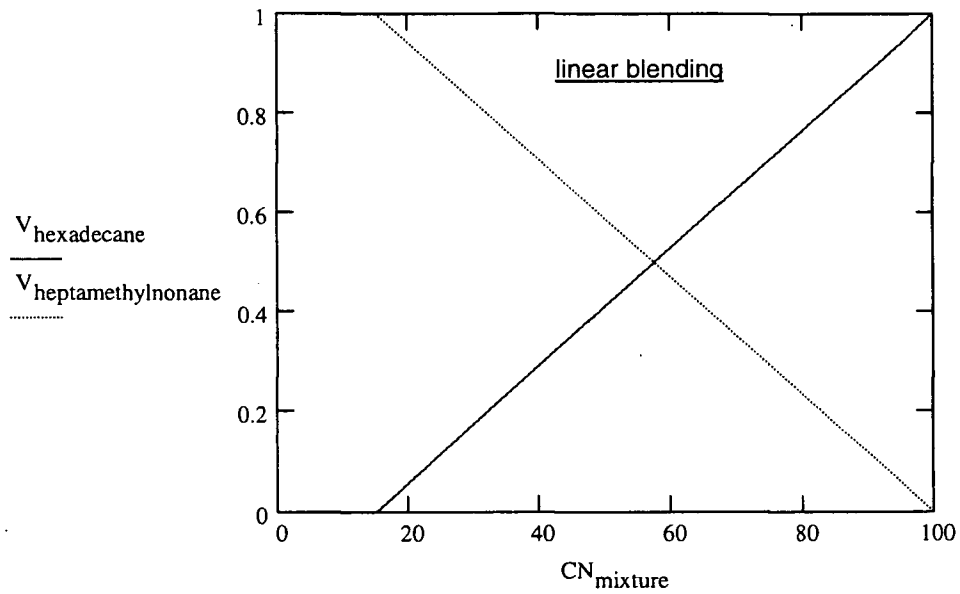
Figure A.1: Linear blending of 2,2,4,4,6,8,8-heptamethylnonane (CN=15) and hexadecane (CN=100) to get a certain cetane number.

Appendix B

B.1 Norm and Properties of Diesel, JP-8, and Jet A

Table B.1: European Diesel fuel Specification, EN 590:1993

Properties applying to all Grades	Limit	Method
Flash Point (°C) min	55	ISO 2719
Ash (%mass) max	0.01	EN 26245
Water (mg/kg) max	200	ASTM D1744
Particulate (mg/l) max	24	DIN 51419
Copper Corrosion (3h at 50 °C) max	1	ISO 2160
Oxidation Stability (g/m^3) max	25	ASTM D2274
Sulfur (% mass) max	0.20 [1]	EN 24260 / ISO 8754
Carbon Residue (%mass) max	0.30 [2]	ISO 10370

Arctic Grades	0	1	2	3	4
CFPP, max	-20	-26	-32	-38	-44
Cloud Point (°C) max	-10	-16	-22	-28	-34
Density (kg/m^3) at 15°C	800-845	800-845	800-840	800-840	800-840
Viscocity (mm^2/s) at40°C	1.50-4.00	1.50-4.00	1.50-4.00	1.40-4.00[4]	1.20-4.00[4]
Cetane Number, min	47	47	46	45	45
Cetane Index	46	46	46	43	43
Distillation (°C)					
10% Vol rec at, max	180	180	180	180	180
50% Vol rec at	Report	Report	Report	Report	Rreport
95% Vol rec at	340	340	340	340	340

Table B.2: Temperature Climate Grades for Diesel - Spec. EN 590

Temperate Climate Grades A to F	Limit	Method
CFPP, max	No.3	EN 116
Density (kg/m^3) at 15°C	820-860	ISO 3675 / ASTM D4052
Viscosity (mm^2/s) at 40°C	2.00-4.50	ISO 3104
Cetane Number, min	49	ISO 5165
Cetane Index, min	46	ISO 4264
Distillation (°C)		ISO 3405
10% Vol. rec at	Report	
50% Vol. rec at	Report	
65% Vol. rec at, min	250	
85% Vol. rec at, max	350	
95% Vol. rec at, max	370	

[1] Sulfur limit will be reduced toward 0.05% mass maximum, in line with EU directives or national standards.

[2] Based on fuel without ignition improver additives. If a higher value is found, fuel should be tested by ASTM D4046 for presence of nitrates. If present, the limit does not apply.

[3] Six grades, with CFPP limits from +5 to -20C in 5C intervals.

[4] Arctic classes may exhibit poor lubricity characteristics and corrective measures (lubricity additives) may have to be used.

[5] EN 590 is currently being revised applying the Unique Acceptance Procedure to include the new sulfur content of 0.05% mass maximum and new lubricity requirement of 460 maximum wear scar diameter using test method CEC-F-06-A-96.

Table B.3: US Diesel Fuel Specification [9]

Property	Test Method ASTM	#2 Diesel Fuel	California Reformulated Test Diesel	#1 Diesel Fuel
Appearance		Clear to tan or Red Dye[2]	clear or Red Dye[2]	clear to tan or Red Dye[2]
Cetane No., min	D 613	40	48[1]	40
Cloud Point, °F, min	D 2500	seasonal by location	seasonal by location	seasonal by location
Viscocity, cSt at 40 °C, min.-to- max. [3]	D 455	1.9 - 4.1	2.0 - 4.1	1.3 - 2.4
Gravity, API min	D 4502		33 - 39	
Copper Strip Corrosion, max	D 130	No.3	No.3	No.3
Flash Point, PMCC, °F	D 93	125 (land), 140 (marine)	130	100
Distillation, °F	D 86			
Initial Boiling Point, min -to- max			340-400	550
90% Recovered, min -to- max[3]		540-640	580-660	
Sulfur, % mass, max.	D 2622			
On Road (EPA)		0.05		0.50

Continued on Next Page...

Table B.3 – Continued

Property	Test Method ASTM	#2 Diesel Fuel	California Reformulated Test Diesel	#1 Diesel Fuel
Off Road (High Sulfur)		0.50		
Vehicle (CARB)			0.050[1]	
Non-Vehicle (High Sulfur)			0.50	
Aromatics, Vol.%	D 1319	35	10[1]	

[1] CARB regulation limits the aromatics to 10-volume % maximum based on 90 day averaging or permits the use of a CARB certified "alternate diesel" formulation. CARB alternate formulations specify the sulfur, cetane number, aromatics, nitrogen and PNA limits. The supplier must confirm that the product is certified per Title 13, California Code of Regulations, Sections 2281 and 2282. CARB originally designated D 1319 as the required test for aromatics. The CARB diesel limits and D 1319 are expressed in volume %. Unfortunately D 1319 was not designed for diesel fuel and has poor reproducibility. For this reason, CARB later allowed the use of a more precise test, D 5186. D 5186 results come in mass %. Therefore, D 5186 results must be converted to volume % using the CARB approved equation: D 1319 (volume %) = 0.916D 5186 (mass %) + 1.33. If the D 5186 test apparatus is not available, the D 1319 results may be used. CARB "alternate diesel formulas" must have aromatics reported in "mass %" using D 5186.

[2] High sulfur diesel must be dyed red at the refinery (EPA regulation). According to IRS regulations this fuel must contain Dye Solvent 164 at a concentration spectrally equivalent to 3.9 pounds per thousand barrels (PTB) (11.13 mg/liter) of solid dye Standard Solvent Red 26. Low sulfur diesel, both EPA and CARB, are generally on road diesels and consequently undyed. However, if they are sold as non-taxable diesel or heating fuel they must be dyed to the above concentration.

[3] In addition to a 90% point specification, some pipeline companies impose a maximum end point specification of 690 F on shippers on the pipeline.

Table B.4: Comparison of US, European, and Japanese Specification for comparable Grade of Diesel fuel. [9]

Property	US: ASTM D 975, Low Sulfur No.2-D	Europe: CEN 590: Grades A-F	Japan: JIS K 2204, Grade No.2
Density at 15°C, g/cm^3		0.820-0.860	
Kinematic Viscocity			
38°C, cSt			2.0 min
40°C, cSt	1.9-4.1	2.0-4.5	
Sulfur, %mass, max	0.05	0.05	0.05
Cetane No., min	40	49	45
Distillation temperature, °C			
% vol recovered			
65		250 min	
85		350 min	
90	282-338		330-350
95		370 max	

Table B.5: MIL-DTL-83133E - Chemical and physical requirements and test methods for F-35 (JP-8). [118]

Property	Min	Max	Test Methods ASTM Standards
Color, Saybolt		[1]	D156[2] or D6045
Total Acid number, mg KOH/gm		0.015	D3242
Aromatics, Vol.%		25.0	D1319
Sulfur, total, mass %		0.30	D129, D1266, D2622, D3120, D4294[2] or D5453
Sulfur Mercaptant, mass %		0.002	D3227
or			
Doctor Test		negative	D4952
Distillation Temperature, °C[3] (D2887 limits given in parentheses)			D86[2], D2887
Initial boiling point		[1]	
10 % recovered		205 (186)	
20 % recovered		[1]	
50 % recovered		[1]	
90 % recovered		[1]	
End point		300 (330)	
Residue, Vol.%		1.5	
Loss, Vol.%		1.5	
Flash point, °C	38	[4]	D56, D93[2] or D3828[4]
Density or Gravity			
Density, kg/L at 15 °C	0.775	0.840	D1298 or D4052 [2]
or			
Gravity, API at 60°F	37.0	51.0	D1298
Freezing point, °C		-47	D2386[2], D5901 or D5972
Viscosity, at -20°C, mm²/s		8.0	D445
Net heat of combustion, MJ/kg	42.8		D3338[5] or D4809[2]

Continued on Next Page...

Table B.5 – Continued

Property	Min	Max	Test Methods ASTM Standards
Hydrogen content, mass %	13.4		D3701[2], D3343
Smoke Point, mm	25.0		D1322
or			
Smoke Point, mm, AND	19.0		D1322
Naphthalene.Vol.%		3.0	D1840
Calculated Cetane Index		[1]	D976[6]
Copper strip corrosion, 2hr at 100°C		No.1	D130
Thermal stability			D3241[7]
change in pressure drop, mmHg		25	
heater tube deposit, visual rating		<3[12]	
Existent gum, mg/100ml		7.0	D381
Particulate matter, mg/L		1.0	D2276[8] or D4552[2]
Filtration time, minutes		15	[8]
Water reaction interference rating		1 b	D1094
Water separation index	[9]		D3948
Fuel system icing inhibitor, Vol.%	0.10	0.15	D5006[10]
Fuel electrical conductivity, ps/m	[11]	[11]	D2624

[1] To be reported - not limited. [2] Referee Test Method. [3] A condenser temperature of 0°C to 4°C shall be used for the distillation by ASTM D 86. [4] ASTM D56 may give results up to 1°C below ASTM D93 results. ASTM D3828 may give results up to 1.7°C below ASTM D93 results. Method IP170 is also permitted. [5] When the fuel distillation test is performed using ASTM D 2887, the average distillation temperature, for use in ASTM D3338 shall be calculated as follow: V=(10%+50%+95%)/3. [6] Mid-boiling temperature may be obtained by either ASTM D86 or ASTM D2887 to perform the cetane index calculation. ASTM D86 values should be corrected to standard barometric pressure. [7] See 4.5.3. for ASTM D3241 test conditions and test limitations. [8] A minimum sample size of 3.79 liters (1 gallon) shall be filtered. For more information see [118]. [9] The minimum microseparometer rating using a Micro-Separometer shall be as follows: see [118]. [10] Test shall be performed in accordance with ASTM D5006 using DiEGME scale of the refractometer. [11] The conductivity must be between 150 and 450 pS/m for F-34 (JP-8) and between 50 and 450 pS/m for F-35, at ambient temperature or 29.4°C,

whichever is lower, unless otherwise directed by the procuring activity. In the case of JP-8+100 with the thermal stability improver additive, the conductivity limit must be between 150 to 700 pS/m at ambient temperature of 29.4 °C, whichever is lower, unless otherwise directed by the procuring activity. [12] Peacock or Abnormal color deposits results in a failure.

Table B.6: Excerpt from Defence Standard 91-87, Issue 5, Turbine Fuel, Aviation Kerosine Type: Containing Fuel System Icing Inhibitor, NATO Code: F-34, Joint Service Designation: AVTUR/FSII.[119]

Test	Property	Unit	Limit	Method
1	Appearance			
1.1	Visual Appearance		Clear, bright and visually free from solid matter and undissolved water at ambient temperature	Visual
1.2	Colour	Report		ASTM D156 or ASTM D6045
1.3	Particulate Contamination, at point of manufacturing	mg/l	max. 1.0	IP423/ ASTM D5452
2	Composition			
2.1	Total Acidity	mg KOH/g	max 0.015	IP354/ ASTM D3242
2.2	Aromatic Hydrocarbon Types			
2.2.1 or	Aromatics	%v/v	max 25.0	IP 156/ ASTM D1319
2.2.2	Total Aromatics	% v/v	max 26.5	IP 436/ ASTM D6379
2.3	Sulphur, total	% m/m	max 0.30	IP 336
2.4	Sulphur, Mercaptan	% m/m	max 0.0030	IP 342/ ASTM D3227
2.5	Doctor Test		Doctor Negative	IP 30
2.6	Refining Components, at point of manufacture			
2.6.1	Hydroprocessed Components	% v/v	Report	
2.6.2	Severely Hydroprocessed Components	% v/v	Report	
3	Volatility			
3.1	Distillation			IP 123/ ASTM D86
3.1.1	Initial Boiling Point	°C	Report	

Continued on Next Page...

Table B.6 – Continued

Test	Property	Unit	Limit	Method
3.1.2	10% Recovery	°C	max 205.0	
3.1.3	50% Recovery	°C	Report	
3.1.4	90% Recpvery	°C	Report	
3.1.5	Final Point	°C	max 300.0	
3.1.6	Residue	% v/v	max 1.5	
3.1.7	Loss	% v/v	max 1.5	
3.2	Flash Point	°C	min 38.0	IP 170
3.3	Density at 15°C	kg/m^3	min 775.0 max 840.0	IP 365/ ASTM D4052
4	Fluidity			
4.1	Freezing Point	°C	max -47.0	IP 16/ ASTM D2386
4.2	Viscocity at -20°C	mm^2/s	max 8.000	IP 71/ ASTM D445
5	Combustion			
5.1	Smoke Point	mm	min 25.0	IP 57/ ASTM D1322
or				
5.2	Smoke Point	mm	min 19.0	IP57 / ASTM D1322
	and Naphthalenes	% v/v	max 3.0	ASTM D1840
5.3	Specific Energy	MJ/kg	min 42.80	
6	Corrosion			
6.1	Copper Strip	Class	max 1	IP 154/ ASTM D130
7	Thermal Stability, JFTOT			IP 323/ ASTM D3241
7.1	Test Temperature	°C	min 260	
7.2	Tube Rating Visual		less than 3. no Peacock (P) or Abnnormal (A)	
7.3	Pressure Differential	mm Hg	max 25	
8	Contaminants			
8.1.1	Existent Gum	mg/100ml	max 7	IP 131/ ASTM D381
or				
8.1.2	Existent Gum with Air	mg/100ml	max 7	IP 131/ ASTM D381
9	Water Separation Characteristics			

Continued on Next Page. . .

Table B.6 – Continued

Test	Property	Unit	Limit	Method
9.1	Microseparometer, at Point of Manufacture			ASTM D3948
9.1.1	MSEP without SDA	Rating	min 85	
9.1.2	MSEP with SDA	Rating	min 70	
10	Conductivity			
10.1	Electrical Conductivity	pS/m	min 50, max 600	IP 271/ ASTM D2624

Appendix C

C.1 Fuel Chemistry

C.2 Combustion of Hydrocarbons

In an ideal combustion process, hydrocarbons (no matter what type) are converted into water and carbon dioxide when ignited in the presence of oxygen. Equation C.1 shows the process for n-heptane.

$$C_7H_{16} + 11O \longrightarrow 7CO_2 + 8H_2O \qquad (C.1)$$
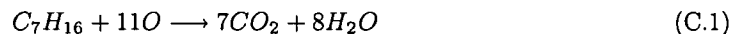
The molecular weight of carbon is 12, the one of hydrogen is 1, and oxygen has a molecular weight of 16. So it can be calculated that 100 grams of n-heptane reacts with 352 grams of oxygen to form 308 grams of carbon dioxide and 144 grams of water. This ration between oxygen and hydrocarbons is known as the stoichiometric ration when combusted under ideal conditions. In reality air is used instead of pure oxygen. This translates the ration of 3.52:1 to 15:1 for air for the combustion of n-heptane on a weight basis. For gasoline a ration of 14.5:1 is required to burn under stoichiometric condition. Although the correct ratio can be only determined on the exact composition of the fuel.

Since air is used instead of pure oxygen, combinations of nitrogen and oxygen are formed under the high temperature reached during the combustion process. Three common oxides are formed, usually referred as NO_x.

Is less than the stoichiometric amount of air present (rich condition) a mixture of carbon monoxide and carbon dioxide and water is formed as a result of the combustion process. If there is too much air present then necessary for a stoichiometric combustion process (lean condition) the formed carbon monoxide will be very low but the NO_x will be high. Figure C.1 shows this controversy relation ship. Since the air-fuel mixture is in reality not totaly homogeneous and the flame gets quenched near the cylinder wall at the cylinder head, the combustion process does not follow the theoretical equation. In addition are several minor impurities present in the fuel that reacts and forms additional combustion products.

C.2.1 Hydrocarbons

These compounds contain, as already the name indicates, carbon and hydrogen only, but there are many thousands of different possibilities depending on how the atoms arrange. The simplest hydrocarbon is methane (CH_4).

The power between atoms depends on the number of electrons in its outer shell. When the outer shell is full, either by sharing electrons with other atoms (covalent binding) or by having
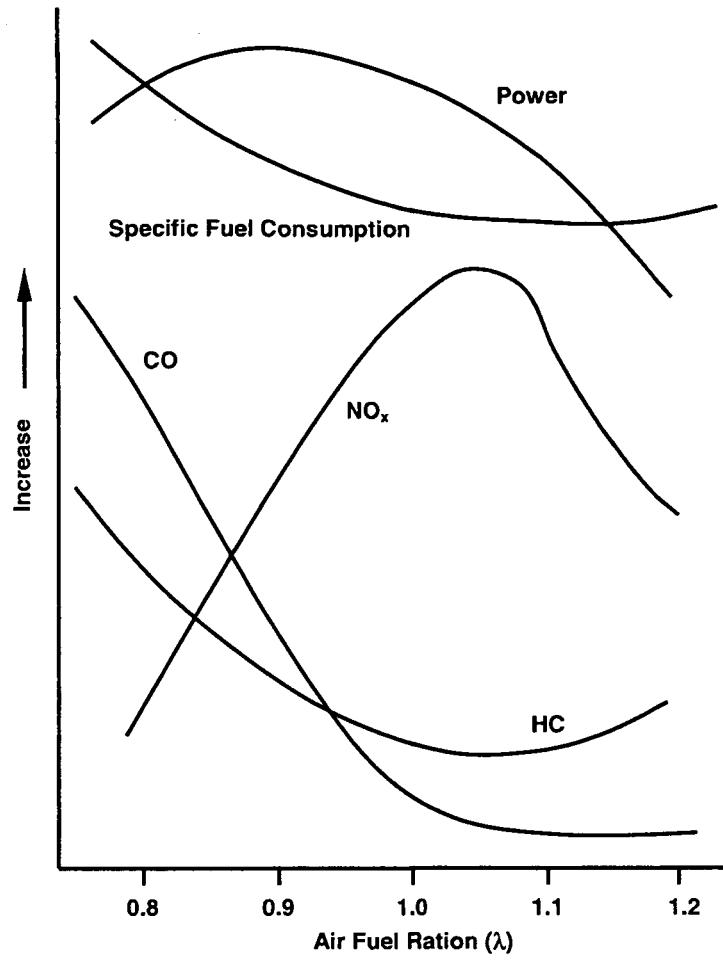
Figure C.1: Influence of air-fuel ration on exhaust emissions.
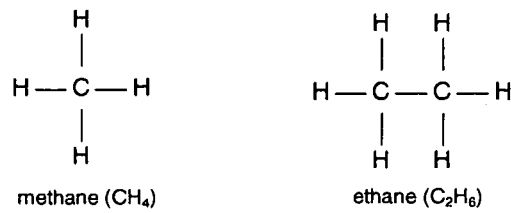
Figure C.2: Chemical structure of hydrocarbons.

electrons donated by another atom (ionic binding), a relative stable chemical compound results. The stability will depend on the strength of the chemical bonds.

Carbon can combine with itself with single, double, and triple bonds. Saturated hydrocarbons have only single bonds, unsaturated ones have double and triple bonds. Unsaturated hydrocarbons react more easily with other components as oxygen.

C.2.2   Paraffins (Alkenes), C_nH_{n+2}

This class consists of a series of saturated hdrocarbons. Methan is the simples member of this group. The carbon atoms can be in a straight line or as branched components. Branched compounds have the same chemical formla but are known as isomers and have different chemical properties as boiling point, octane quality, ... The group CH_3 is called methyl group and can bind instead of the hydrogen.

$$CH_3 \cdot CH_2 \cdot CH_2 \cdot CH_3 \qquad\qquad CH_3 \cdot CH \cdot CH_3$$
$$|$$
$$CH_3$$

n-butane   isobutane or 2-methylpropane
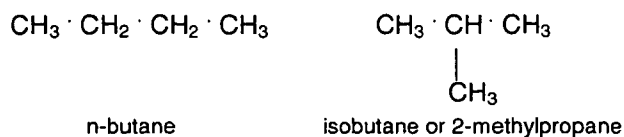
Figure C.3: Chemical structure of paraffins.

C.2.3   Cycloparaffins (Naphthalenes), C_nH_{2n}

In this group CH_2-atoms are arranged in a circle as the name indicates already. Most stable structures, which gives the minimum of distortion of the carbon bond angles, have either five or six carbon atoms. The hydrogen attached to each carbon atom can be replaced by methyl or other groups.

$$CH_2 - CH_2 \qquad\qquad\qquad CH_2$$
$$|\quad\quad| \qquad\qquad\qquad / \quad\quad \backslash$$
$$CH_2 - CH_2 \qquad\qquad CH_2 \qquad CH_2$$
$$\qquad\qquad\qquad\qquad\qquad | \qquad\qquad |$$
$$\qquad\qquad\qquad\qquad CH_2 - CH_2$$

cyclobutane   cyclopentane
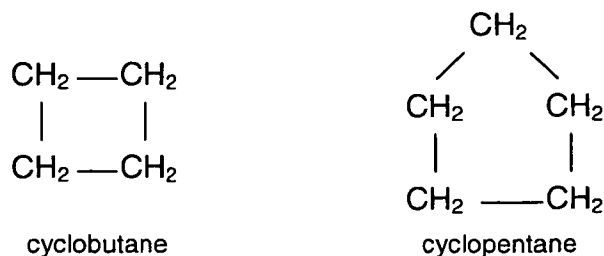
Figure C.4: Chemical structure of cycloparaffins.

C.2.4   Alkenes (Olefins), C_nH_{2n}

This group of fuels has the same carbon to hydrogen ratio and also the general formula as the class of cycloparaffins, but there chemical characteristics are different. The carbon atoms are in

a straight line or branched with one or more double bond. The position of the double bond is indicated by the number of the first carbon atom to which it is attached. The double bond in this group is very reactive and therefore easy to oxidize.

$$CH_2 = CH \cdot CH_2 \cdot CH_2 \cdot CH_3$$
1-pentene
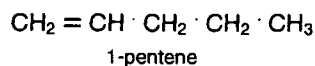
Figure C.5: Chemical structure of alkenes.

C.2.5   Aromatic Hydrocarbons, C_nH_{2n-6}

This class got its name because some of these components have an pleasant "aromatic" smell. The group has six carbon atoms arranged in a sexangle with apparently double bonds. The simples member is benzene C_6H_6. These aromatic rings are not very reactive as other components with double bonds. That's because the double bond behave as they were not in a fixed position and resonates between the two possible positions. Also several aromatic rings can merge together and form polynumeric aromatics.

benzene   which can be written as   or

naphthalene
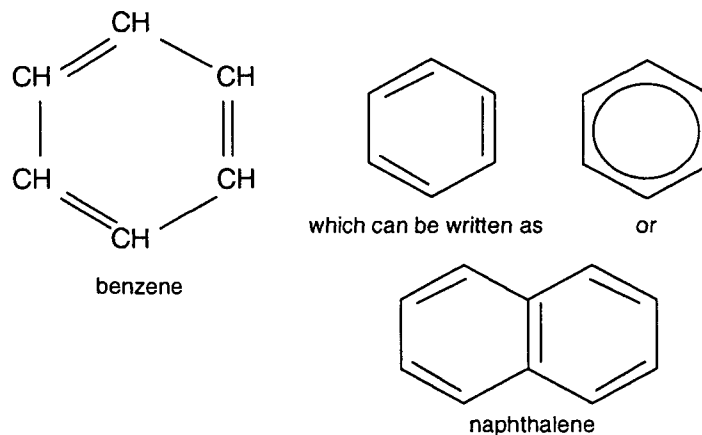
Figure C.6: Chemical structure of aromatic hydrocarbons.

C.3   Combustion of Oxygenates

Oxygenates requires proportionally less oxygen for ideal combustion. Equation shows the chemical formula for ideal combustion of methanol.

$$2CH_3OH + 3O \longrightarrow 2CO_2 + 4H_2 \tag{C.2}$$
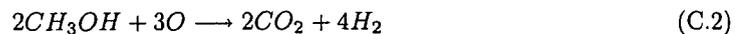
It can bee seen that if methanol or any other oxygenate is mixed with gasoline and used in engine calibrated for hydrocarbon fuels, there will be an excess of oxygen present which will reduce the

formation of carbon monoxide and unburned hydrocarbons in the exhaust gases provided that the mixture is within the flammable range.

C.3.1   Alcohols

Alcohols are hydrocarbons with one or more additional OH-group. Their common formula is $C_nH_{2n+1}OH$. This additional OH-group gives the characteristic properties as solubility in water. Alcohols are used in automotive fuels and fuel component. Methanol (CH_3OH) is the simplest molecule in this group.

C.3.2   Ethers

Alkyl ethers are isomeric with the monohydric alcohols, but contain oxygen linked to two alkyl groups instead of to one alkyl group and a hydrogen atom. Their chemical formula is $(C_nH_{2n+1})_2O$.

Appendix D

D.1 Further Results

D.1.1 Arrhenius Plot
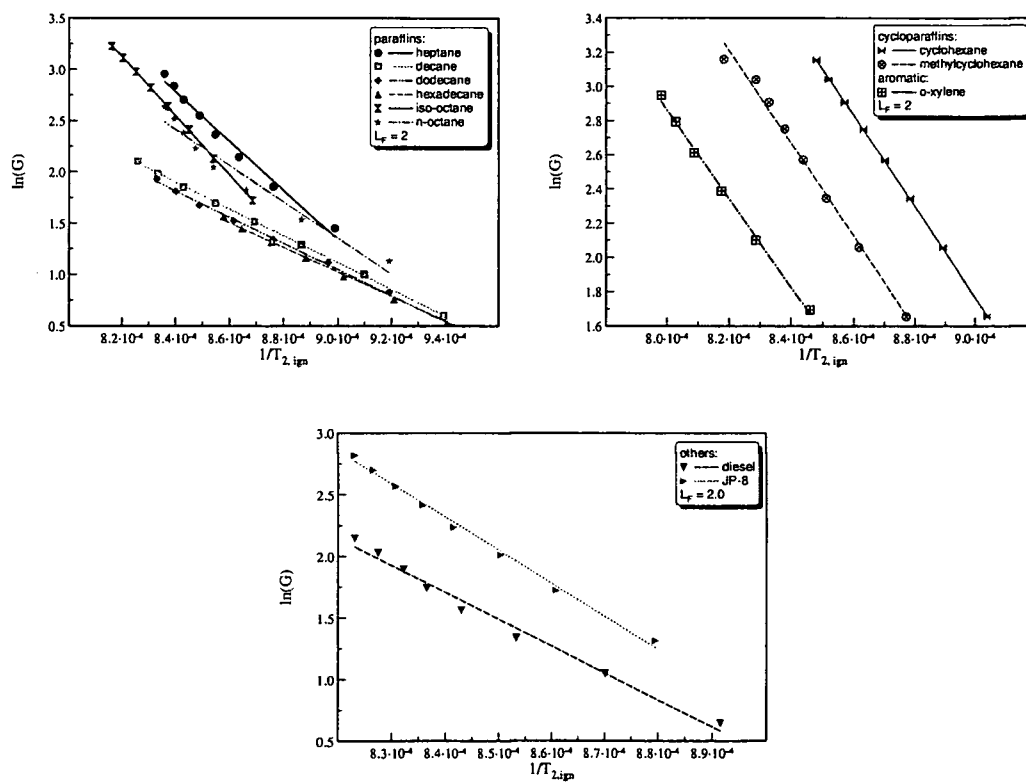
Figure D.1: "Arrhenius" Plot with $L_F = 2.0$ for paraffins, cycloparafins, aromatics, and others. To obtain the kinetic parameters the linear approximation of the experimental data points was used. The symbols represent the data calculated from the experimental points.

D.1.2   Liquid Pool Extinction and Autoignition
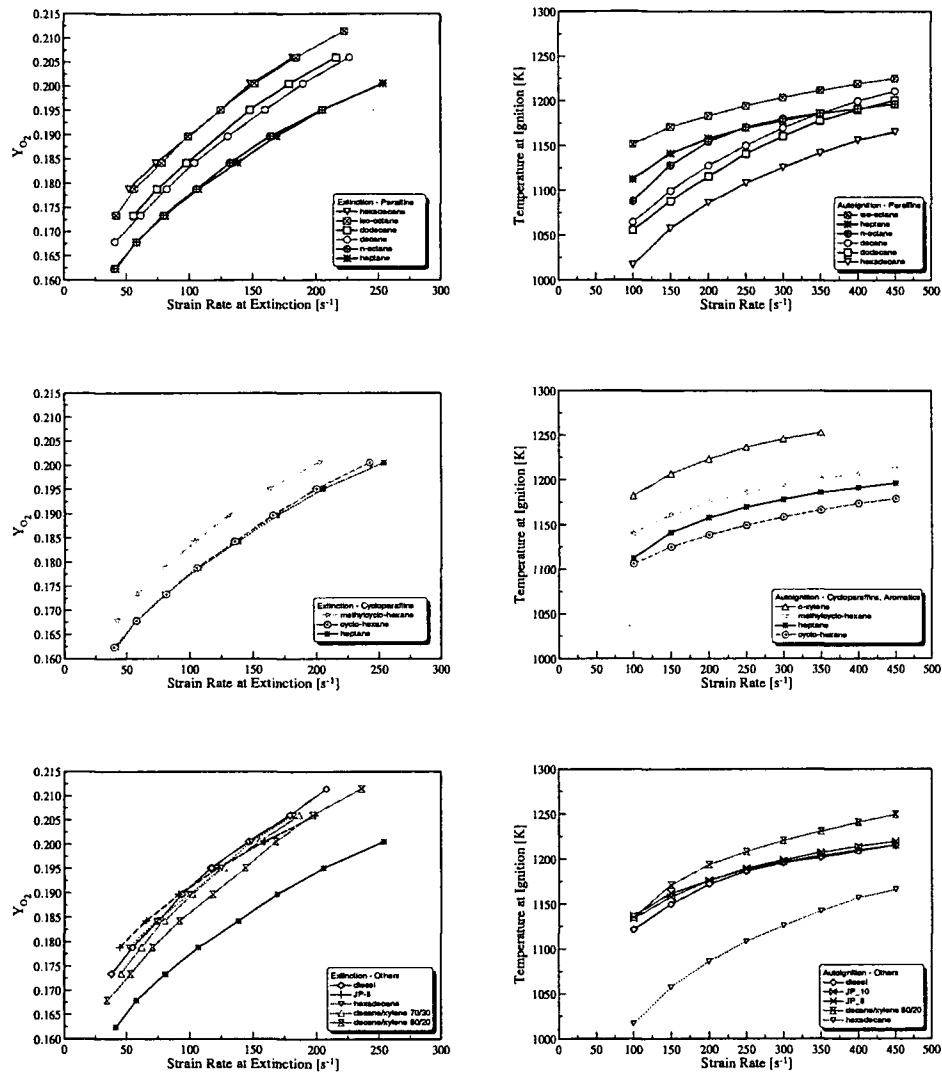
Figure D.2: For better distinction the data for extinction and autoignition from Figure 5.11 and 5.9 are divided in their fuel groups. On the right hand side autoignition data are shown, on the left hand side extinction data.

D.1.3 Calculation of Activation Energy and Frequency Factor

For the calculation the program MathCAD was used.

Stagnation Point Boundary over the Surface of a Liquid Pool $\quad$ $kmol := 1000 \cdot mol$ $\quad$ $kJ := 1000 \cdot J$ $\quad$ $TOL := 0.000000001$

Component Properties (Nitrogen):

$$bar := 10^5 Pa$$

Molecular Mass $\qquad M_N := 28.013 \cdot \dfrac{kg}{kmol}$ $\qquad R := 8.314 \dfrac{J}{mol \cdot K}$

Component properties (heptane):

Molecular Mass $\qquad M_F := 100.21 \cdot \dfrac{gm}{mol}$

Heat of vaporization $\qquad Q_L := 31.7191968 \cdot \dfrac{kJ}{mol}$ $\qquad\qquad q_L := \dfrac{Q_L}{M_F}$ $\qquad q_L = 316.52726 \dfrac{kJ}{kg}$

Boiling temperature $\qquad T_g := 371 \cdot K$

Oxidizer temperature $\qquad T_2 := 1158 \cdot K$

Heat capacity $\qquad a := 0.0292664 \cdot 10^2$ $\quad b := 0.14879769 \cdot 10^{-2}$ $\quad c := -0.0568476 \cdot 10^{-5}$ $\quad d := 0.10097038 \cdot 10^{-9}$

$$e := 0.06753351 \cdot 10^{-13}$$

$$c_P(T) := \dfrac{R}{M_N} \cdot \left(a + \dfrac{b}{K} \cdot T + \dfrac{c}{K^2} \cdot T^2 + \dfrac{d}{K^3} \cdot T^3 + \dfrac{e}{K^4} \cdot T^4 \right)$$

$$c_P(T_2) = 1.20389 \dfrac{kJ}{kg \cdot K}$$

Prndtl Number $\qquad Pr := 0.7$

Lewis Number $\qquad L_F := 2.16675$

Initial Guesses: $\qquad A_2 := 0.08998$ $\qquad\qquad B_2 := -1.92938$

$\qquad\qquad C_2 := 2.46485$ $\qquad\qquad F_2 := 0.6052$

$$\gamma := \dfrac{q_L}{c_P(T_2) \cdot T_2} \qquad \gamma = 0.22705$$

Calculation of the boundary conditions

for large η:

$\eta_1 := 5$ $\qquad\qquad \eta 1 >> 1,\ 1/\eta 1^2 << 1$ (neglectible), $B2 << 1$

Asymtotic solution of the energy equation

$$\theta_f(\eta, C_2) := \dfrac{C_2}{\sqrt{2\pi} \cdot \eta} \cdot \exp\left(-\dfrac{\eta^2}{2} \right)$$

$$\theta'_f(\eta, C_2) := \dfrac{C_2}{\sqrt{2\pi}} \cdot \exp\left(-\dfrac{\eta^2}{2} \right)$$

$$f(\eta, A_2, C_2) := \eta + \frac{A_2}{\eta^3} \cdot \exp\left(\frac{-\eta^2}{2 \cdot Pr}\right) + \frac{\gamma \cdot C_2}{2 \cdot \sqrt{2\pi} \cdot (1 - Pr) \cdot \eta^4} \cdot \exp\left(\frac{-\eta^2}{2}\right)$$

$$f'(\eta, A_2, C_2) := 1 - \frac{A_2}{Pr \cdot \eta^2} \cdot \exp\left(\frac{-\eta^2}{2 \cdot Pr}\right) - \frac{\gamma \cdot C_2}{2 \cdot \sqrt{2\pi} \cdot (1 - Pr) \cdot \eta^3} \cdot \exp\left(\frac{-\eta^2}{2}\right)$$

$$f''(\eta, A_2, C_2) := \frac{A_2}{Pr^2 \cdot \eta} \cdot \exp\left(\frac{-\eta^2}{2 \cdot Pr}\right) + \frac{\gamma \cdot C_2}{2 \cdot \sqrt{2\pi} \cdot (1 - Pr) \cdot \eta^2} \cdot \exp\left(\frac{-\eta^2}{2}\right)$$

$$c_P(T_2) = 1.20389 \times 10^3 \, m^2 \, s^{-2} K^{-1}$$

Asymtotic solution for the balance equation for fuel

$$y_{Ff}(\eta, F_2, L_F) := \frac{F_2}{\sqrt{2\pi} \cdot \sqrt{L_F} \cdot \eta} \cdot \exp\left(\frac{L_F \cdot \eta^2}{2}\right)$$

$$y'_{Ff}(\eta, F_2, L_F) := \frac{F_2 \cdot \sqrt{L_F}}{\sqrt{2 \cdot \pi}} \cdot \exp\left(\frac{L_F \cdot \eta^2}{2}\right)$$

$$\eta 2 := 0$$

$$f_{B''} := 0$$

$$\theta_{B''} := \frac{c_P(T_2) \cdot (T_2 - T_g)}{q_L} \qquad \theta_{B''} = 2.99329$$

Calculation of the equation for fuel

Definition of the system of ordinary differential equations:

$$Pr \cdot f''' + f \cdot f'' + f'^2 + (1 - \gamma\theta) = 0 \text{ AND} \qquad \frac{1}{L_F} \cdot (y_F'') + f \cdot y_F' = 0 \qquad \text{AND} \qquad \theta'' + f \cdot \theta' = 0 \qquad \text{Equ. (1)-(3)}$$

Definition of the initial conditions

$$y(\eta, A_2, B_2, C_2, F_2, L_F) := \begin{pmatrix} f(\eta + B_2, A_2, C_2) \\ f'(\eta + B_2, A_2, C_2) \\ f''(\eta + B_2, A_2, C_2) \\ \theta_f(\eta + B_2, C_2) \\ \theta'_f(\eta + B_2, C_2) \\ y_{Ff}(\eta + B_2, F_2, L_F) \\ y'_{Ff}(\eta + B_2, F_2, L_F) \end{pmatrix} \begin{matrix} f \\ f' \\ f'' \\ \theta \\ \theta' \\ y_F \\ y'_F \end{matrix} \quad y(\eta_1, A_2, B_2, C_2, F_2, L_F) = \begin{pmatrix} 3.0706612218 \times 10^0 \\ 9.9986856128 \times 10^{-1} \\ 4.2492697373 \times 10^{-4} \\ 2.8711556427 \times 10^{-3} \\ -8.8162279396 \times 10^{-3} \\ 1.9563028906 \times 10^{-6} \\ -1.3015803283 \times 10^{-5} \end{pmatrix}$$

Definition of the system of differential equations: 4/19/2005

$$D(x,y) := \begin{bmatrix} y_1 \\ y_2 \\ \left[\dfrac{(-2 \cdot y_0 \cdot y_2 + \gamma \cdot y_3) + \left[(y_1)^2 - 1 \right]}{2 \cdot Pr} \right] \\ y_4 \\ -y_0 \cdot y_4 \\ y_6 \\ -L_F \cdot y_0 \cdot y_6 \end{bmatrix}$$

$f' = y_1$

$f'' = y_2$

$f''' = \left[\dfrac{(-2 \cdot y_0 \cdot y_2 + \gamma \cdot y_3) + \left[(y_1)^2 - 1 \right]}{2 \cdot Pr} \right]$

$\theta' = y_4$

$\theta'' = -y_0 \cdot y_4$

$y'_F = y_6$

$y''_F = -L_F \cdot y_0 \cdot y_6$

$Z(\eta_1, \eta_2, A_2, B_2, C_2, F_2, L_F) := rkadapt\left(y(\eta_1, A_2, B_2, C_2, F_2, L_F), \eta_1, \eta_2, 0.0000001, D, 5, 0.1\right)$

$\eta_1 = 5 \qquad \eta_2 = 0 \qquad A_2 = 0.08998 \qquad\qquad B_2 = -1.92938$

Given $\qquad\qquad\qquad C_2 = 2.46485 \qquad\qquad F_2 = 0.6052$

$\left[\left(Z(\eta_1, \eta_2, A_2, B_2, C_2, F_2, L_F)^T \right)^{\langle 4 \rangle} \right]_2 = f_{B''}$

$\left[\left(Z(\eta_1, \eta_2, A_2, B_2, C_2, F_2, L_F)^T \right)^{\langle 4 \rangle} \right]_4 = \theta_{B''}$

$\left[\left(Z(\eta_1, \eta_2, A_2, B_2, C_2, F_2, L_F)^T \right)^{\langle 4 \rangle} \right]_5 = \left[\left(Z(\eta_1, \eta_2, A_2, B_2, C_2, F_2, L_F)^T \right)^{\langle 4 \rangle} \right]_1$

$\left[\left(Z(\eta_1, \eta_2, A_2, B_2, C_2, F_2, L_F)^T \right)^{\langle 4 \rangle} \right]_7 = L_F \cdot \left[\left(Z(\eta_1, \eta_2, A_2, B_2, C_2, F_2, L_F)^T \right)^{\langle 4 \rangle} \right]_1 \cdot \left[1 - \left[\left(Z(\eta_1, \eta_2, A_2, B_2, C_2, F_2, L_F)^T \right)^{\langle 4 \rangle} \right]_6 \right]$

$R := Find(A_2, B_2, C_2, F_2)$

$$R := \begin{pmatrix} 0.08998 \\ -1.92938 \\ 2.46485 \\ 0.6052 \end{pmatrix}$$

$\left[\left(Z(\eta_1, \eta_2, A_2, B_2, C_2, F_2, L_F)^T \right)^{\langle 4 \rangle} \right]_7 = -0.10884$

$A_2 := R_0$

$B_2 := R_1$

$C_2 := R_2$

$F_2 := R_3$

$S := Rkadapt\left(y(\eta_1, A_2, B_2, C_2, F_2, L_F), \eta_1, \eta_2, 10, D\right)$

	0	1	2	3	4
0	5	3.0706617412	0.999868562	0.0004249241	0.0028711524
1	4.5	2.5708338571	0.9992813303	0.0024364637	0.0127499139
2	4	2.0717408401	0.9964062132	0.0108400878	0.0475630695
3	3.5	1.5757194311	0.9855321441	0.0368878074	0.1436293893
4	3	1.089610588	0.9540259177	0.0954989882	0.3516059115
5	2.5	0.6281455358	0.8839686439	0.1894593659	0.706757503
6	2	0.2142987056	0.7625853362	0.2947680279	1.191112705
7	1.5	-0.1264192877	0.5936471539	0.3740892111	1.7309404266
8	1	-0.3746085808	0.3963614021	0.4072088475	2.2400184416
9	0.5	-0.5218438062	0.1931939188	0.400151976	2.66455445
10	0	-0.5695130607	-0.0000000829	0.3701861041	2.9932912383

$S =$

Heptane

$S := \text{Rkadapt}\big(y(\eta_1, A_2, B_2, C_2, F_2, L_F), \eta_1, \eta_2, 1000, D\big)$

Graphs of the solution $n := 0..999$

f

$\dfrac{S_{n,1}}{}$

THETA

$\dfrac{S_{n,4}}{}$

f'

$\dfrac{S_{n,2}}{}$

yF

$\dfrac{S_{n,6}}{}$

f''

$\dfrac{S_{n,3}}{}$
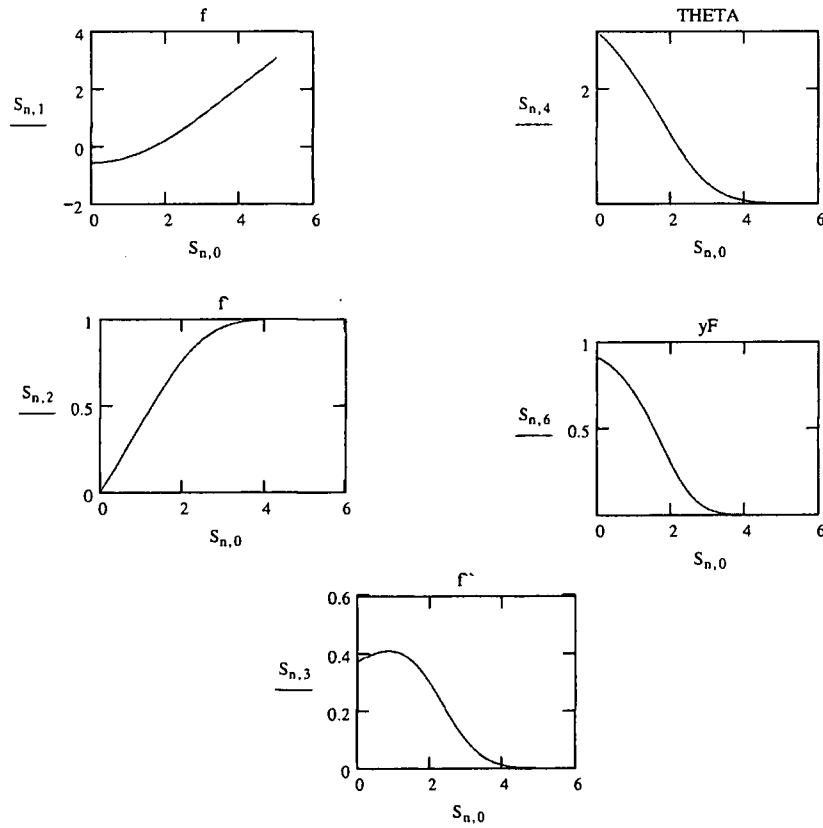
The chemical reaction between the fuel and oxygen is represented by the following one-step, irreversible process: 4/19/2005

CmHn + (m+n/4) O2 -> m CO2 + (n/2) H2O
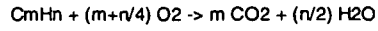
Guess a value of the activation temperature Ta

$T_a := 2.38753 \times 10^4 K$ $\beta := \gamma \cdot \dfrac{T_a}{T_2}$ $\eta_r := 0.5$ (guess) $R' := 8.314 \dfrac{J}{mol \cdot K}$ $W_{air} := 0.21 \cdot 32.0 \dfrac{kg}{kmol} + 0.79 \cdot 28.01 \dfrac{kg}{kmol}$

$\Delta_i := 0.4503$ for $L_F = 2.16675$

$a_2 := 200 \cdot \dfrac{1}{s}$ $p := 101300 Pa$ $Y_{O2.2} := 0.23301$ $W_{O2} := 32.0 \dfrac{kg}{kmol}$

$Q_F := 4465 \dfrac{kJ}{mol} - Q_L$ $q_F := \dfrac{Q_F}{M_F}$

$\eta_r := 0.4$

Given

$q_F = 4.42399 \times 10^4 \dfrac{kJ}{kg}$

$\dfrac{\beta \cdot C_2}{\sqrt{2\pi \cdot \eta_r}} \cdot \exp\left(-\dfrac{\eta_r}{2}\right) = 1$

$\eta_r(\beta) := Find(\eta_r)$

$j := 0..7$

$a_2 := \begin{pmatrix} 100 \\ 150 \\ 200 \\ 250 \\ 300 \\ 350 \\ 400 \\ 450 \end{pmatrix} \dfrac{1}{s}$ $T_{2ign} := \begin{pmatrix} 1112.4 \\ 1141.1 \\ 1158.0 \\ 1169.8 \\ 1178.0 \\ 1186.2 \\ 1191.3 \\ 1196.4 \end{pmatrix} K$ $\beta(T_2) := \gamma \cdot \dfrac{T_a}{T_{2ign}}$ $\beta(T_2) = \begin{pmatrix} 4.87309708676437 \\ 4.75053299388019 \\ 4.68120310821821 \\ 4.63398290247622 \\ 4.60172597565083 \\ 4.5699150221857 \\ 4.55035104450322 \\ 4.53095386101361 \end{pmatrix}$

$\eta_{r_j} := \eta_r(\beta(T_2)_j)$

$\eta_r = \begin{pmatrix} 1.8758 \\ 1.85122 \\ 1.83711 \\ 1.82742 \\ 1.82076 \\ 1.81415 \\ 1.81007 \\ 1.80602 \end{pmatrix}$

$G_j := \Delta_i \cdot \eta_{r_j} \cdot \dfrac{C_2^{L_F} \cdot W_{O2} \cdot R' \cdot q_L \cdot a_{2_j} \cdot \sqrt{L_F} \cdot T_{2ign_j}}{F_2 \cdot Y_{O2.2} \cdot q_F \cdot p \cdot W_{air}} \cdot \left(\dfrac{\eta_{r_j} \cdot \sqrt{2\pi}}{\beta(T_2)_j}\right)^{(1-L_F)} \cdot \dfrac{mol \cdot s}{m^3}$ $G = \begin{pmatrix} 4.70378E+000 \\ 7.04123E+000 \\ 9.37727E+000 \\ 1.17121E+001 \\ 1.40467E+001 \\ 1.63788E+001 \\ 1.87123E+001 \\ 2.10442E+001 \end{pmatrix}$ $\ln(G) = \begin{pmatrix} 1.54837 \\ 1.95178 \\ 2.23829 \\ 2.46062 \\ 2.64239 \\ 2.79599 \\ 2.92918 \\ 3.04663 \end{pmatrix}$

$slope\left(\dfrac{1}{T_{2ign}}, \ln(G)\right) = -2.38752 \times 10^4 K$

$y(x) := slope\left(\dfrac{1}{T_{2ign}}, \ln(G)\right) \cdot x + intercept\left(\dfrac{1}{T_{2ign}}, \ln(G)\right)$

Arrhenius plot
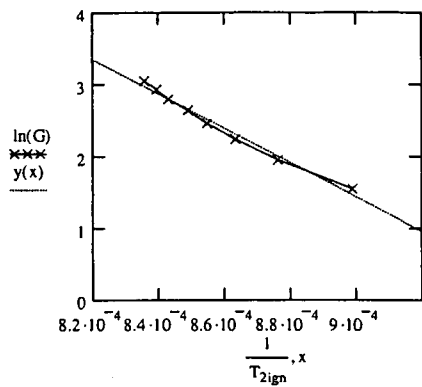
$$T_a := -\text{slope}\left(\frac{1}{T_{2ign}}, \ln(G)\right)$$ $T_a = 2.38752 \times 10^4 \, K$ $E_a := T_a \cdot R'$ $E_a = 198.49842 \, \frac{kJ}{mol}$

$$B := \exp\left(\text{intercept}\left(\frac{1}{T_{2ign}}, \ln(G)\right)\right)$$ $B = 9.06158 \times 10^9$

D.1.4 Multicomponent Results

(a) JP-8

(b) Jet A
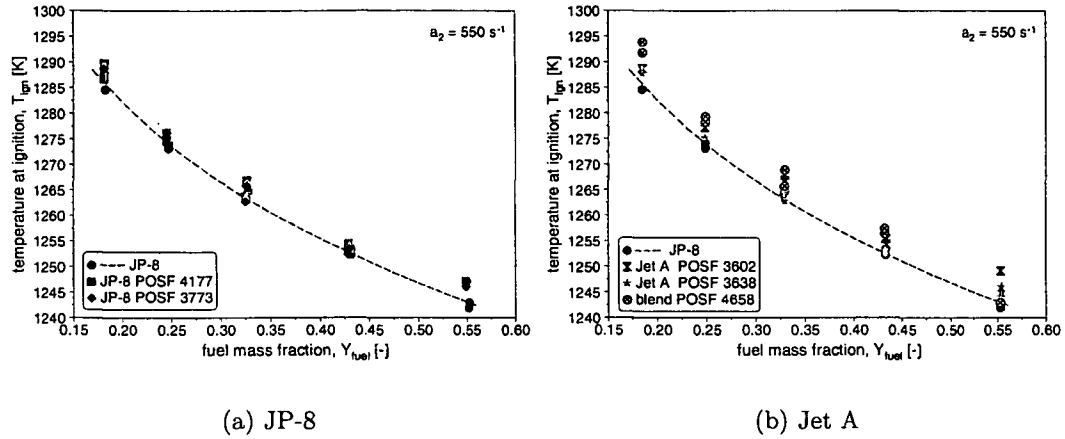
Figure D.3: Autoignition data for JP-8 and Jet A at constant strain rate, $a_2 = 550$ s^{-}1. Symbols represent experimental data, lines represent best fit curves.

(a) $Y_{fuel} = 0.4$

(b) $a_2 = 550$s^{-1}
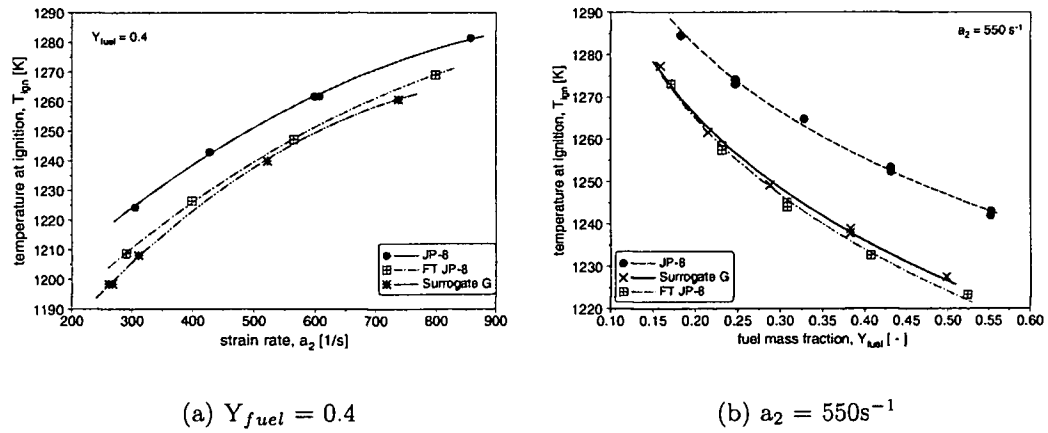
Figure D.4: Autoignition results for Fischer-Tropsch JP-8 (FT JP-8) and its surrogate G. Symbols represent experimental data, lines represent best fit curves.

(a) $Y_{fuel} = 0.4$

(b) $a_2 = 550s^{-1}$
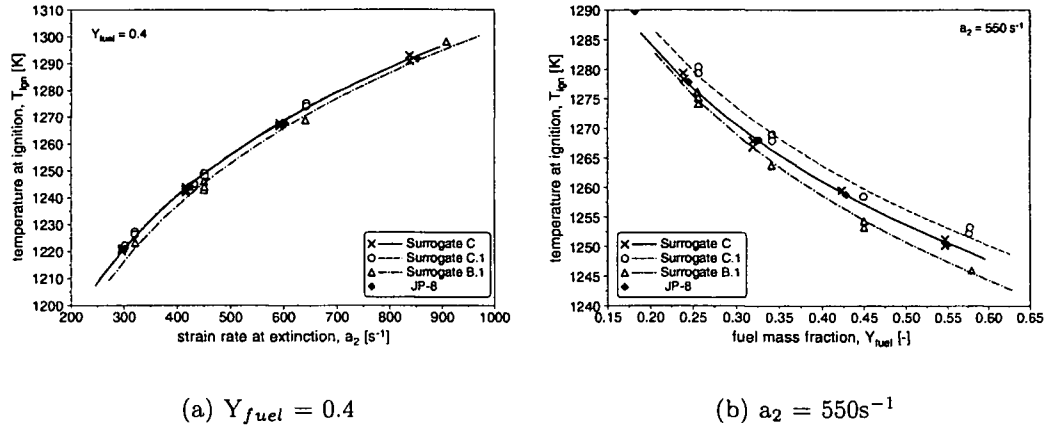
Figure D.5: Autoignition results for surrogate B.1, C, and C.1. Symbols represent experimental data, lines represent best fit curves.

(a) $Y_{fuel} = 0.4$

(b) $a_2 = 550s^{-1}$
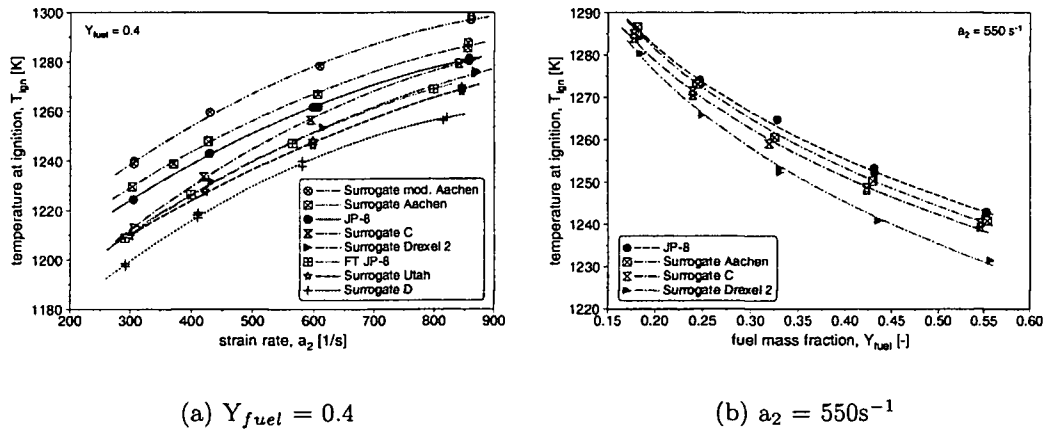
Figure D.6: Autoignition results for surrogates. Symbols represent experimental data, lines represent best fit curves.
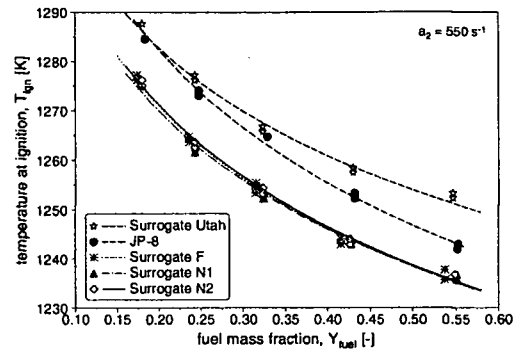
(a) $Y_{fuel} = 0.4$

Figure D.7: Autoignition results for surrogate N. Symbols represent experimental data, lines represent best fit curves.
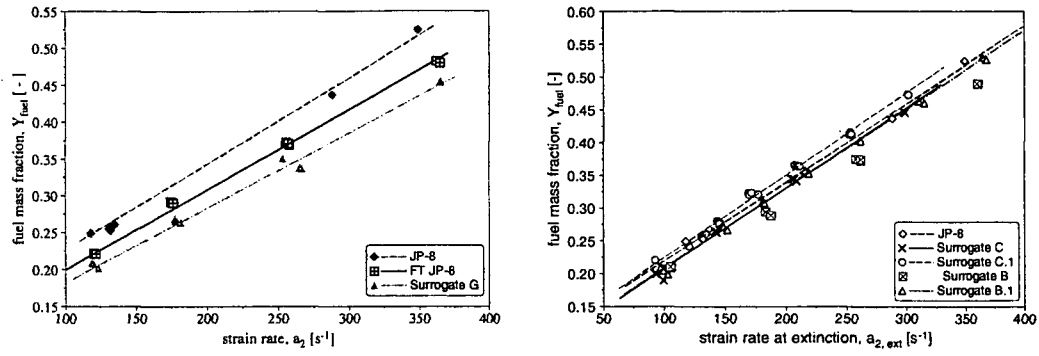
(a) Surrogate G

(b) Surrogate C
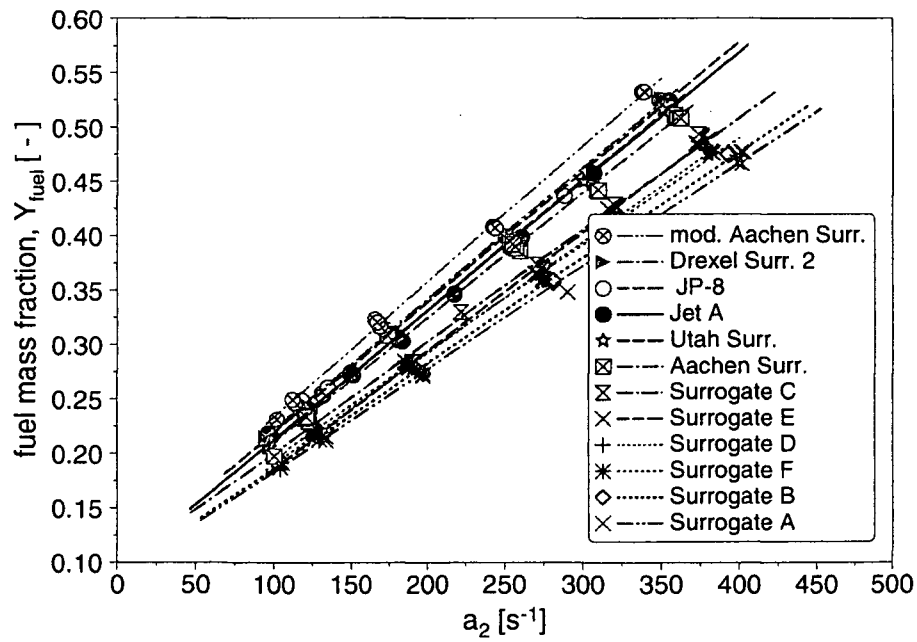
(c) var. surrogates

Figure D.8: Extinction results for various surrogates. Symbols represent experimental data, lines represent best fit curves.

Curriculum Vitae

Stefan Helmuth Humer

- Date of Birth: 02/24/1973, Salzburg, Austria
- Citizenship: Austrian

Education

79/09-83/06	Elementary school in Salzburg
83/09-91/06	BundesRealGymnasium ($\simeq$ high school), Akademiestrasse, Salzburg
91/10-92/04	Military duty, Salzburg
92/10-01/01	Technische Universität Wien, Austria (University of Technology Vienna)
	Study of mechanical engineering, since 1996 specializing during the 2nd part of the study in the field of engine-combustion and vehicle manufacturing
01/03	Dipl.-Ing. (*simeq* Master of Science)
01/04-	Ph.D.-study at University of Technology Vienna in cooperation with University of California, San Diego, California, USA

Teaching and Working Experience

99/09-00/05	DaimlerChrysler AG; Stuttgart - Untertrkheim Forschung und Technologie, Abteilung PKW Motorenversuch (FT1/MP) composition of a diploma-thesis
01/04-03/06	Teaching Assistant for "Chemical Engineering Thermodynamics" at UCSD, (each spring quarter)
03/06-03/12	Teaching Assistant for "Heat Transfer" (MAE 101C) at UCSD
01/04-04/11	Research Associate, Department of Mechanical and Aerospace Engineering, University of California, San Diego
05/05-	Research Associate Level II Department of Mechanical and Aerospace Engineering, UCSD

Publications

- S. Humer, R. Seiser, and K. Seshadri, Nonpremixed and Premixed Extinction and Autoignition of C_2H_4, C_2H_6, C_3H_6, and C_3H_8, *Proceedings of the Combustion Institute*, 29, p.1597-1604, 2002

- S. Humer, et all, Experimental and Kinetic Modeling Study of Combustion of JP-8, its Surrogates and Reference Components in Laminar Nonpremixed Flows, *Proceedings of the Combustion Institute,* in press 2006

- R. Seiser, S. Humer, K. Seshadri, and E. Pucher, Experimental Investigation of Methanol and Ethanol Flames in nonuniform Flows, *Proceedings of the Combustion Institute,* in press 2006

- S. Humer, R. Seiser, K. Seshadri, and E. Pucher, Extinction of Methanol and Ethanol Flames in Premixed Flows, SAE, 07SFL-89, in press 2007

Skills and Qualifications

- fluent (written and oral) in German

- Computer skills in Mircosoft, LaTex, SolidWorks, AutoCAD, Chemkin 3.7+

- knowledge of Fluent, Gambit